2005

Development of a numerical model of rock failure mechanisms associated with the impact of lateral displacement

Jong Wook Lee
University of Wollongong

DEVELOPMENT OF A NUMERICAL MODEL OF ROCK FAILURE MECHANISMS ASSOCIATED WITH THE IMPACT OF LATERAL DISPLACEMENT

A thesis submitted in partial fulfillment of the
requirements for the award of the degree

MASTER OF ENGINEERING
BY RESEARCH

from

School of Civil, Mining and Environmental Engineering
UNIVERSITY OF WOLLONGONG

by

JONG WOOK LEE
B. Eng. (Hons)

Faculty of Engineering
August 2005

THESIS CERTIFICATION

CERTIFICATION

I, Jong Wook Lee, declare that this thesis, submitted in partial fulfillment of the requirements for the award of Master of Engineering by Research, in the School of Civil, Mining and Environmental Engineering, University of Wollongong, is wholly my own work unless otherwise referenced or acknowledged. The document has not been submitted for qualifications at any other academic institution.

…….

Jong Wook Lee

Date

ACKNOWLEDGEMENTS

The thesis could not have been completed without the valuable support from a group of people. The author would like to acknowledge the support of the following.

The thesis supervisors Associate Professor Najdat I. Aziz and Associate Professor Ernest Y. Baafi, for their excellent guidance, strong support and sincere encouragement throughout this study.

Dr. Yonglian Sun, visiting fellow, for his advice and suggestions in FLAC modelling.

Bill Huuskes from Metropolitan Colliery for his support in providing all the necessary information related to the fieldwork, Dr. Ken Mills from SCT Pty Ltd for continual dialogue and discussions on the project, BHP Billiton staff and other members of the ACARP Project partners.

Walter Keilich, my co-research colleague, for effective research partnership.

This thesis would not have come to fruition without the financial support from ACARP Project 22083 (Development of protection strategies, damage criteria and practical solutions for protecting undermined river channels).

Finally, the author would like to thank his family for their constant support and encouragement during the study.

ABSTRACT

Ground subsidence due to mining has been the subject of research for several decades, and it remains to be an important problem, which confronts the mining close to ecologically sensitive areas. This thesis is concerned with the development of a numerical simulation model of ground deformation, extended to ground movement under river channel systems present at the base of valleys. A number of numerical models have been developed for better understanding of the strata interactions using the two-dimensional explicit finite difference code FLAC Version 4.0.

The proposed model simulation is focused on the ground deformation, down to 30 meters below the river valley. Ground displacement, mainly lateral displacement has been observed by field monitoring and accordingly, artificial lateral displacement was created to study the deformational behaviour beneath the bottom of the valley. Lateral displacement around valley areas caused the closure of the valley and bulging of the valley floor, known as upsidence. Most of the numerical simulations carried out with FLAC demonstrated that valley closure and valley floor bulging were dependent on the shape and dimension of modelled geometry, strata properties, loading rate of lateral displacement, the magnitude and shape of loading, the presence of bedding planes and the presence of an underground water table.

The inclusion of bedding planes or joints with known rock types was recommended for ground deformation simulations. The use of UDEC instead of FLAC was considered as an alternative to provide a better understanding of the effects of joints and bedding planes on subsidence and upsidence. Further studies are required for strata interaction when an underground water table is introduced to the model.

TABLE OF CONTENTS

LIST OF TABLES

LIST OF FIGURES

LIST OF SYMBOLS AND ABBREVIATIONS

ACARP	Australian Coal Association Research Program
SCT	Strata Control Technology
WRS	Waratah Rivulet Site
FLAC	Fast Lagrangian Analysis of Continua
GIIC	Graphical Interface for Itasca Codes
FISH	FLACish
UBI	Ubiquitous-Joint Model
P.L.	Proportional Limit
RMR	Rock Mass Classification System
MGA	Map Grid Australia System
ISG	Integrated Survey Grid System
RL	Reduced Level
ALD	Applied Lateral Displacement

σ_{yy}	Vertical Stress
σ_{xx}	Horizontal Stress
σ_1	Major Principal Stress
σ_2	Intermediate Principal Stress
σ_3	Minor Principal Stress
σ_n	Normal Stress
σ_{ult}	Ultimate Stress
τ	Shear Stress
μ	Coefficient of Friction for the Crack Surfaces
σ_{cr}	Stress Normal to the Crack required to close it.
γ	Unit Weight of Rock
z	Thickness of Rock Layer
ρ	Density of Rock
g	Gravity
ν	Poisson's Ratio for the Rock Mass
ε	Strain
E	Young's Modulus of Elasticity
G	Shear Modulus

K	Bulk Modulus
σ_t	Tensile Strength
c	Cohesion
ϕ	Internal Friction Angle
θ	Joint Angle
ϕ_j	Friction of the Weak Plane
c_j	Cohesion of the Weak Plane
σ_j^t	Tensile Strength of the Weak Plane
m_coh	Cohesion in UBI
m_dil	Dilation Angle in UBI
m_fric	Friction Angle in UBI
m_g	Shear Modulus in UBI
m_k	Bulk Modulus in UBI
m_ten	Tensile Strength in UBI
m_jang	Joint Angle in UBI
m_jcoh	Joint Cohesion in UBI
m_jfric	Joint Friction Angle in UBI
m_jten	Joint Tension Limit in UBI
n	Porosity
e	Void Ratio
k	Permeability
C_w	Compressibility of Fluid
ρ_w	Fluid Mass Density
σ'	Effective Stress
σ	Total Stress
pp	Pore Pressure
ρ_{dry}	Dry Density
ρ_{wet}	Wet Density

LIST OF EQUATIONS

CHAPTER 1
INTRODUCTION

1.1 GENERAL BACKGROUND

In ACARP Project Nos. C8005 and C9067, Waddington Kay and Associates (WKA, 2002) addressed a number of issues related to the impacts of mine subsidence on the strata and hydrology of river valleys and development of management guidelines for undermining cliffs, gorges and river systems. The report was based on several years of field data gathered from a number of underground coal mining operations. The main conclusions reported were:

a) Distinct patterns of ground movement are present whenever creeks, rivers and gorges are undermined,
b) The major influences on the closure and upsidence movements are:
    - the location of the creek or river valley relative to the perimeter of the mined goaf area;
    - the depth of the valley;
    - the maximum incremental subsidence in the panel being mined; and
    - the pre-existing magnitudes and directions of in-situ horizontal stresses.
c) The impacts of mining on the hydrology of the river systems in the Southern Coalfield are temporary.

WKA then recommended the following:

a) Further research should be carried out to determine the way in which the in-situ horizontal stress influences the subsidence impacts on creeks, river valleys and gorges and to develop improved methods for predicting the impacts, and
b) Future research would be advantageous:

- in the development and testing of methods for remediation of damage to creeks and rivers;
- a study of the longer-term impacts of subsidence on creek and river hydrology; and
- baseline studies to record present conditions in areas that are to be mined in future.

As a consequence of WKA's ACARP reports, a second successful submission was made to ACARP to "develop and demonstrate protection strategies, damage criteria and practical solutions for protecting undermined river channels". This project is known as ACARP Project 22083. This application group comprised; BHP Billiton, Strata Control Technology operations Pty Ltd (SCT), CSIRO Division of Mining and Exploration, University of Wollongong, Waddington Kay and Associates and Helensburgh Coal Pty Ltd (Metropolitan Colliery). Three field sites in the Appin and Helensburgh area were identified for investigations. One of the sites chosen for this thesis is located on one of several major rock bars along the section of Waratah Rivulet within the current mining area operated by Metropolitan Colliery. The site (Fig. 1.1) is known as the Waratah Rivulet Site 1 (WRS 1). The site was identified as being suitable to study the behaviour of rock because it is the first major rock bar on the Waratah Rivulet to come under the influence of mining induced subsidence. The major concern in this study was the changes in flow paths at the rock bars (Fig. 1.2) due to surface and subsurface fractures developed as a result of mining operation. Continuous field monitoring found that there has no on going water loss as a result of fracturing. However, when subsurface flows feature predominantly while there is not enough flow on the surface of rock bar, the ecosystem is destroyed and there is oxidization at the fractured rock surface.

In search of a possible solution for the protection of rock bars from the effect of underground mining operation, it is necessary to understand how strata behave when undermining cliffs, gorges and river systems.

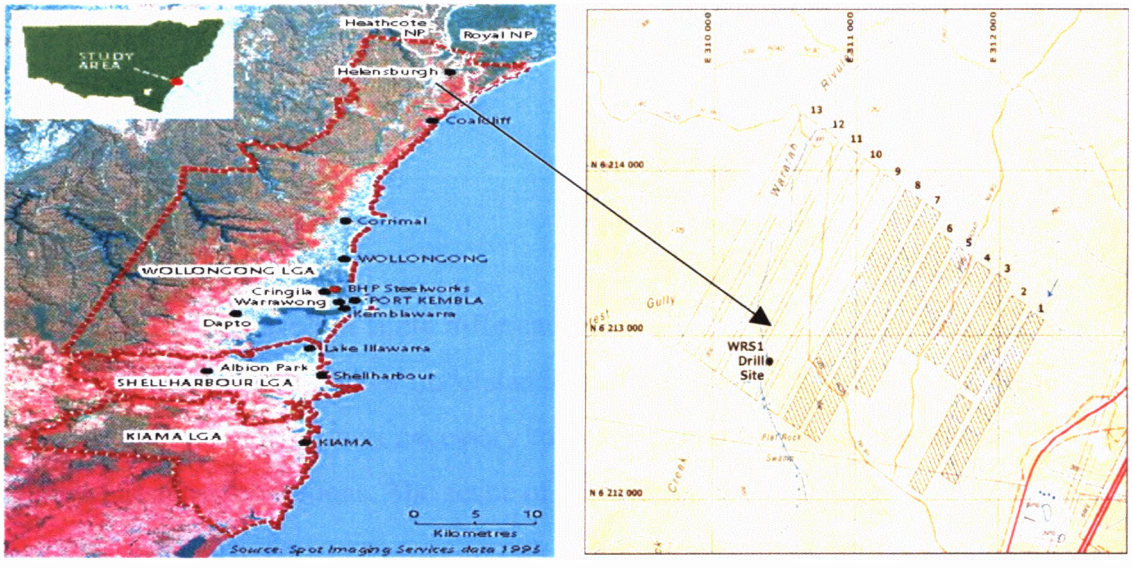

(a) Regional Map (b) Location of WRS 1

Figure 1.1 Location of study site (Mills, 2002)

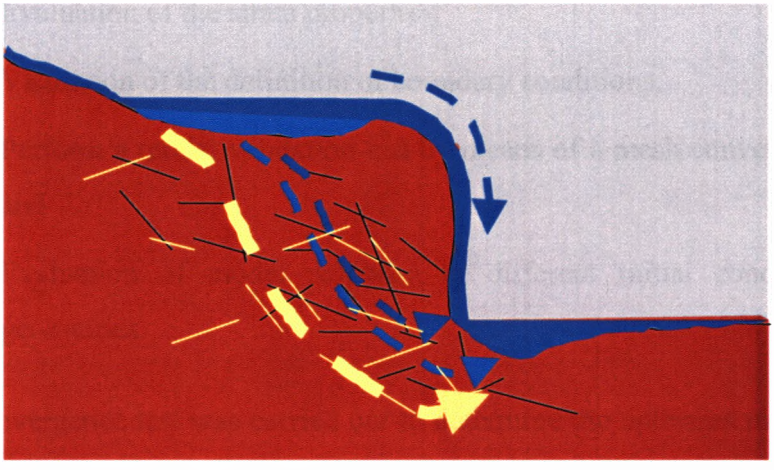

Figure 1.2 Natural state flow conditions (Mills, 2002)

1.2. OBJECTIVES OF THE STUDY

The objectives of this thesis are:

1. The primary objective of this thesis is to determine the key deformation processes associated with the impact of lateral movements on river valleys and gorges, and

2. The approach used was to develop a numerical model to mimic the deformation processes using a finite element model.

1.3. SCOPE OF WORK

The 2-Dimensional explicit finite difference code FLAC V4.0 was chosen as the modelling techniques for better understanding of the strata interaction. To achieve the objective of thesis, it was necessary to perform number of simulations under different assigned conditions. The scope of work involves:

- Familiarisation of FLAC V4.0,
- Evaluation of the constitutive behaviour of in-situ strata,
- Evaluation of the in-situ stress conditions,
- Evaluation of the strata properties,
- Validation of the definition of boundary conditions,
- Perform a model validation test by means of a mesh convergence test, and
- Evaluation of model response to different initial conditions and geometries.

A mesh convergence test was carried out to determine the optimum mesh density for further simulation. The mesh convergence test was also used to validate the numerical accuracy of the solution.
No attempt was made to compare the various numerical models with field data as the models had different conditions to the field site.

1.4 THESIS ORGANISATION

Chapter 1 provides general background information about ACARP Projects C8005 and C9067, which were carried out by Waddington Kay and Associates.

Their findings and recommendations are briefly listed. Chapter 1 also contains an introduction for this thesis, its objectives and scope of study undertaken. Chapter 2 provides a literature review on rock mechanics. In particular this chapter was focused on the mechanics of rock deformation. Chapter 3 provides an overview of FLAC while Chapter 4 details procedures undertaken in writing the FLAC codes for this thesis. Chapter 5 contains the results for the mesh convergence tests in FLAC and Chapter 6 presents the results of simulations undertaken in FLAC. Finally Chapter 7 provides conclusions for this thesis and recommendations for future studies.

CHAPTER 2
LITERATURE REVIEW

2.1 INTRODUCTION

This chapter briefly presents some of the fundamental concepts and relevant equations of rock mechanics. The main emphasis was placed on rock mechanics, stresses in rock, properties of rocks, criteria of rock failure, in-situ strength of rocks and rock mass properties. Familiarisation of terms and fundamental concepts used in this chapter is important in the understanding of topics included in various chapters presented in this thesis.

2.2 STRESSES IN ROCK

Rock at depth is subjected to stresses resulting from the weight of the overburden, and from locked in stresses of tectonic origin known as virgin stress. The state of stress at a point in undisturbed rock is in equilibrium state as shown in Fig. 2.1 that illustrates the general stress components in undisturbed, homogeneous and isotropic rock.

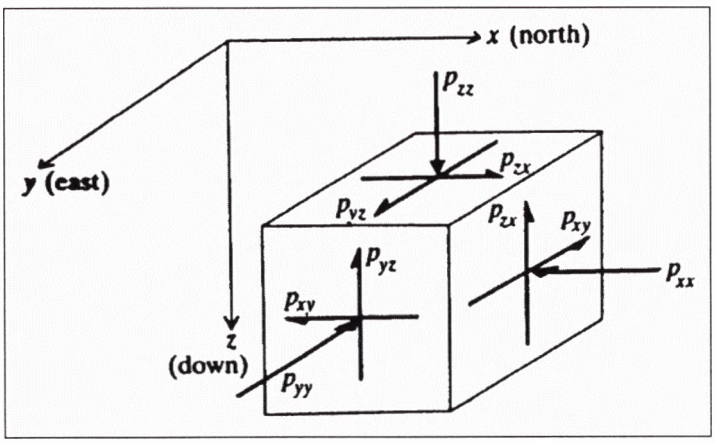

Figure 2.1 Stress components in undisturbed rock (Brady & Brown, 1993)

The stress at a point varies in magnitude with increased depth from the ground surface. Near the surface, the natural rock stresses are influenced by the weight of the rock, tectonic stresses, jointing, fractures and restraint against lateral expansion. In general, both vertical and horizontal stresses increase with depth of overburden. Vertical stress at any given point in the ground can be found by:

$$\sigma_{zz} = \gamma \times z \tag{2.1}$$

where,

σ_{zz} = vertical stress at a point, Pa
γ = unit weight of rock,
z = thickness of rock layer, m

$\gamma = \rho \times g$
ρ = density of rock, kg/m^3
g = gravity, m/sec^2

In Equation 2.1, the following assumptions are made:

1. The rock is linear-elastic, isotropic and homogeneous,
2. The lateral rock constraint or confinement is complete, and
3. There are no stresses of tectonic origin such as those accompanying folding, shrinkage, or other distortions of the earth's crust.

A common but unjustified assumption in the estimation of the in-situ horizontal stress is given by Equation 2.2 (Vutukuri & Katsuyama, 1994):

$$\sigma_{xx} = \sigma_{yy} = \left(\frac{\nu}{1-\nu}\right) \times \sigma_{zz} \tag{2.2}$$

where,

$\sigma_{xx} = \sigma_{yy}$ = horizontal normal stress components, Pa
σ_{zz} = vertical stress at a point, Pa
ν = Poisson's ratio for the rock mass

The shear stress components σ_{xy}, σ_{yz}, σ_{zx} are assumed to be zero and the normal stresses defined by Equations 2.1 and 2.2 are the principal stresses, which are denoted by the symbols σ_1, σ_2 and σ_3. σ_1 is known as the major principal stress,

σ_3 is the minor principal stress, and σ_2 is the intermediate principal stress. Based on field studies have shown that (Hooker et al., 1972; Brown and Hoek, 1978) Equation 2.2 is rarely satisfied, and also that the vertical direction is rarely a principal stress direction. This state of affairs arises from the complex load path and the geologic history to which an element of rock is typically subjected in reaching its equilibrium state. Rock in-situ is in state of stress equilibrium prior to being disturbed or excavated. Three kinds of in-situ stress fields exist in a rock. They are a uniaxial stress (unidirectional) field, a biaxial stress (two directional) field and a hydrostatic stress field (Obert and Duvall, 1967).

A uniaxial stress field is one where the rock material is subjected to compressive or tensile stresses in one direction only. This state of stress would be encountered in rock at shallow depth below ground surface, and also near free vertical surfaces. A biaxial stress field is one where the rock medium is subjected to compressive or tensile stresses in two mutually perpendicular directions. The state of stress condition would be encountered at greater depth over a wide range of depth, depending upon the type of rock, and at a depth of approximately 1000 m and greater. A hydrostatic stress field is one where the rock medium is subjected to equal stress in three mutually perpendicular directions. This means that σ_{xx}, σ_{yy} and σ_{zz} are all of equal magnitude or pressure. Such conditions may be encountered in undisturbed ground at greater depth, and in semi-viscous or plastic rocks. The three stress fields are illustrated in Fig. 2.2.

2.3 DEFORMATION OF ROCKS

The term deformation of rock means any changes in its original form. This is caused by the externally applied loads on in-situ rock, or by tectonic forces (compressive and/or shear forces). In nature, the common modes of deformation may be folding, faulting (shear), and solid flow. Stress in rock generates strain and displacement. Stress is an abstract concept and can only be determined by strain

measurement. There are three idealized stress-strain relationships and Fig. 2.3 illustrates how various materials deform.

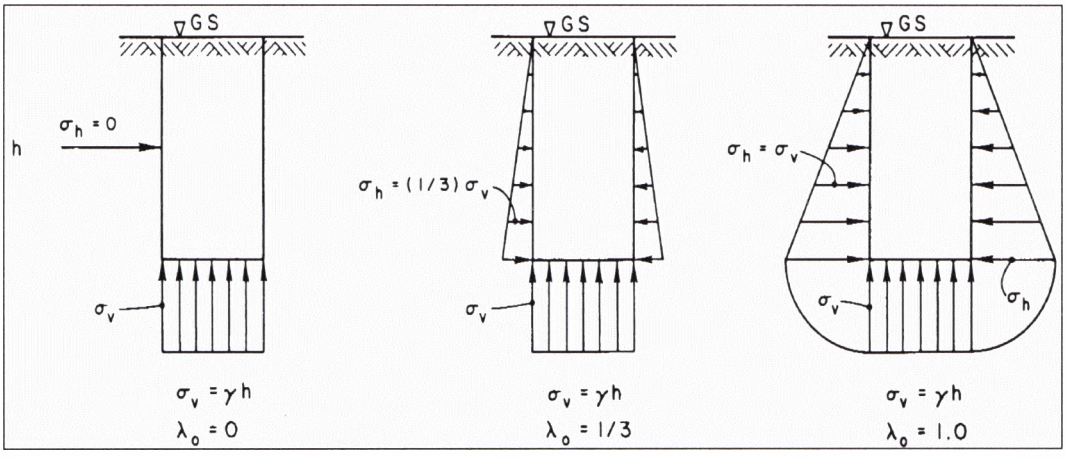

(a) Uniaxial unconstrained stress field

(b) Laterally constrained biaxial stress field

(c) Hydrostatic stress field (in semi viscous or plastic rocks)

Figure 2.2 Three assumed kinds of stress fields (Jumikis, 1979)

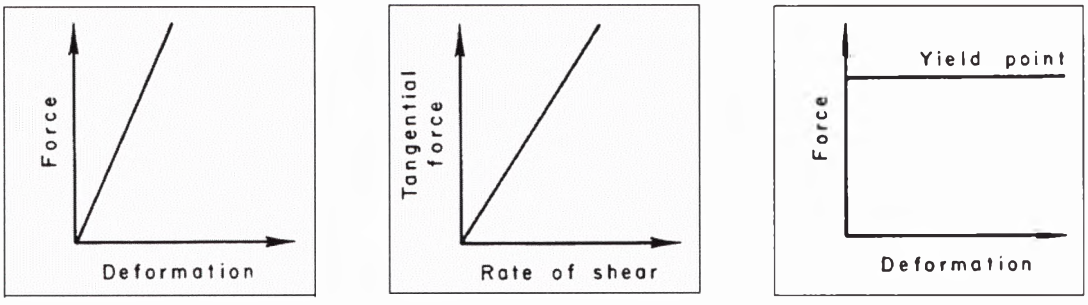

(a) Elastic substance represented by straight line. Elastic Deformation

(b) Viscous substance. Viscous deformation

(c) Perfectly plastic substance. Plastic deformation or plastic flow condition

Figure 2.3 Three idealised substances, characterised somewhat by the modes according to which they deform (Jumikis, 1979)

Fig. 2.3(a) illustrates elastic deformation of an elastic material represented by a straight-line stress-strain diagram. Fig. 2.3(b) shows viscous deformation of a viscous substance represented by a straight-line shear-force versus rate of shear diagram. Fig. 2.3(c) represents plastic deformation of a perfectly plastic substance

represented by a straight-line stress-strain diagram. According to Jumikis (1979), rock deformation and strength are affected by the deformability factors, including:

- Various rock defects, joints and beddings,
- Rock petrographic structure (rock matrix),
- Geometric orientation and attitude of the rock formation (dip and strike),
- Degree of weathering or alteration of the rock,
- Elastic, plastic, and rheological properties of rock,
- Anisotropy of rock,
- Direction and magnitude of acting loads on rock,
- Degree of compression and/or decompression of rock,
- Fissures and/or hair cracks brought about by blasting and/or excavation of, or drilling in the rock,
- Seismic factors, and
- State of stress (internal stress) within the rock mass.

While elastic deformation entails changes in the volume of rock, plastic deformations (the relative movement or sliding of the ruptured or sheared-off parts of the rock past each other) take place usually at a constant volume. Fig. 2.4 shows an idealized stress-strain relationship diagram for a ductile material.

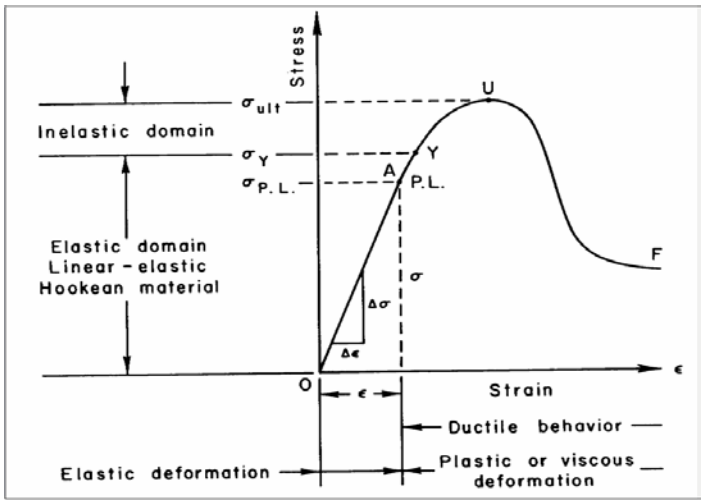

Figure 2.4 Stress-strain diagram for ductile material

Fig. 2.4 shows that up to a certain magnitude of the externally applied stress σ_Y (yield point *Y*) on the rock, the corresponding strain ε is constant. In other words, the stress σ (or $\Delta\sigma$) is proportional to strain ε (or $\Delta\varepsilon$) by Hooke's law:

$$\sigma = E \times \varepsilon \tag{2.3}$$

or

$$\Delta\sigma = E \times \Delta\varepsilon \tag{2.4}$$

where,

$E = \frac{\sigma}{\varepsilon}$ Hooke's coefficient of proportionality, known as Young's modulus of elasticity, defined for uniaxial stress; the modulus of elasticity E represents the stiffness of the material. The E-value is different for various materials.

Point *Y* in Fig. 2.4, is known as the elastic yield point at which the transition from elastic to ductile behaviour of the material takes place. The corresponding stress σ_Y at point *Y* is called the yield stress. Plasticity is characterized by the existence of a yield point beyond which permanent strains appear. Upon continuing the loading beyond the yield point *Y* up to the ultimate stress σ_{ult} to point *U* on the stress-strain curve, failure of the material takes place, and with increasing strain beyond *U* the stress drops, as shown by the part *UF* of the curve. It means that the material deforms without limit under this stress unless constrained. Thus, Fig. 2.4 represents a stress-strain curve for a perfectly elasto-plastic material.

From Fig. 2.4, three domains can be distinguished, namely: the elastic domain, the partly elastic-plastic domain and the plastic domain. The domains of the partly elastic-plastic and the plastic are also known as the inelastic domain. Deformation in the inelastic domain is generally termed plastic or viscous deformation. A material is called purely elastic if the deformation is recovered when the stress is removed. Whereas a material is called purely plastic if the deformation does not disappear when the stress is removed and if the stress determines the amount, but not the rate of deformation. On the other hand, a material is called purely viscous if the stress acting upon it determines the rate of deformation.

Due to deformation of rock, many kinds of rock fail or fracture at the proportional limit P.L. (Fig. 2.4) of elasticity or somewhat beyond it very near to the yield stress. Such materials are referred to as brittle. Rocks are characterised as failing in brittle fracture if they fail with no previous plastic deformation. Rocks are referred to as ductile if they deform plastically before failure. After previous plastic deformation, the rock fails by ductile rupture. For ductile materials, there is no brittle fracture. Under normal temperature and pressure, rocks usually tend to exhibit a brittle kind of rupture of failure mechanism. The term "fracture" is used here in the sense of brittle fracture or failure; this implies a complete loss of cohesion across a surface. Because of most of the rock materials are brittle, the plasticity domain of such rocks and thus their plastic deformation and degree of plasticity are relatively very small.

No material is perfect. All materials combine in some proportion of the characteristics of elasticity, plasticity and flow. When a material deforms slowly in a continuous way, this kind of permanent deformation is known as creep, a deformation phenomenon when strain increases linearly with time. Creep, a complex response of strain to stress, is the time-dependent movement (plastic displacement) of rock under a sustained load. In other words, creep is the phenomenon of increase in strain during the course of time under constant stress. The amount of creep depends upon the stress level: at a high stress, creep accelerates, and failure is attained quickly. Creep was not considered in the numerical modelling for this thesis.

2.4 CRITERIA OF ROCK FAILURE

Fracture is the dominant mechanism of rock failure at the relatively low pressures and temperatures at shallow depths in the earth's crust. Fracturing may be defined as the processes that involve at least the momentary loss of cohesion, the ability to resist differential stress, separation into two or more parts, and the release of stored elastic strain energy (Griggs and Handin, 1960). In general there are two

basic types of fractures, namely, extension fractures and shear fractures. Extension fractures occur normal to the least principal compressive stress, σ_3, these are termed tensile fractures if σ_3 is tensile. In the shear fracture, particle motion is parallel to the fracture surface, which may be inclined from 45° to a few degrees to the direction of the maximum principal compressive stress, σ_1. Fracture criteria express relationships between stress components that will cause fracture. Some of the better-known criteria of failure that are considered to be reasonably acceptable in rock mechanics are the maximum tensile stress, Coulomb, Mohr, Griffith, Bieniawski, Hoek and Brown, and Johnston criteria. The theory and applications of these criteria are provided in Appendix A.

2.5 ROCK MASS CLASSIFICATION SYSTEM (RMR)

The basic aim of a rock mass classification system is to derive representative in-situ rock mass properties for stiffness and strength parameters for numerical modelling input. Because of the presence of fissures, cracks, joints, gaps, stratification, discontinuities, planes of weakness, and layer anisotropy, compressibility of in-situ rock, the strength properties of an intact laboratory rock specimen is considerably greater than that of properties of in-situ rocks. In other words, the strength of the intact laboratory rock specimen should be reduced by some factor. It is not part of scope of this thesis to describe how laboratory rock properties are adjusted to the corresponding in-situ rock properties. However the reduction factor found in the paper by Mohammad et al. (1997) and was used as a benchmark for this thesis. In the simplest terms, maximum axial compressive strength was reduced by around a quarter and stiffness (Young's Modulus) by around a half.

2.6 VALLEY BULGING

River valleys are formed by the complex interaction of various processes of weathering and erosion. According to Fell et al. (1992), the mean horizontal

stresses, in many geological environments worldwide, were found in general, significantly greater than vertical stresses at depth less than 500 meters and that at greater depths the stresses tended to equalise. The author believed that the high measured stresses in most situations resulted from strain energy, which had been locked into the rocks during their formation. It is assumed that as the vertical load on highly stressed rock is slowly lowered by erosion (Fig. 2.5), vertical stresses are relieved progressively by upward expansion. However, because the rock remains confined laterally, the horizontal stresses decrease in accordance with the Poisson's ratio. This results in the near surface imbalance.

Fell et al. (1992) noted that gentle anticlines, in some cases with associated thrust faults as shown in Fig. 2.6 have been recorded across many river valleys cutting through near-horizontal sedimentary rocks of moderate to low strength. The phenomenon is referred to as 'valley bulging'. Most of the features shown in Fig. 2.6 have clearly developed as a result of buckling and shear failure under high horizontal compressive stresses. The stresses were concentrated beneath the valley floor as a result of load transfer as the excavation of the valley removed lateral support from the rock layers above the floor, and vertical load from the rock beneath the floor. The steeply-dipping joints next to the cliff faces probably opened up due to expansion of the rock layers under the influence of horizontal stresses both across and parallel to the valley.

The work by Hutchinson (1987) describes the various rockslide mechanisms that were identified in what is known as the Vaiont slide. These mechanisms included buckling, wedging and shear on low angle discontinuities on the surface of a slope, all of which can equally occur as the base of a valley fails under the action of compressive stress. A diagram indicating each of these mechanisms was provided by the author and has been reproduced in Fig. 2.7, but redrawn in a horizontal configuration to represent the base of a valley.

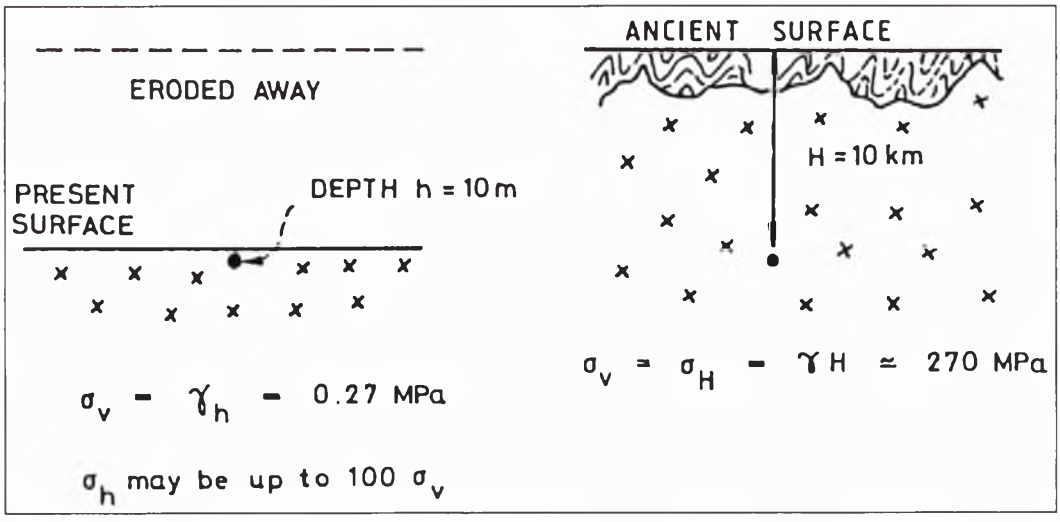

Figure 2.5 Probable cause of high horizontal stresses at shallow depths.

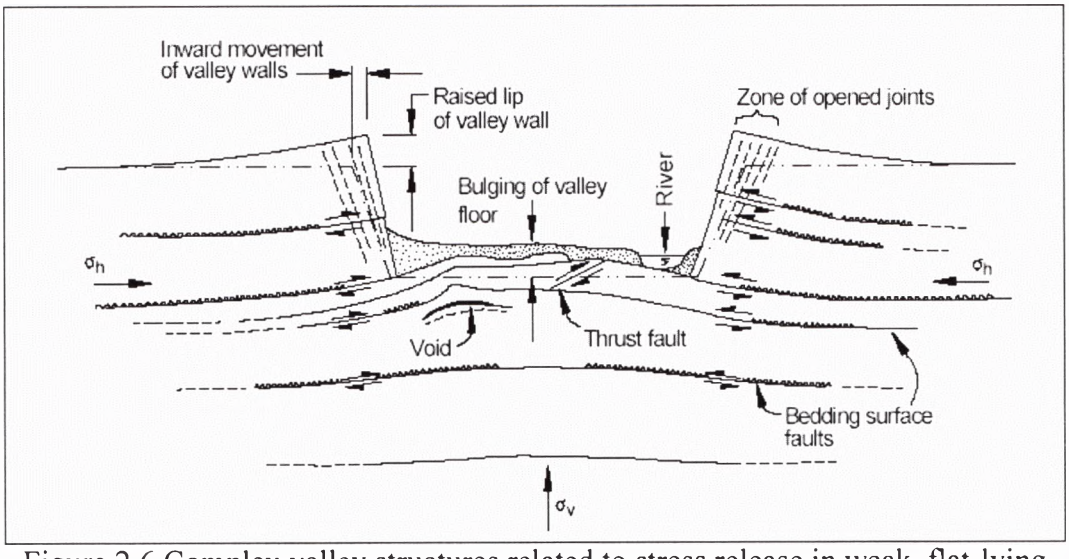

Figure 2.6 Complex valley structures related to stress release in weak, flat-lying rocks (based on Patton and Hendren, 1972)

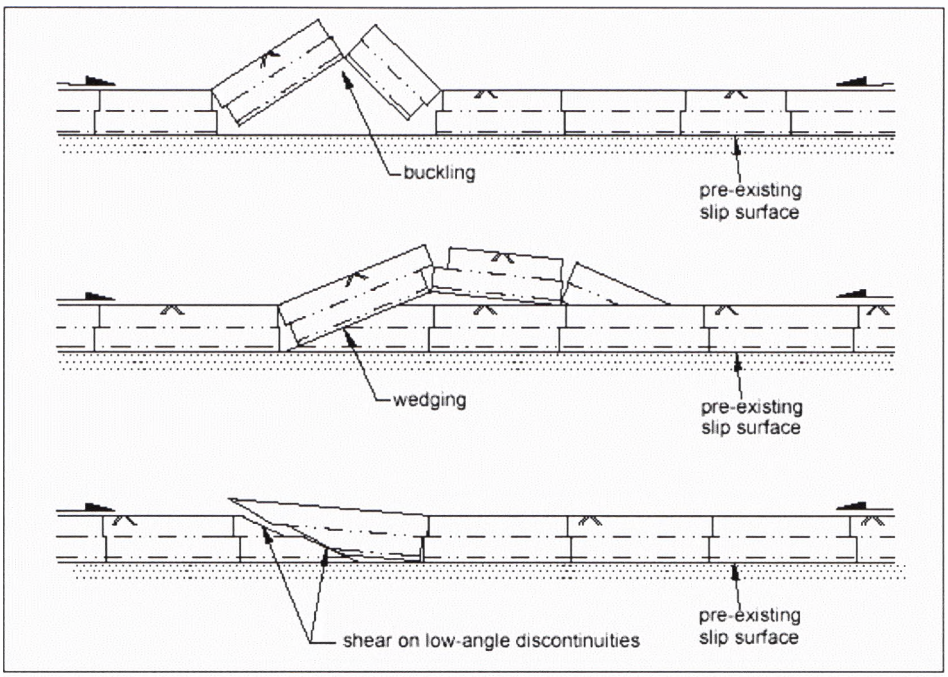

(a) Buckling, (b) Wedging, (c) Shear on Low Discontinuities

Figure 2.7 Possible failure mechanisms in the bottom of a valley (based on Hutchison, 1987)

CHAPTER 3
FLAC THEORY AND BACKGROUND

3.1 INTRODUCTION

FLAC V4 was used for the numerical modelling of the key processes associated with strata deformation. FLAC stands for Fast Lagrangian Analysis of Continua. FLAC was chosen as the most appropriate modelling program due to its ability to efficiently handle the non-linear effects of a yielding state via various plastic constitutive laws in large strain, along with the ability to create complex grid geometries with ease using the new GIIC (Graphical Interface for Itasca Codes). In addition, FLAC contains many desirable features that include:

- Interface elements to simulate distinct planes along which slip and/or separation can occur,
- Ground water (fully coupled) models with automatic phreatic surface calculation,
- Extensive facility for generating plots of virtually any problem variable, and
- Built-in programming language FISH (short for FLACish), which allows the user to write their own functions to tailor analyses to suit specific needs.

In this chapter, an explanation of the terms and concepts are described, including theory and implementation of constitutive models used in this thesis. In addition, a general guide to the principles of developing a numerical model is discussed.

3.2 FINITE DIFFERENCE METHOD

FLAC is described as an explicit, finite difference program that performs a Lagrangian analysis. The finite difference method is one of the oldest numerical

techniques used for the solution of sets of differential equations, given initial values and/or boundary conditions. In the finite difference method, every derivative in the set of governing equations is replaced directly by an algebraic expression written in terms of the field variables such as stress or displacement at discrete points in space; these variables are undefined within elements. FLAC uses an explicit, time marching method to solve the algebraic equations.

Even though FLAC wants to find a static solution to a problem, the dynamic equations of motion are included in the formulation. One reason for doing this is to ensure that the numerical scheme is stable when the physical system being modelled is unstable. With non-linear materials, there is always the possibility of physical instability, for instance, the sudden collapse of a pillar. The general calculation sequence embodied in FLAC is illustrated in Fig. 3.1. This procedure first invokes the equations of motion to derive new velocities and displacements from stresses and forces. Then strain rates are derived from velocities, and new stresses from strain rates.

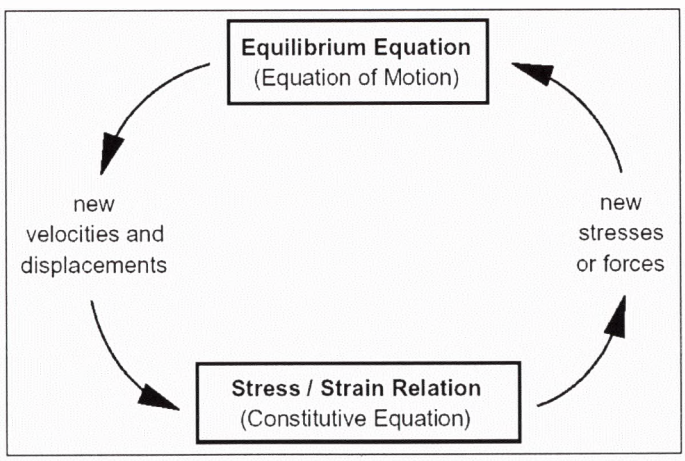

Figure 3.1 Basic explicit calculation cycle (Itasca, 2001c)

It takes one time step for every cycle around the loop. The important thing to realize is that each box in Fig. 3.1 updates all of its grid variables from known values that remain fixed while control is within the box. For example, the lower

box takes the set of velocities already calculated and, for each element, computes new stresses. The velocities are assumed to be frozen for the operation of the box – i.e., the newly calculated stresses do not affect the velocities. Since one loop of the cycle occupies one time step, neighbouring elements really cannot affect one another during the period of calculation.

Finally, since it is not required to form a global stiffness matrix, it is a trivial matter to update coordinates at each time step in large-strain mode. The incremental displacements are added to the coordinates so that the grid moves and deforms with the material it represents. This is termed a Lagrangian formulation. The constitutive formulation at each step is a small-strain one, but is equivalent to a large-strain formulation over many steps.

3.3 GENERATION OF GRID

The grid defines the geometry of the problem. The physical shape of a FLAC grid need not be rectangular or square. The rows and columns can be distorted so that the boundary fits some given shape; holes can be made in the grid; separate grids can be stuck together to create more complicated bodies. Furthermore, the zones can vary in size across a grid within a practical ratio. With any numerical method, the accuracy of the results depends on the grid used to represent the physical system. In general, finer meshes (more zones per unit length) lead to more-accurate results. Furthermore, the aspect ratio (ratio of height to width of a zone) also affects accuracy. It should be kept in mind that the greatest accuracy is obtained for a model with equal, square zones. If the model must contain different zone sizes, then a gradual variation in size should be used for maximum accuracy. As a general rule, the aspect ratio of a zone should be kept as close to unity as possible: anything above 5:1 (Itasca, 2001c) is potentially inaccurate. However, high aspect-ratio zones are quite acceptable in regions of low strain gradient, such as remote boundary regions.

The primary dilemma of generating grids is the difficulty of satisfying both the requirement to minimise boundary influence, and to provide sufficient zoning in the region of interest. It is not advisable to have large jumps in zone size between different regions of the grid. In fact, for reasonable accuracy, the ratio between areas of adjacent zones should not exceed roughly 4:1 (Itasca, 2001c). It is better to use a smooth variation and grade the zoning from a fine mesh in the region of interest to a coarse mesh near the boundaries.

3.4 CONSTITUTIVE MODELS

The constitutive behaviour and associated material properties dictate the type of response the model will display upon disturbance (e.g., deformation response due to excavation). There are ten basic constitutive models in FLAC V4 arranged into null, elastic, and plastic model groups as:

- Null model group:
  1) Null model:

     A null material model is used to represent material that is removed or excavated.

- Elastic model group:
  2) Elastic, isotropic model:

     This model provides the simplest representation of material behaviour. This model is valid for homogeneous, isotropic, continuous materials that exhibit linear stress-strain behaviour with no hysteresis on unloading.
  3) Elastic, transversely isotropic model:

     This model gives the ability to simulate layered elastic media in which there are distinctly different elastic moduli in directions normal and parallel to the layers.

- Plastic model group:
  4) Drucker-Prager model:

This model may be useful to model soft clays with low friction angles. However this model is not generally recommended for application to geologic materials.

5) Mohr-Coulomb model:

   This model is the conventional model used to represent shear failure in soils and rocks.

6) Ubiquitous-Joint model:

   This model is an anisotropic plasticity model that includes weak planes of specific orientation embedded in a Mohr-Coulomb solid.

7) Strain-hardening/softening model:

   This model allows representation of non-linear material softening and hardening behaviour based on prescribed variations of the Mohr-Coulomb model properties (cohesion, friction, dilation, tensile strength) as functions of the deviatoric plastic strain.

8) Bilinear strain-hardening/softening ubiquitous-joint model:

   This model allows representation of material softening and hardening behaviour for the matrix and the weak plane based on prescribed variations of the ubiquitous-joint model properties (cohesion, friction, dilation, tensile strength) as functions of deviatoric and tensile plastic strain. The variation of material strength properties with mean stress can also be taken into account by using the bilinear option.

9) Double-yield model:

   This model is intended to represent materials in which there may be significant irreversible compaction in addition to shear yielding, such as hydraulically placed backfill or lightly cemented granular material.

10) Modified Cam-clay model:

    This model may be used to represent materials when the influence of volume change on bulk property and resistance to shear need to be taken into consideration, such as soft clay.

There are also six time-dependent (creep) material models available in the creep model option for FLAC. As mentioned in Chapter 2, creep is outside the scope of this thesis, hence was not considered in the developing a numerical model.

All models are implemented using the same incremental numerical algorithm, given the former stress state and the total strain increment for the current time step, the corresponding stress increment is determined and the new stress state calculated. Note that all models operate on effective stresses only; pore pressures are used to convert total stresses to effective stresses before the constitutive model is called. The reverse process occurs after the model calculations are completed. These built-in ten basic constitutive models can be controlled via FISH code to modify the behaviour of the models. For example, in the built-in Ubiquitous-Joint (UBI) model, properties of cohesion, friction, dilation and tensile strength are assumed to remain constant after the onset of plastic yield. This is illustrated in Fig. 3.2. On the other hand, using the modified (FISH) UBI model, the

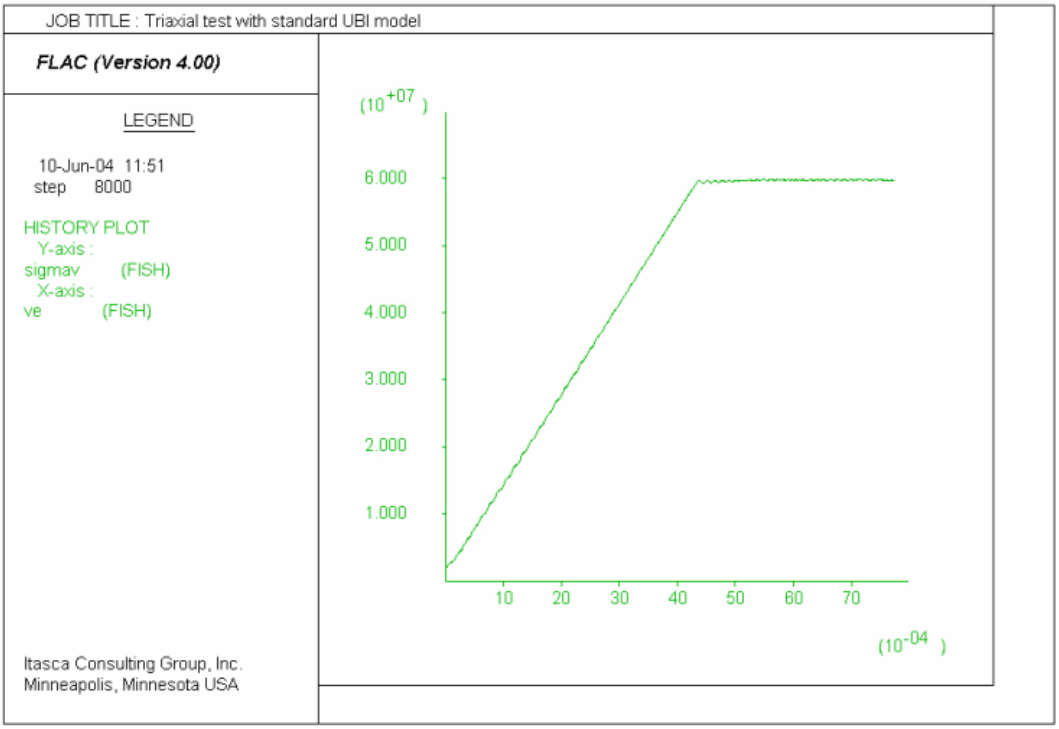

Figure 3.2 Triaxial test with standard UBI model

user can control the cohesion, friction, dilation and tensile strength once yield is detected. For example, when fracture develops within a rock, it involves loss of cohesion and this is illustrated in Fig. 3.3.

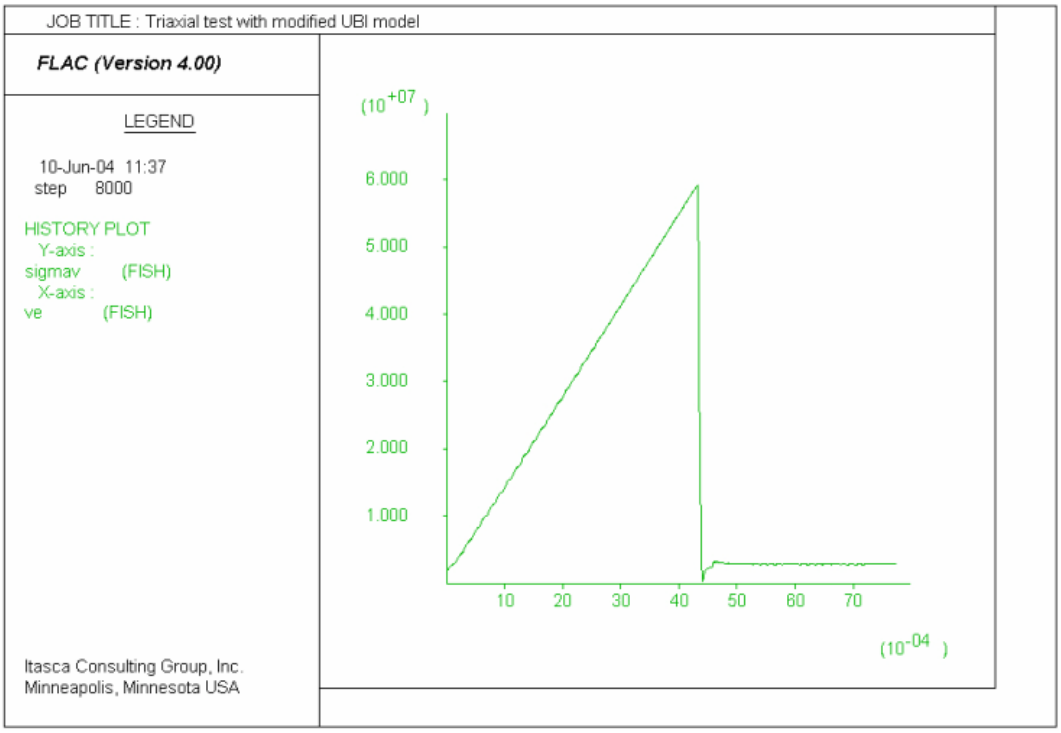

Figure 3.3 Triaxial test with modified UBI model

For this thesis, the UBI modified model had been chosen as a basic constitutive model. This model simulated the rock strata as initially behaving as an elastic material until a yield condition is detected, determined by the friction and cohesion strength properties of the individual strata horizons. The yielded strata were then modelled as a perfectly plastic medium undergoing flow.

3.4.1 Ubiquitous-Joint Modified Model

This model accounts for the presence of an orientation of weakness (weak plane) in a FLAC Mohr-Coulomb model. Yield was considered to occur in either the solid or along the weak plane, or both, depending on the stress state, the

orientation of the weak plane, and the material properties of the solid and weak plane.

In the model, stresses corresponding to the elastic guess for the step were first analysed for general failure and relevant plastic corresponding was made. The resulting stress components (labelled as σ_{ij}) were then examined for failure on the weak plane. Figure 3.4 illustrates a weak plane existing in a Mohr-Coulomb solid and the global (xy) and local (x' y') coordinate frames.

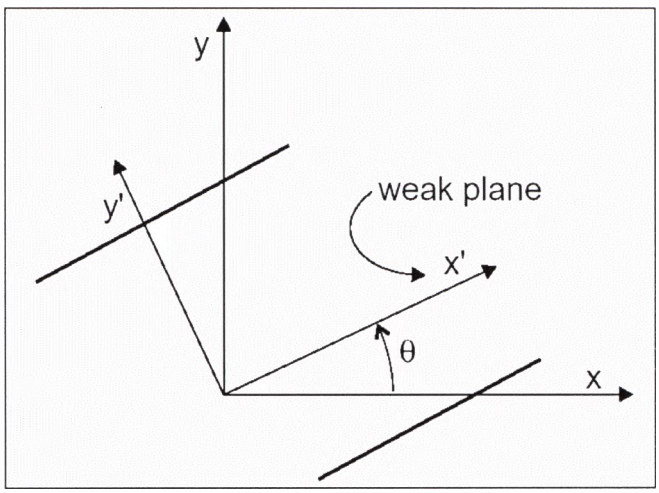

Figure 3.4 A weak plane oriented at an angle θ to the global reference frame (Itasca, 2001c)

The corresponding local stress components σ'_{22} and τ were calculated using Equation 3.1 and 3.2 (Itasca, 2001c):

$$\begin{aligned}
\sigma'_{11} &= \sigma_{11}\cos^2\theta + 2\sigma_{12}\sin\theta\cos\theta + \sigma_{22}\sin^2\theta \\
\sigma'_{22} &= \sigma_{11}\sin^2\theta - 2\sigma_{12}\sin\theta\cos\theta + \sigma_{22}\cos^2\theta \\
\sigma'_{33} &= \sigma_{33} \\
\sigma'_{12} &= -(\sigma_{11} - \sigma_{22})\sin\theta\cos\theta + \sigma_{12}(\cos^2\theta - \sin^2\theta)
\end{aligned} \qquad (3.1)$$

where,

θ = the joint angle (measured counter clockwise from the x-global axis), and

$$\tau = \left|\sigma'_{12}\right|$$
$$\gamma = \left|e'_{12}\right| \tag{3.2}$$

If corrections must be applied to the components σ_{ij} to give the new stress state for the step. In this situation we have

$$f^s = -\tau - \sigma'_{22}\tan\phi_j + c_j \tag{3.3}$$

and

$$f^t = \sigma^t_j - \sigma'_{22} \tag{3.4}$$

where,

ϕ_j = friction of the weak plane, °
c_j = cohesion of the weak plane, Pa
σ^t_j = tensile strength of the weak plane, Pa

see Fig. 3.5 for illustration of the weak-plane failure criterion.

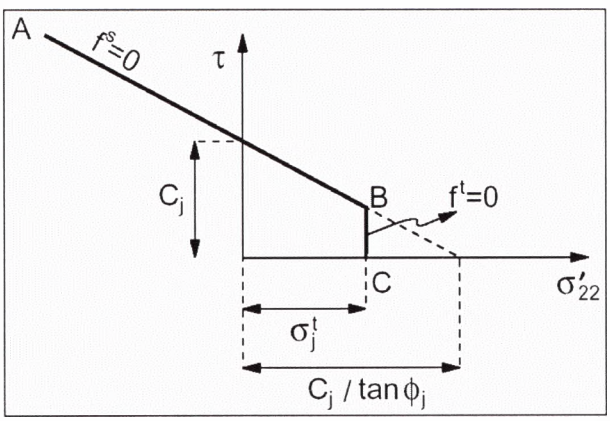

Figure 3.5 Weak-plane failure criterion in FLAC (Itasca, 2001c)

either $h(\sigma'_{22},\tau) > 0$ or $h(\sigma'_{22},\tau) \le 0$ (from Equations 3.5 and 3.6 and Figure 3.6).

$$h = \tau - \tau^p_j - \alpha^p_j(\sigma'_{22} - \sigma^t_j) \tag{3.5}$$

where,

τ^p_j and α^p_j are constants defined as

$$\tau_j^p = c_j - \tan\phi_j \alpha_j^t$$
$$\alpha_j^p = \sqrt{1+\tan\phi_j^2} - \tan\phi_j \tag{3.6}$$

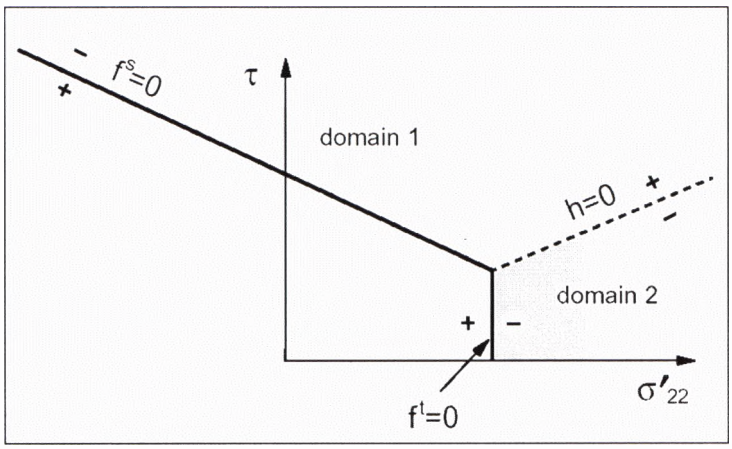

Figure 3.6 Ubiquitous-joint model: domains used in the definition of the weak-plane flow rule (Itasca, 2001c)

When ($h(\sigma_{22}^{'},\tau) > 0$), shear failure takes place on the weak plane. New stresses are evaluated by adding the corrections Equation 3.7 to σ_{ij}.

$$\begin{aligned}
\Delta\sigma_{11} &= -2\Delta\sigma_{12}^{'}(\cos\theta\sin\theta) + \Delta\sigma_{11}^{'}\cos^2\theta + \Delta\sigma_{22}^{'}\sin^2\theta \\
\Delta\sigma_{22} &= 2\Delta\sigma_{12}^{'}(\cos\theta\sin\theta) + \Delta\sigma_{11}^{'}\sin^2\theta + \Delta\sigma_{22}^{'}\cos^2\theta \\
\Delta\sigma_{33} &= \Delta\sigma_{33}^{'} \\
\Delta\sigma_{12} &= \Delta\sigma_{12}^{'}(\cos^2\theta - \sin^2\theta) + (\Delta\sigma_{11}^{'} - \Delta\sigma_{22}^{'})\sin\theta\cos\theta
\end{aligned} \tag{3.7}$$

When ($h(\sigma_{22}^{'},\tau) \le 0$), weak-plane tensile failure is declared and new stresses are calculated using the corrections to give Equation 3.8:

$$\begin{aligned}
\Delta\sigma_{11} &= (\sigma^t - \sigma_{22}^{'})(\frac{\alpha_2}{\alpha_1}\cos^2\theta + \sin^2\theta) \\
\Delta\sigma_{22} &= (\sigma^t - \sigma_{22}^{'})(\frac{\alpha_2}{\alpha_1}\sin^2\theta + \cos^2\theta) \\
\Delta\sigma_{33} &= (\sigma^t - \sigma_{22}^{'})\frac{\alpha_2}{\alpha_1} \\
\Delta\sigma_{12} &= -(\sigma^t - \sigma_{22}^{'})(1 - \frac{\alpha_2}{\alpha_1})\sin\theta\cos\theta
\end{aligned} \tag{3.8}$$

In large-strain mode, the orientation of the weak plane is adjusted to account for body rotations and hence:

$$\Delta\theta = e_{12}^{'} + \omega \tag{3.9}$$

where,

$$\begin{aligned}
e_{12}^{'} &= -(e_{11} - e_{22})\sin\theta\cos\theta + e_{12}(\cos^2\theta - \sin^2\theta) \\
\omega &= \frac{1}{2}(\dot{u}_{1,2} - \dot{u}_{2,1})
\end{aligned} \tag{3.10}$$

and $\Delta\theta$ is expressed in radians.

The default value for the weak-plane tensile strength is zero if $\phi = 0$ and $\sigma_{j,\max}^t$ i.e.

$$\sigma_{j,\max}^t = \frac{c_j}{\tan\phi_j} \tag{3.11}$$

The default value is also retained in the code if the value assigned for the weak-plane tensile strength exceeds $\sigma_{j,\max}^t$. If the computed value of $\sigma_{22}^{'}$ exceeds $\sigma_{j,\max}^t$ in a zone, then the tensile strength is set to zero for that zone. This simulates instantaneous softening.

3.5 MODEL PROPERTIES

Once the grid generation was completed and one or more material models are assigned to all zones in the model, properties must be assigned to all the zones. As

mentioned in Chapter 3, FLAC has ten built-in constitutive (material) models. Each one of the models requires different model properties. For example, elastic model requires properties of density, bulk modulus and shear modulus. While Mohr-Coulomb model requires additional properties such as cohesion, tensile strength, dilation and friction angle.

Since the selected model for this thesis was the ubiquitous-joint modified model, its model properties will be discussed further. Under ubiquitous-joint modified model, its function identification in the code is named as *m_ubi*, and requires that the following parameters be specified in the FISH command (Itasca 2001a):

m_coh	cohesion, Pa
m_dil	dilation angle, °
m_fric	friction angle, °
m_g	shear modulus, Pa
m_k	bulk modulus, Pa
m_ten	tensile strength, Pa
m_jang	joint angle (measured counter clockwise from x-axis – refer to Fig. 3.4), °
m_jcoh	joint cohesion, Pa
m_jfric	joint friction angle, °
m_jten	joint tension limit, Pa

Each of above parameters is defaulted to zero if not specified. In practice the selection of material properties is often the most difficult aspect because of the high uncertainty in the material properties. It should be kept in mind when performing any analysis, that the problem will always involve a data-limited system since field data will never be known with certainty. However, with the appropriate selection of material properties based on realistic assumptions, important insight to the physical problem can still be gained.

In addition to above parameters, further parameters are required for underground flow. The properties that relate to underground flow are porosity, permeability, bulk modulus of fluid, mass density of water and saturation.

3.5.1 Porosity

Porosity is a dimensionless number defined as the ratio of void volume to total volume of an element. It is related to the void ratio by the expression:

$$n = \frac{e}{1+e} \tag{3.12}$$

where,

n = porosity

e = void ratio

The default value of porosity, if not specified, is 0.5. Porosity should be given as positive number between 0 and 1, but small values (say, less than 0.2) should be used with great caution, because the apparent stiffness of the pore fluid is proportional to $\frac{K_w}{n}$. For low values of porosity, the stiffness may become very large in comparison to the stiffness of the solid material, causing the FLAC solution to take a very long time to converge.

3.5.2 Permeability

The permeability required by FLAC is the mobility coefficient (coefficient of the pore pressure terms of Darcy's law). The relation between hydraulic conductivity, commonly used when Darcy's law is expressed in terms of head, and permeability as:

$$k = \frac{k_H}{g\rho_w} \tag{3.13}$$

where,

k = permeability, m^3sec/kg

k_H = hydraulic conductivity, m/sec

g = gravitational acceleration, m/sec^2

ρ_w = fluid mass density, kg/m^3

In reality, permeability is a tensor quantity, with a direction and two principal values. In FLAC, if the keyword *perm* is assigned with the *Property* command, then permeability is assumed to be isotropic. To specify an anisotropic permeability, the components k_{ij} should be assigned instead – with keyword *k11*, *k22* and *k12*, which correspond to the components k_{xx}, k_{yy} and k_{xy}, respectively.

3.5.3 Bulk Modulus of Fluid

The bulk modulus is defined in the following expression (Itasca 2001b):

$$K_w = -\frac{\Delta P}{\Delta V / V} \tag{3.14}$$

where,

K_w = bulk modulus, Pa

ΔP = change in pressure for a volumetric strain of $\Delta V / V$

The compressibility of a fluid is the reciprocal of bulk modulus:

$$K_w = \frac{1}{C_w} \tag{3.15}$$

where,

C_w = compressibility of a fluid, 1/Pa, i.e. m^2/N

3.5.4 Density of Water

The given value of density is used solely to compute the gravitational forces on elements of fluid in conjunction with the value of gravity. If FLAC is configured

for groundwater, then the dry density of the solid material must be used. FLAC will compute the saturated density of each element, using the known density of water, the porosity and the saturation.

3.5.5 Saturation

Saturation is defined as the ratio of pore volume occupied by fluid to total pore volume. In FLAC's formulation, pore pressure is set to zero if the saturation at any point is less than exactly 1. The effect of dissolved and trapped air may be allowed by reducing the local fluid modulus, while keeping the saturation at 1 (i.e. assume that there is an equivalent fluid present throughout the pore space). Although no pore pressures are present in a partially saturated region, the trapped fluid still has weight (body force act), and the fluid moves under the action of gravity. The user may give the initial saturation, but it is also updated during FLAC's calculation cycle, as necessary, to preserve the mass balance. Saturation may be declared to be fixed at any grid point; for example, water may enter and leave at a fixed saturation grid point, even if the pressure is zero.

3.6 BOUNDARY CONDITIONS

The boundary conditions in a numerical model consist of the values of field variables (e.g., stress, displacement) that are prescribed at the boundary of the numerical grid. Boundaries are of two categories: real and artificial. Real boundaries exist in the physical object being modelled – e.g., a tunnel surface or the ground surface. Artificial boundaries do not exist in reality, but they must be introduced in order to enclose the number of zones chosen to represent a region of infinite extent. It must be remembered that artificial boundaries are placed sufficiently far away form the area of interest to assume that the behaviour in that area is not greatly affected.

3.7 EFFECT OF WATER

FLAC models the flow of fluid (e.g., groundwater) through a permeable solid, such as rock. The flow modelling may be done by itself; independent of the usual mechanical calculation of FLAC, or it may be done in parallel with the mechanical modelling, so as to capture the effects of fluid/solid interaction. Geologic materials appear to be weaker if a pressurised fluid, such as water, occupies their pore space. This effect is represented in FLAC by the incorporation of an effective stress that accounts for pore pressure in a zone. The pore pressures in FLAC are taken to be positive in compression; thus the effective stress σ' is related to the total stress σ and pore pressure p by (Itasca 2001d):

$$\sigma' = \sigma + p \tag{3.16}$$

where,

σ' = effective stress, Pa

σ = total stress, Pa

p = pore pressure, Pa

The basic flow model handles both fully saturated flow and flow in which a phreatic surface develops. In this case, pore pressures are zero above the phreatic surface, and the air phase is considered as passive.

In case where groundwater exists, establishing vertical stresses in the model can be quite confusing. In order to establish initial stress equilibrium in a groundwater problem, the following points should be noted:

- Saturation should be zero above the water table, and 1 below it,
- The pore pressure should be zero above the water table, and have a gradient of $\rho_w g$ below it,
- The gradient of the total vertical stress should be:

$$g \times (\rho + s \times n \times \rho_w) \tag{3.17}$$

where,

g = gravity, m/sec^2, assumed as either 9.8 or 10 m/sec^2
ρ = dry density of solid, kg/m^3
ρ_w = density of water, kg/m^3
s = saturation, dimensionless
n = porosity, dimensionless

- If k_{0x} is the ratio of effective σ_{xx} to effective σ_{yy}, then the total σ_{xx} should be:

$$\sigma_{xx} = k_{0x}(\sigma_{yy} + pp) - pp \tag{3.18}$$

where,

pp = pore pressure, Pa

This calculation can be carried out either manually or by using FISH codes. When writing FISH codes for this situation, a user must understand how to solve such problems manually. For this reason, the manual procedures of determining vertical and horizontal stresses are illustrated in Example 3.1:

Example 3.1

Consider an impermeable box of height 10 meters and width of 5 meters which contains a solid, elastic material, fixed at the sides and base. Assume that only the bottom 5 meters is fully saturated. The dry density of the solid is 2000 kg/m^3, and its porosity is 0.5. This problem is illustrated in Fig. 3.7.

Step 1 Understand the given data:

- Dimension of each zone is 1 m × 1 m.
- Saturation (s) is 0 at Point A and above, and 0.5 at Point B.
  Saturation is 1 at Point C and below.
- Dry density (ρ_{dry}) = 2000 kg/m^3 and water density (ρ_{wet}) = 1000 kg/m^3.
- Porosity (n) = 0.5.

- Remember that compressive stresses are negative, and pore pressure is positive in FLAC
- Assumed gravity as 10 m/sec^2.

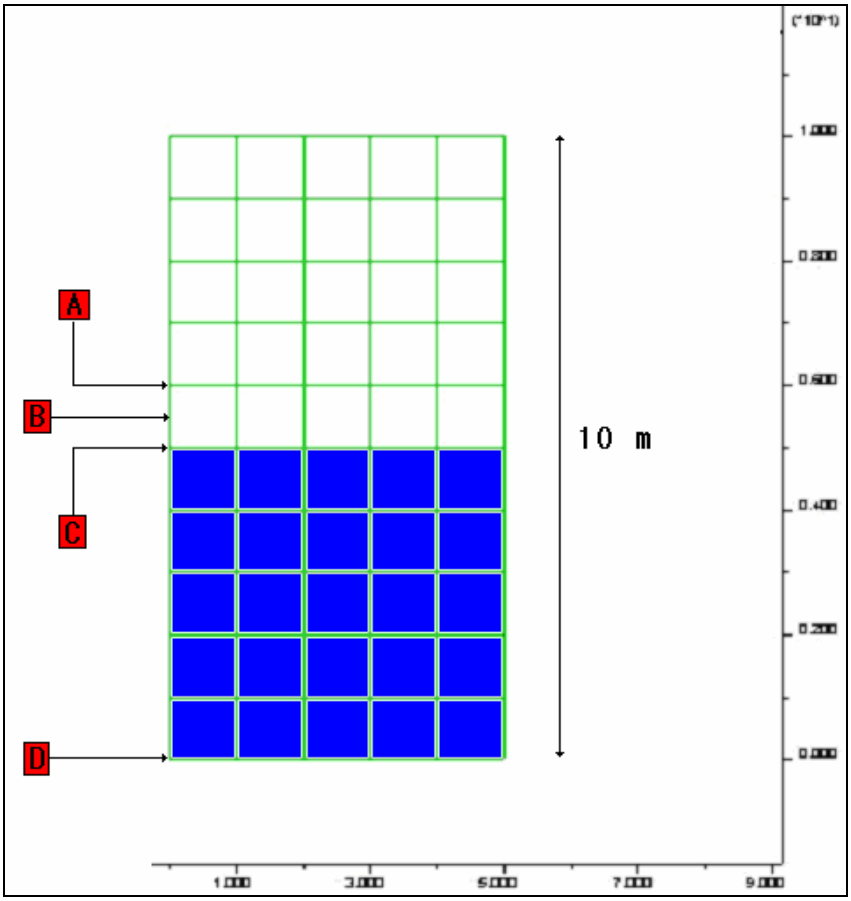

Figure 3.7 Establish an initial stress equilibrium in a groundwater example problem

Step 2 Calculate the vertical stresses:

- At Point A:

  Due to the overburden of 4 m, vertical stress using Equation 3.17:

$$\sigma_{yy\ (at\ A)} = 4\ m \times 10\ m/sec^2 \times (2000\ kg/m^3 + 0\ m \times 0.5 \times 1000\ kg/m^3) = -80\ kPa$$

- At Point B:

Average saturation is 0.5. Hence additional vertical stress is:

$$\sigma_{yy\ (additional)} = 0.5\ \text{m} \times 10\ \text{m/sec}^2 \times (2000\ \text{kg/m}^3 + 0.5\text{m} \times 0.5 \times 1000\ \text{kg/m}^3)$$
$$= -11.25\ \text{kPa}$$
$$\sigma_{yy\ (at\ B)} = -80\ \text{kPa} + -11.25\ \text{kPa} = -91.25\ \text{kPa}$$

- At Point C:

  Average saturation is 0.5. Hence additional vertical stress is:

$$\sigma_{yy\ (additional)} = -11.25\ \text{kPa}$$
$$\sigma_{yy\ (at\ C)} = -91.25\ \text{kPa} + -11.25\ \text{kPa} = -102.50\ \text{kPa}$$

- At Point D:

  Saturation is 1. Hence additional vertical stress is:

$$\sigma_{yy\ (additional)} = 5\ \text{m} \times 10\ \text{m/sec}^2 \times (2000\ \text{kg/m}^3 + 1\ \text{m} \times 0.5 \times 1000\ \text{kg/m}^3)$$
$$= -125.0\ \text{kPa}$$
$$\sigma_{yy\ (at\ D)} = -102.50\ \text{kPa} + -125.0\ \text{kPa} = -227.50\ \text{kPa}$$

Step 3 Calculate the pore pressures:

- Pore Pressure at Point D is:

$$pp = 1000\ \text{kg/m}^3 \times 10\ \text{m/sec}^2 \times 5\ \text{m}$$
$$= 50.0\ \text{kPa}$$

Step 4 Calculate the horizontal stress:

- Using Equation 3.18, and assume k_{0x} is 2, horizontal stress at Point D is:

$$\sigma_{xx} = 2 \times (-227.50\ \text{kPa} + 50\ \text{kPa}) - 50\ \text{kPa}$$
$$= -405.0\ \text{kPa}$$

Example 3.1 illustrates the procedure of calculating vertical and horizontal stresses when underground water is present and it shows that the process can be very complicated. The process becomes much more complicated if more than one material layer involved in the model. For this reason, FISH code should be used to perform the necessary computations.

3.8 EQUILIBRIUM STATE

Each grid point in the model is surrounded by up to four zones that contribute forces to the grid point. At equilibrium – or steady plastic flow – the algebraic sum of these is almost zero (i.e., the forces acting on one side of the grid point nearly balance those acting on the other). During time stepping, the maximum unbalanced force is determined for the whole grid. The unbalanced force is important in assessing the state of the model, but its magnitude must be compared with the magnitude of typical forces acting in the grid; in other words, it is necessary to know what constitutes a small force. The ratio of maximum unbalanced force to the representative internal force will never decrease to zero; however, a value of 0.01 or 0.001 may be acceptable as denoting equilibrium, depending on the degree of precision required. The largest ratio of maximum unbalanced force to average applied force amongst all of the grid points is called the equilibrium ratio. By default in FLAC, the equilibrium state is considered to be achieved when the equilibrium ratio in the model drops below the value of 0.001. The default ratio limit can be changed by the user, depending on the degree of precision required. In this thesis, the equilibrium ratio of 0.00001 (i.e., 1×10^{-5}) was used.

The maximum unbalanced force can be plotted against stepping to display the equilibrium state as shown in Fig. 3.8, which shows that the initial maximum unbalanced force is about 5×10^5 N and after 14466 steps, this force has practically approached zero.

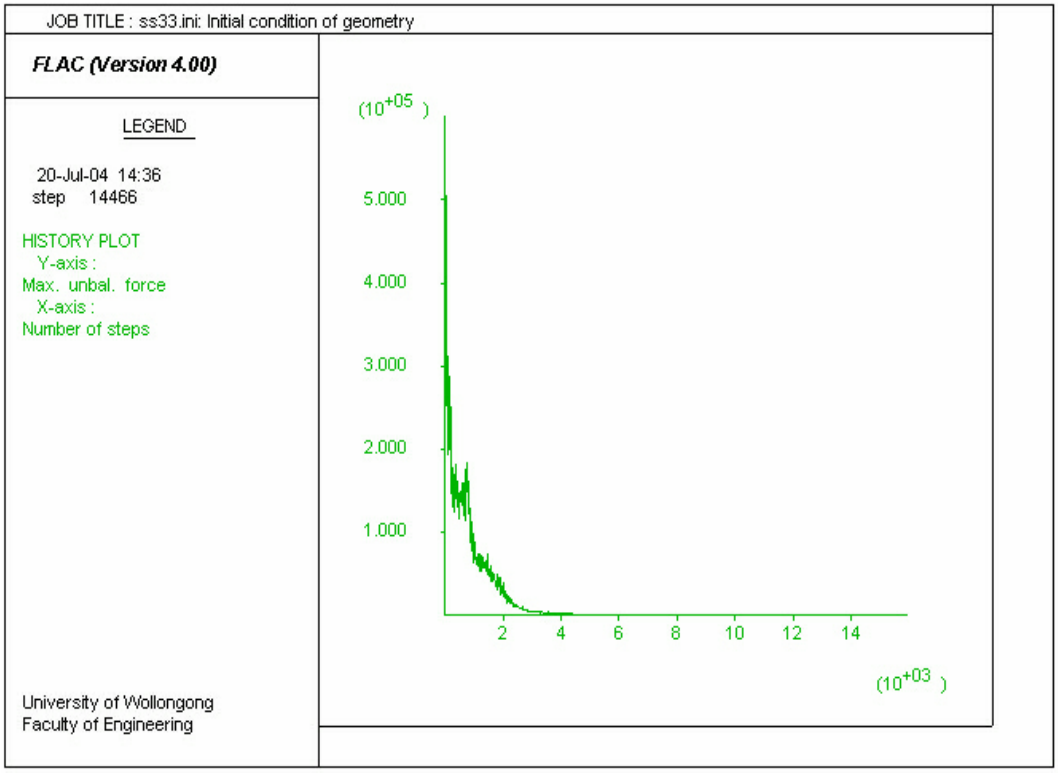

Figure 3.8 Maximum unbalanced force history in FLAC

CHAPTER 4
FLAC MODELLING APPROACH

4.1 INTRODUCTION

In this chapter, the procedure used to develop FLAC numerical simulation model is described. A number of fundamental components of a problem must be examined including:

- A finite difference grid;
- Constitutive behaviour and material properties; and
- Boundary and initial conditions.

The grid defines the geometry of the study area. The constitutive behaviour and associated material properties dictate response of the model when disturbed (e.g., deformation response due to lateral movement). Boundary and initial conditions define the in-situ state. After defining these conditions, the initial equilibrium state of the model is calculated. The model is then subjected to external loading (e.g., apply lateral displacement or change loading conditions), and the resulting response of the model was evaluated. The general modelling procedure used in this thesis is illustrated in Appendix B.

4.2 GEOMETRY OF MODEL

The geometry of the model was developed based on the field site WRS 1. There is an on-going survey measurement program for ground movements at WRS 1 by the Metropolitan Colliery. The survey line, that traverses the WRS 1 site is known as Line 3 (or L3), see Fig. 4.1. This survey data had been used for generating the surface topography of the model. The survey data used in this thesis was measured on July 22nd 2002, as summarised in Table 4.1.

Figure 4.1 Location of Survey Line 3 (Mills, 2002)

Table 4.1 Metropolitan Colliery Subsidence Coordinates for Line 3 (July 2002) using MGA system.

Line	Peg Number	Northing	Easting	RL
3	1025	6212903	309300	238
3	1026	6212899	309314	234
3	1027	6212896	309327	231
3	1028	6212893	309342	230
3	1029	6212891	309352	228
3	1030	6212887	309362	226
3	1031	6212885	309373	226
3	1032	6212886	309392	226
3	1033	6212886	309401	228
3	1034	6212886	309409	230
3	1035	6212884	309421	235

The survey Line 3 extends approximately 120 meters across the WRS 1 site. However, to obtain a representation of the valley in which WRS 1 is located, the survey Line 3 was extended to the corresponding topographic peaks, and the coordinates noted. A topographic map of the Appin region from the Central Mapping Authority of NSW was used to extend the survey Line 3 and obtain the coordinates.

The subsidence coordinates in Table 4.1 were measured using the Map Grid Australia (MGA) system. However the Central Mapping Authority of NSW utilises the Integrated Survey Grid system (ISG). A conversion was required to transform the surveyed coordinates of Line 3 to the ISG system to enable the plotting and extension of Line 3. Using a software package called Geodetic Transformations (Geoscience Australia), it was found that the conversion factor for changing coordinates from MGA to ISG were –103E and –185N. The survey coordinates using the ISG system are summarised in Table 4.2.

Table 4.2 Metropolitan Colliery Subsidence Coordinates for Line 3 (July 2002) using ISG system

Line	Peg Number	Northing	Easting	RL
3	1025	6212718	309197	238
3	1026	6212714	309211	234
3	1027	6212711	309224	231
3	1028	6212708	309239	230
3	1029	6212706	309249	228
3	1030	6212702	309259	226
3	***1031***	***6212700***	***309270***	***226***
3	1032	6212701	309289	226
3	1033	6212701	309298	228
3	1034	6212701	309306	230
3	1035	6212699	309318	235

It was noted that peg 1031 is located in close proximity of WRS 1. Using peg 1031 as the datum line (RL = 0), the new reduced levels of the other pegs were then calculated. In addition, only Easting and RL values were used in developing the geometry, since all numerical simulations were performed based on two-dimensions. Furthermore, Easting coordinates were reduced by a factor of 300,000 to simplify the coordinate system. In other words, the Easting coordinate for peg 1031 in FLAC was 9270 E. The adjusted survey coordinates are summarized in Table 4.3.

Table 4.3 Surface topography in FLAC, coordinates of Line 3

Line	Peg Number	Easting	RL
3	1025	9197	12
3	1026	9211	8
3	1027	9224	5
3	1028	9239	4
3	1029	9249	2
3	1030	9259	0
3	1031	9270	0
3	1032	9289	0
3	1033	9298	2
3	1034	9306	4
3	1035	9318	9

Table 4.4 Coordinates of surface topography (extended line)

Line	Peg Number	Easting	RL
New	New	8840	84
New	New	8870	74
New	New	8910	64
New	New	8930	54
New	New	8960	44
New	New	9000	34
New	New	9050	24
New	New	9180	14
3	1025	9197	12
3	1026	9211	8
3	1027	9224	5
3	1028	9239	4
3	1029	9249	2
3	1030	9259	0
3	1031	9270	0
3	1032	9289	0
3	1033	9298	2
3	1034	9306	4
3	1035	9318	9
New	New	9330	14
New	New	9350	24
New	New	9385	34
New	New	9410	44
New	New	9440	54
New	New	9480	64
New	New	9520	74

Using the surface topography coordinates in Table 4.4, FLAC generated the following geometry, Fig. 4.2.

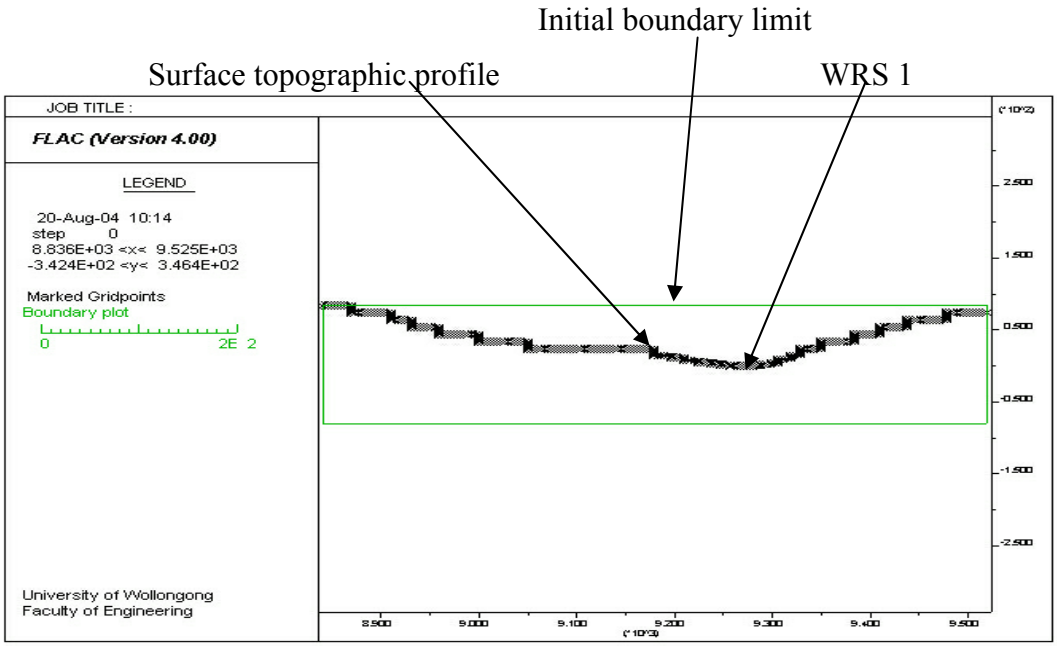

Figure 4.2 Preliminary Geometry of Model

Once the region above the surface topographic profile was excavated, the geometry that represents the physical site was generated (Fig. 4.3). This geometry of the area was then scaled down to focus on the immediate region around WRS 1. The final model geometry for the study is illustrated in Fig. 4.4.

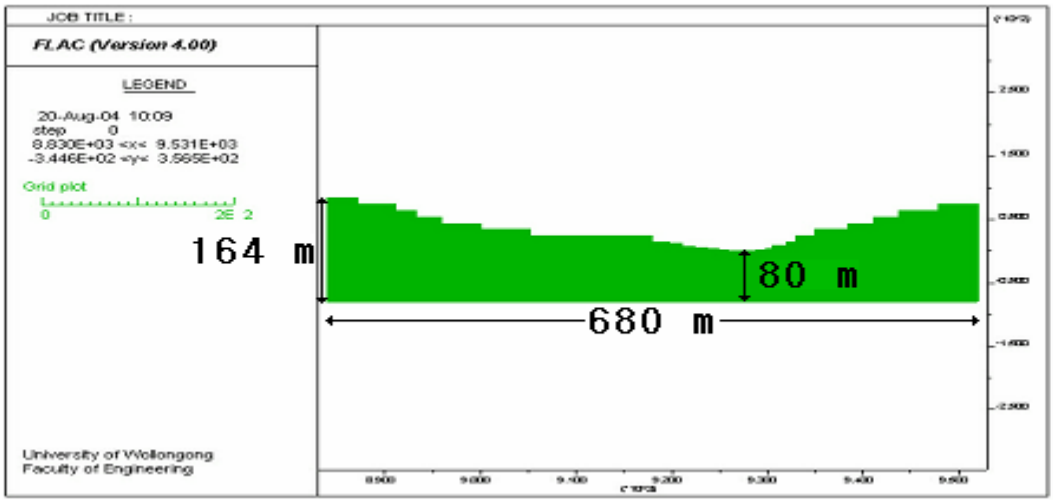

Figure 4.3 Secondary geometry of model

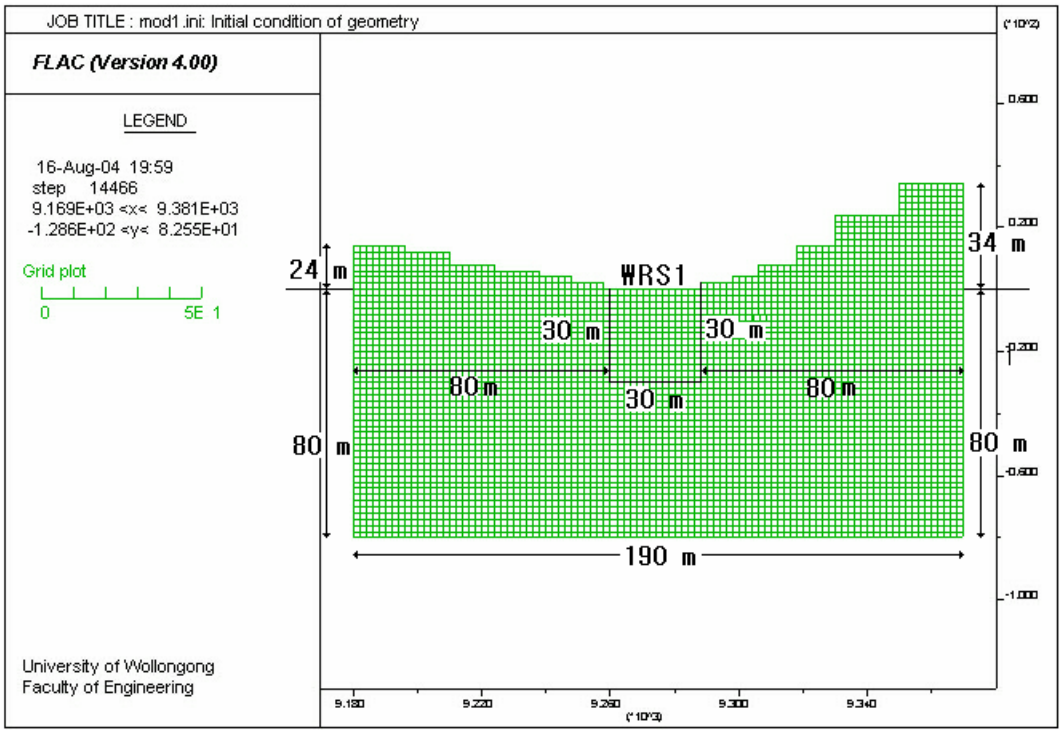

Figure 4.4 Final geometry of model

There are a number of points to be noted regarding to Fig. 4.4.

- Relatively smaller geometry than Fig. 4.3.
- The highest point on the model is 34 meters (right hand side of model).
- The depth is 80 meters below the bottom of WRS 1.
- The centre of WRS 1 is 95 meters from either side of the artificial boundary.
- Area of interest is 30 meters below WRS 1 and 15 meters on either side of WRS 1. Fine mesh density had been used in this area to increase the accuracy of numerical modelling results.
- Dimensions of the model will remain constant while different mesh densities are employed.

An example of FLAC coding for generating the grid is provided below:

```
grid 190,114

gen 9180,-80  9180,-30  9260,-30  9260,-80  i=1,81    j=1,51
gen 9180,-30  9180,0    9260,0    9260,-30  i=1,81    j=51,81
gen 9180,0    9180,34   9260,34   9260,0    i=1,81    j=81,115
gen 9260,-80  9260,-30  9290,-30  9290,-80  i=81,111  j=1,51
gen 9260,-30  9260,0    9290,0    9290,-30  i=81,111  j=51,81
gen 9260,0    9260,34   9290,34   9290,0    i=81,111  j=81,115
gen 9290,-80  9290,-30  9370,-30  9370,-80  i=111,191 j=1,51
gen 9290,-30  9290,0    9370,0    9370,-30  i=111,191 j=51,81
gen 9290,0    9290,34   9370,34   9370,0    i=111,191 j=81,115
```

Note that the entire FLAC coding used is provided in Appendix C.

4.3 INITIAL CONDITIONS FOR MODEL

After generating the model grids, the necessary input parameters to the model was assigned to study the behaviour of the model and the procedure is explained below.

4.3.1 Constitutive Model

The UBI modified constitutive model was used as a basis for model development. An example of FLAC coding for specifying a constitutive model is provided below:

```
call ubi.fis
model m_ubi
```

Due to the extensive length of the FISH version of the UBI joint model, the coding is not included here. However, the full coding is provided in Appendix D.

4.3.2 Strata Properties

Strata properties used were provided by SCT Pty Ltd. The summary of strata properties is provided in Table 4.5.

Table 4.5 Summary of strength and stiffness properties from vertical hole WRS 1/2

Sample	Material	Depth	Young's modulus	Poisson's ratio	Bulk modulus	Shear modulus	Density	sigma 1	sigma 3	Cohesion	Friction angle	Tensile strength
ID	description	m	E, GPa	v	K, GPa	G, GPa	kg/m^3	MPa	MPa	MPa	o	MPa
033-1	Sandstone	0 ~ 2	13.0	0.21	7.5	5.4	2389	57.9	0.5	12	44	10.2
033-2	Sandstone	2 ~ 2.12	13.0	0.21	7.5	5.4	2383	60.2	0.5	11	47	8.7
033-3	Sandstone	2.12 ~ 3.62	7.5	0.21	4.3	3.1	2421	29.8	0.5	7	37	7.0
033-4	Sandstone	3.62 ~ 5.12	8.0	0.21	4.6	3.3	2440	34.7	0.5	8.3	36	8.5
033-5	Sandstone	5.12 ~ 8.01	11.0	0.21	6.3	4.5	2384	49.1	0.5	9.7	44	8.2
033-6	Sandstone	8.01 ~ 10.95	13.0	0.21	7.5	5.4	2422	80.8	0.5	15	47	11.8
033-7	Siltstone	10.95 ~ 15.2	5.4	0.21	3.1	2.2	2686	40.1	0.5	11	32	12.2
033-8	Sandstone	15.2 ~ 18.5	12.0	0.21	6.9	5.0	2414	57.8	0.5	10	49	7.5
033-9	Sandstone cg	18.5 ~ 21.7	11.0	0.21	6.3	4.5	2416	48.8	0.5	8.7	49	6.5
033-10	Conglomerate	21.7 ~ 26.6	11.0	0.21	6.3	4.5	2395	31.0	0.5	5.9	45	4.9
033-11	Sandstone fg	26.6 ~ 27.3	6.1	0.21	3.5	2.5	2657	38.7	0.5	8.3	41	7.6

Bulk and shear moduli were calculated using Equations 4.1 and 4.2.

$$K = \frac{E}{3(1-2\gamma)} \tag{4.1}$$

$$G = \frac{E}{2(1+\gamma)} \tag{4.2}$$

where,

K = Bulk Modulus, Pa
G = Shear Modulus, Pa
E = Young's Modulus, Pa
γ= Poisson's ratio

Tensile strengths were calculated using Equation 4.3.

$$\sigma_t = \frac{2c\cos\phi}{1+\sin\phi} \tag{4.3}$$

where,

σ_t = Tensile strength, Pa
c = Cohesion, Pa
ϕ = Internal friction angle, °

The strength and stiffness of strata in Table 4.5 are laboratory values. These values were reduced prior to assignment in the numerical model. Table 4.6, Table 4.7 and Table 4.8 shows a summary of strength and stiffness properties with quarter, half and three-quarter reductions respectively.

Table 4.6 Quarter reductions in strength and stiffness properties

Sample	Material	Depth	Bulk modulus	Shear modulus	Density	Friction angle	Cohesion	Tensile strength
ID	description	m	K, GPa	G, GPa	kg/m^3	o	MPa	MPa
033-1	Sandstone	0 ~ 2						
033-2	Sandstone	2 ~ 2.12	5.6	4.0	2389	44	8.6	7.3
033-3	Sandstone	2.12 ~ 3.62	3.2	2.3	2421	37	5.1	5.0
033-4	Sandstone	3.62 ~ 5.12	3.4	2.5	2440	36	6.1	6.3
033-5	Sandstone	5.12 ~ 8.01	4.7	3.4	2384	44	7.2	6.1
033-6	Sandstone	8.01 ~ 10.95	5.6	4.0	2422	47	11.3	8.9
033-7	Siltstone	10.95 ~ 15.2	2.3	1.7	2686	32	7.9	8.7
033-8	Sandstone	15.2 ~ 18.5	5.2	3.7	2414	49	7.4	5.6
033-9	Sandstone cg	18.5 ~ 21.7	4.7	3.4	2416	49	6.2	4.6
033-10	Conglomerate	21.7 ~ 26.6	4.7	3.4	2395	45	4.2	3.5
033-11	Sandstone fg	26.6 ~ 27.3	2.6	1.9	2657	41	6.1	5.5

Table 4.7 Half reduction in strength and stiffness properties

Sample	Material	Depth	Bulk modulus	Shear modulus	Density	Friction angle	Cohesion	Tensile strength
ID	description	m	K, GPa	G, GPa	kg/m^3	o	MPa	MPa
033-1	Sandstone	0 ~ 2						
033-2	Sandstone	2 ~ 2.12	3.7	2.7	2389	44	5.8	4.9
033-3	Sandstone	2.12 ~ 3.62	2.2	1.5	2421	37	3.2	3.2
033-4	Sandstone	3.62 ~ 5.12	2.3	1.7	2440	36	3.9	4.0
033-5	Sandstone	5.12 ~ 8.01	3.2	2.3	2384	44	4.6	3.9
033-6	Sandstone	8.01 ~ 10.95	3.7	2.7	2422	47	7.3	5.8
033-7	Siltstone	10.95 ~ 15.2	1.6	1.1	2686	32	5.1	5.7
033-8	Sandstone	15.2 ~ 18.5	3.4	2.5	2414	49	4.7	3.5
033-9	Sandstone cg	18.5 ~ 21.7	3.2	2.3	2416	49	3.9	2.9
033-10	Conglomerate	21.7 ~ 26.6	3.2	2.3	2395	45	2.6	2.2
033-11	Sandstone fg	26.6 ~ 27.3	1.8	1.3	2657	41	3.9	3.5

Table 4.8 Three-quarter reduction in strength and stiffness properties

Sample	Material	Depth	Bulk modulus	Shear modulus	Density	Friction angle	Cohesion	Tensile strength
ID	description	m	K, GPa	G, GPa	kg/m^3	o	MPa	MPa
033-1	Sandstone	0 ~ 2						
033-2	Sandstone	2 ~ 2.12	1.9	1.3	2389	44	2.6	2.2
033-3	Sandstone	2.12 ~ 3.62	1.1	0.8	2421	37	1.4	1.3
033-4	Sandstone	3.62 ~ 5.12	1.1	0.8	2440	36	1.7	1.8
033-5	Sandstone	5.12 ~ 8.01	1.6	1.1	2384	44	2.0	1.7
033-6	Sandstone	8.01 ~ 10.95	1.9	1.3	2422	47	3.3	2.6
033-7	Siltstone	10.95 ~ 15.2	0.8	0.6	2686	32	2.3	2.6
033-8	Sandstone	15.2 ~ 18.5	1.7	1.2	2414	49	2.0	1.5
033-9	Sandstone cg	18.5 ~ 21.7	1.6	1.1	2416	49	1.6	1.2
033-10	Conglomerate	21.7 ~ 26.6	1.6	1.1	2395	45	1.0	0.8
033-11	Sandstone fg	26.6 ~ 27.3	0.9	0.6	2657	41	1.7	1.5

4.3.3 Boundary Conditions for Model

The generated grid had the left and right hand sides fixed from movement in the x-direction, and the bottom fixed in the x and y-directions. An example of FLAC coding for setting boundary conditions for model is provided below:

fix x y j=1
fix x i=1
fix x i=191

Fixed boundaries are illustrated in Fig. 4.5.

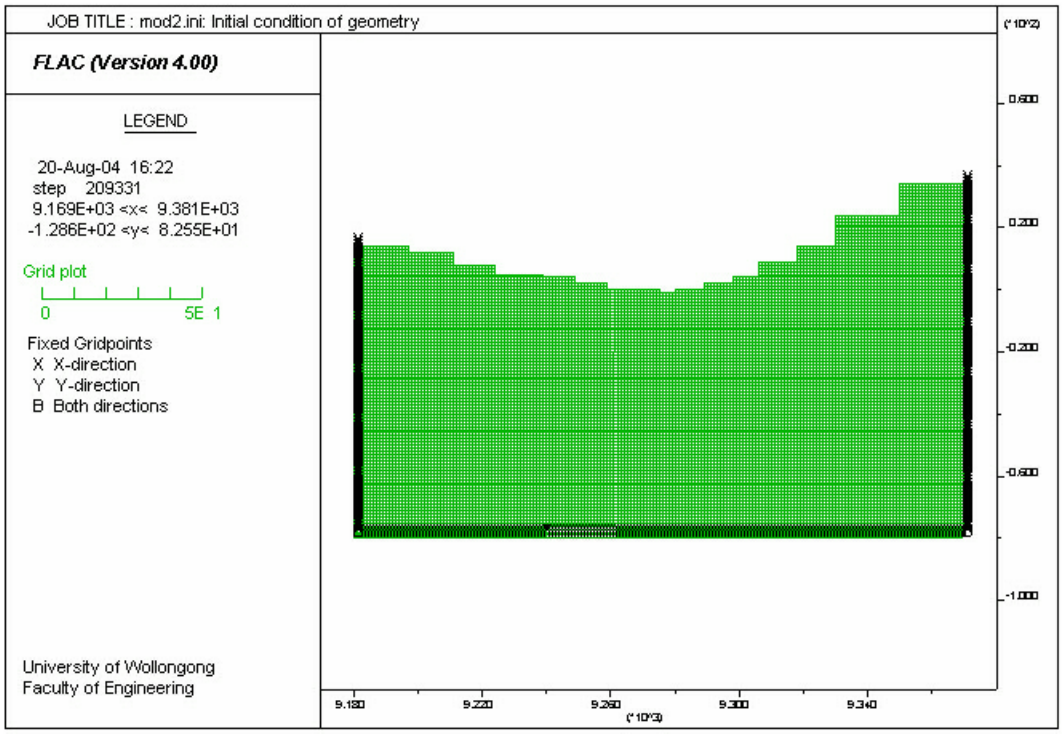

Figure 4.5 Boundary conditions of numerical model

4.3.4 Local In-Situ Stress

Prior to making any changes to the model, the model must be in its initial equilibrium state. This in-situ state must be re-generated based on local known geological conditions. In the model, the most significant geological conditions considered were pore pressure, bedding planes, horizontal and vertical stresses based on the k ratio. The value of k is the ratio of vertical to horizontal stress. For example, when the k ratio is 2, it means that horizontal stress is twice the vertical stress. An example of FLAC coding for initialising horizontal and vertical stress for the model is provided below:

```
set echo off
ca ininv.fis
set k0x=2
set k0z=1
ininv
set echo on
```

The FISH function (ininv.fis) was used to initialise vertical and horizontal stresses and is provided below:

```
;**** ini_syy ************************************
; Initialises vertical stresses
; variables:
;            h ……....height of zone j
;            bot ……..vertical stress at the bottom of zone j
;            top ……..vertical stress at the top of zone j
def ini_syy
top = 0.0
loop jj (1,jzones)
 j=jgp-jj
 h=abs(y(1,j)-y(1,j+1))
 bot=top+ygrav*h*(density(1,j))
 loop i (1,izones)
  syy(i,j)=0.5*(bot+top)
 end_loop
 top=bot
end_loop
end
;**** ini_shor ************************************
; Initialises horizontal stresses
; variables:
;            k0x..... ratio of sxx to syy
;            k0z..... ratio of szz to syy
; parameters (SET):
;               k0x
;            k0z
def ini_shor
loop i (1,izones)
 loop j (1,jzones)
  sxx(i,j)=k0x*(syy(i,j))
  szz(i,j)=k0z*(syy(i,j))
 end_loop
end_loop
end
def ininv
  ini_syy
  ini_shor
end
```

4.3.5 Pore Pressure

Inclusion of pore pressure in the model requires extra coding and more time to reach the equilibrium state. Modifications were required for the FISH function, ininv.fis, in order to initialise the vertical and horizontal stresses under pore pressures in a model. The coding is provided below:

```
;***** ini_pp ****************************************
; Initialises zone pore pressures
; parameters (SET):
;                   wth ..... height of the water table

def ini_pp
loop i (1,igp)
  loop j (1,jgp)
    if y(i,j)>wth then
      sat(i,j)=0.0
    else
      sat(i,j)=1.0
      gpp(i,j)=-1.0*abs((y(i,j)-wth))*wdens*ygrav
    end_if
  end_loop
end_loop
loop i (1,izones)
  loop j (1,jzones)
    pp(i,j)=0.25*(gpp(i,j)+gpp(i,j+1)+gpp(i+1,j+1)+gpp(i+1,j))
  end_loop
end_loop
end

;**** ini_syy ****************************************
; Initialises vertical stresses
; variables:
;             h ..... height of zone j
;             bot ..... vertical stress at the bottom of zone j
;             top ..... vertical stress at the top of zone j
def ini_syy
top = 0.0
loop jj (1,jzones)
  j=jgp-jj
```

```
 h=abs(y(1,j)-y(1,j+1))
 bot=top+ygrav*h*(density(1,j)+porosity(1,j)*0.5*(sat(1,j)+sat(1,j+1))*wdens)
 loop i (1,izones)
  syy(i,j)=0.5*(bot+top)
 end_loop
 top=bot
end_loop
end

;**** ini_shor ***************************************
; Initialises horizontal stresses
; variables:
;          k0x..... ratio of effective sxx to effective syy
;          k0z..... ratio of effective szz to effective syy
; parameters (SET):
;            k0x
;          k0z
def ini_shor
loop i (1,izones)
 loop j (1,jzones)
  sxx(i,j)=k0x*(syy(i,j)+pp(i,j))-pp(i,j)
  szz(i,j)=k0z*(syy(i,j)+pp(i,j))-pp(i,j)
 end_loop
end_loop
end
def ininv_1
 ini_pp
 ini_syy
 ini_shor
end
```

4.3.6 Bedding Planes

In the model, only one bedding plane was added at 10 meters below the surface of WRS 1. The inclusion of bedding planes in the model requires additional time to reach equilibrium state. Simulating the model with the inclusion of one bedding plane at 10 meters below the surface was sufficient enough to provide a good insight into the effect of bedding planes in a model. Fig. 4.6 illustrates a model

with a bedding plane at 10 meters below the ground level. The effect of bedding plane in a model is illustrated in Chapter 6.

FLAC coding for adding a bedding plane in a model is as follows:

```
call ubi.fis
model m_ubi
mod null j=70
ini y add 1 j=1,70
int 1 Aside from 1,70 to 191,70 Bside from 1,71 to 191,71
set echo off
ca mod2_half_r_fish_properties.txt
set echo on
int 1 ks=6.3e10 kn=6.3e10 fric=44
```

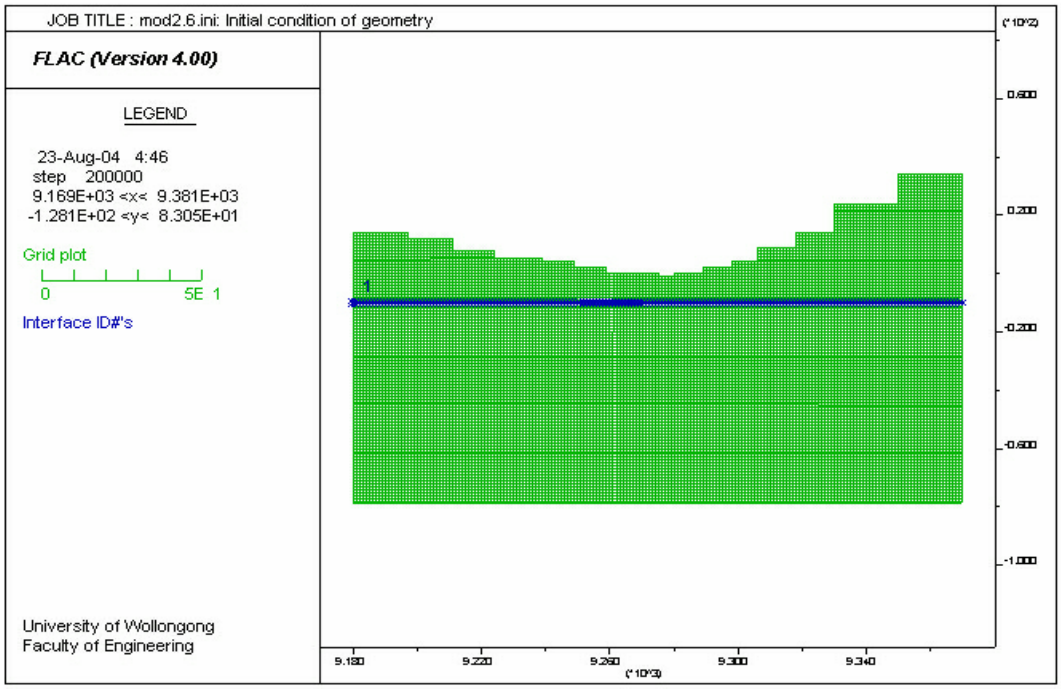

Figure 4.6 Bedding plane in a Numerical Model

4.4 APPLYING LATERAL DISPLACEMENT

Lateral displacement was applied to the model to study the strata interaction. In this thesis, two types of loading pattern were used. In the first case loading was

kept constant, whereas in second case the magnitude of the loading rate increased as depth increased. Both types of loading patterns are illustrated in Fig. 4.7.

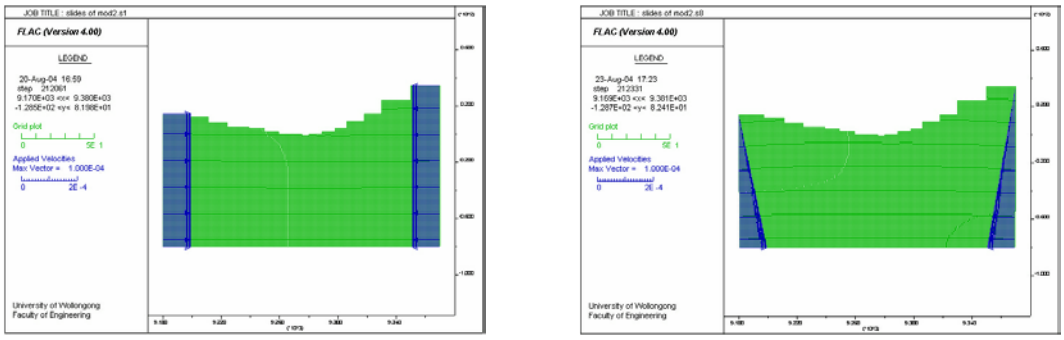

(a) Type one loading pattern (b) Type two loading pattern

Figure 4.7 Lateral displacement loading Pattern

4.4.1 Velocity Rate

In applying lateral displacement to a model, the pattern of loading will have an effect on how the strata will behave. However another important factor is the rate of loading. With FLAC, the loading velocity controls the rate of loading. For example, when the loading rate is 1×10^{-4} m/s, it means that 0.1 mm of load is applied every one second. The following two numerical examples explain how FALC works.

Example A

When the loading rate is 1×10^{-4} m/s and the desired displacement is 0.5 meter, the number of calculation steps required are:

$$\text{Velocity} \times \text{Step} = \text{Displacement}$$

$$\text{Step} = 0.5 \text{ m} \div (1 \times 10^{-4} \text{ m/s})$$

$$= 5000 \text{ steps}$$

Example B

When the loading rate is 1×10^{-5} m/s and the desired displacement is 0.5 meter, the number of calculation steps required are:

$$\text{Step} = 0.5 \text{ m} \div (1 \times 10^{-5} \text{ m/s})$$
$$= 50000 \text{ steps}$$

It can be seen from Example A and B, when the loading rate is low, more time is required to reach the desired displacement.

CHAPTER 5
GRID CONVERGENCE TEST IN FLAC

5.1 INTRODUCTION

In FLAC modelling, generated grids must satisfy both the requirement to minimise boundary influence and provide sufficient zoning in the region of interest. Consequently the highest grid density should be generated in region of interest, and conversely low grid density is acceptable in region of least interest. The accuracy of the simulated results depends on the grid density used to represent the physical system. However, complications may arise in grid generation when the dimensions of the physical model are large. As illustrated in Chapter 4, the dimensions of the model used in this thesis were 190 m (horizontal) by 114 m (vertical). Allowing each zone size of 1 m by 1 m, then the required grid size would be 190 by 114, which is equivalent to 21,660 zones. Each zone can be made to represent greater area, simply by changing the size of grid. Generally it is desirable to use more zones to represent a physical model to improve the accuracy of results. The downside of increasing the number of zones is that FLAC takes more time to converge compared to a model with lesser number of zones. Accordingly, a grid convergence test was carried out to determine the optimum number of zones required for a given physical system and allowing a better validation of the model results.

In this thesis, four models were used for the grid convergence test. All four models had the same input parameters and initial conditions, except that the sizes of grid and mesh density were different. A summary of the four models is listed in Table 5.1. The dimensions of the areas of interest were 30 m by 30 m with respect to zone dimension of the study region (see Figure. 4.4, pp. 43). Models 1 to 4 were represented by a grid of 15 by 15, 30 by 30, 60 by 60 and 100 by 100 respectively.

5.2 GRID CONVERGENCE TEST RESULTS IN FLAC

Fig. 5.1 shows the common geometry shape for all models used in the grid convergence test. Once the model had reached the equilibrium state, lateral displacement was applied at the artificial boundary toward the centre of the valley as shown in Fig. 5.2.

Fig. 5.3 shows the contours of vertical displacement for Model 1. It shows that due to applied lateral displacement the strata had moved toward centre of the valley. The magnitude of the strata movement was greater at nearby boundaries where the artificial displacement was applied. However there appears to be less movement at the centre/bottom of the valley.

Fig. 5.4 shows the stratification movements both toward the centre of the valley as well as upwards. The velocity vectors at the centre of the valley in Fig. 5.4 clearly show there was no noticeable upward movement of the ground past 30 meters of depth. The trend was similar for all other models (refer to Fig. 5.5, Fig. 5.6 and Fig. 5.7). For Model 1, the general trend of the strata movement was both lateral and upward (see Fig. 5.8). On the other hand, for Models 2, 3 and 4, the strata started to move downward once it reached certain depths. This phenomenon is termed the turning point movement and is clearly observed in Fig. 5.9, Fig. 5.10 and Fig. 5.11. The turning point for Model 2, Model 3 and Model 4 was at 16 meters, 20 meters and 21 meters respectively below the surface.

Fig. 5.12 shows the plastic state of the material for Model 1 after applying 212 mm of lateral displacement. In respect to the legend in Fig. 5.12, *0* denotes the material is in elastic state, *1* denotes plastic shear state and *2* denotes elastic state now, but plastic in the past. The plastic state in Fig. 5.12 indicates that fractures would develop at the centre/bottom of the valley and propagate toward the boundary. This phenomenon was not shown in Fig. 5.12, however the dynamic simulation file showing this trend is included in this thesis's CD. The movie file can only be viewed with the FLAC movie program.

Under Model 1 conditions, 212 mm of lateral displacement was applied without boundary interference in model results. For Models 2, 3 and 4, 273mm, 272 mm and 315mm of lateral displacement was applied respectively without boundary interference. Contour plots of the vertical displacement (see Fig. 5.13, Fig. 5.14 and Fig. 15) were of little difference to Model 1, and the trend is similar. The plasticity state for all models displayed similar trends (see Fig. 5.16 through Fig. 5.18).

There were also pre-selected monitoring stations for strata movements for all four models. It consisted of six monitoring stations from the surface to 30 meters depth with an interval of 6 meters; this is illustrated in Fig. 5.19. Fig. 5.20 through Fig. 5.25 show comparison of all four models. Fig. 5.26 shows strata movements at different depths for Model 2. As mentioned earlier, the magnitude of strata movements decreased as depth increased. This phenomenon can be seen in Fig. 5.26.

5.3 SUMMARY

The grid convergence test facilitated the changes necessary to reduce run times or to improve accuracy. Without sacrificing a great deal in accuracy of the result it is recommended to reduce the model size to minimise run time. A summary of the grid convergence test is provided in Table 5.2. Model 1 has too coarse grid density and a detailed study would be rather difficult under this model conditions. Model 4 has the finest grid density. One obvious problem associated with this model is the running time to reach an equilibrium state. With almost 700,000 steps, the model could not reach the pre-assigned equilibrium state ratio of 1×10^{-5}. To execute 700,000 steps, it required 253 hours (more than 10 days). In considering all the factors presented in this chapter, including running time, Model 2 was selected as a base model for the parametric study as discussed in Chapter 6.

Table 5.1 Summary of initial conditions for models used for grid convergence test in FLAC

	Model 1	Model 2	Model 3	Model 4
Grid size	95,57	190,114	220,144	420,268
No. of zones	5,415	21,660	31,680	112,256
Single zone dimension of study region	2 m × 2 m	1 m × 1 m	0.5 m × 0.5 m	0.3 m × 0.3 m
Constitutive model	m_ubi	m_ubi	M_ubi	m_ubi
Stiffness/strength reduction factor	Half reduction	Half reduction	Half reduction	Half reduction
Bedding plane	No	No	No	No
Loading pattern	→[ ]←	→[ ]←	→[ ]←	→[ ]←
Loading rate	1×10^{-4} m/s	1×10^{-4} m/s	1×10^{-4} m/s	1×10^{-4} m/s

Table 5.2 Summary of grid convergence test results in FLAC

	Model 1	Model 2	Model 3	Model 4
Steps to reach equilibrium state	14,460	209,330	274,180	697,950
Time taken to reach equilibrium state	0.23 hrs	13.08 hrs	26.57 hrs	252.88 hrs
Maximum unbalance force	2.5 N	1.6 N	8.8 N	3.3 N
Equilibrium ratio	1.17×10^{-5}	3.27×10^{-5}	2.39×10^{-5}	4.29×10^{-4}
Maximum allowable applied displacement	212 mm	273 mm	272 mm	315 mm

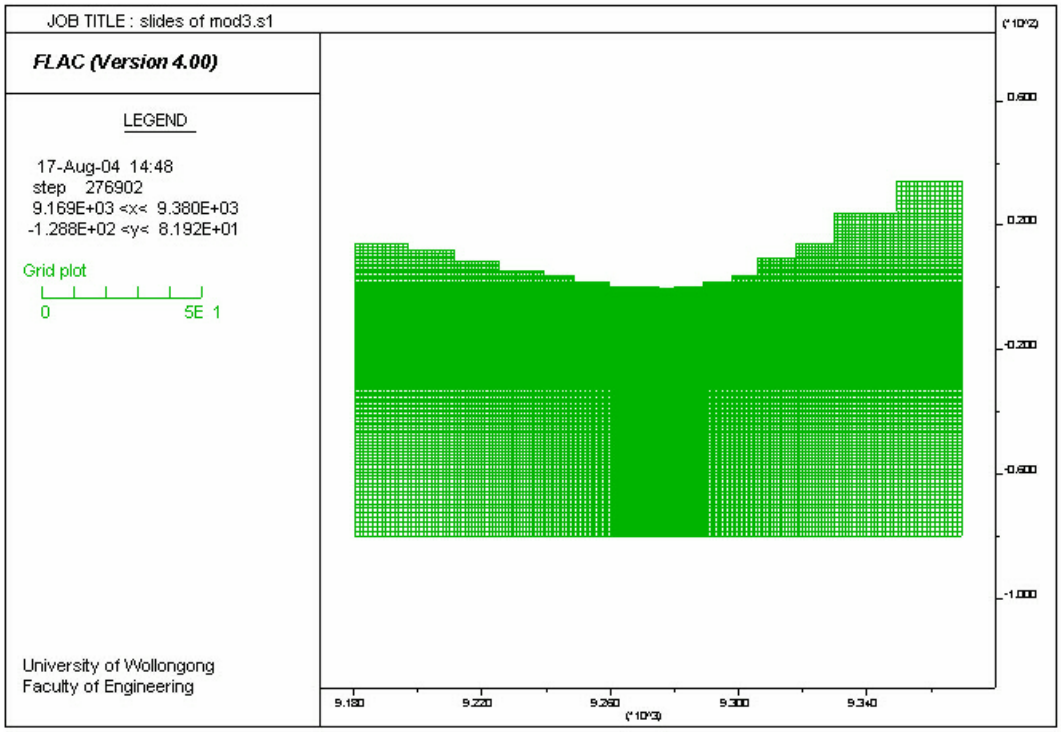

Figure. 5.1 Common geometry shape for all models

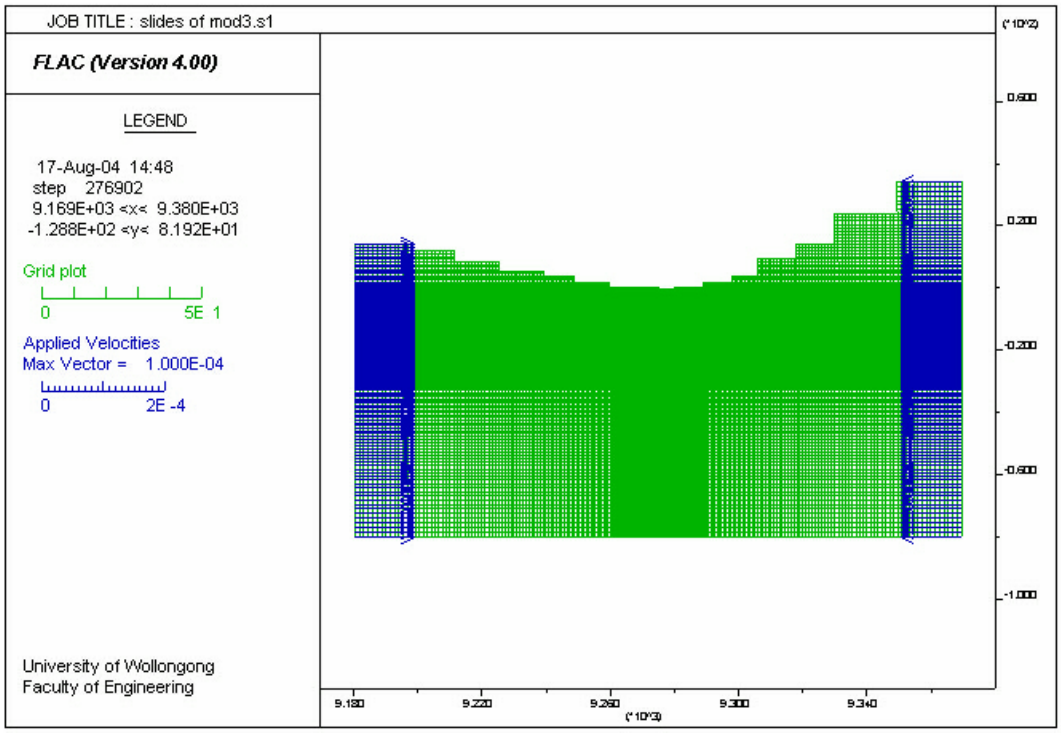

Figure. 5.2 Applying lateral displacements at the boundary

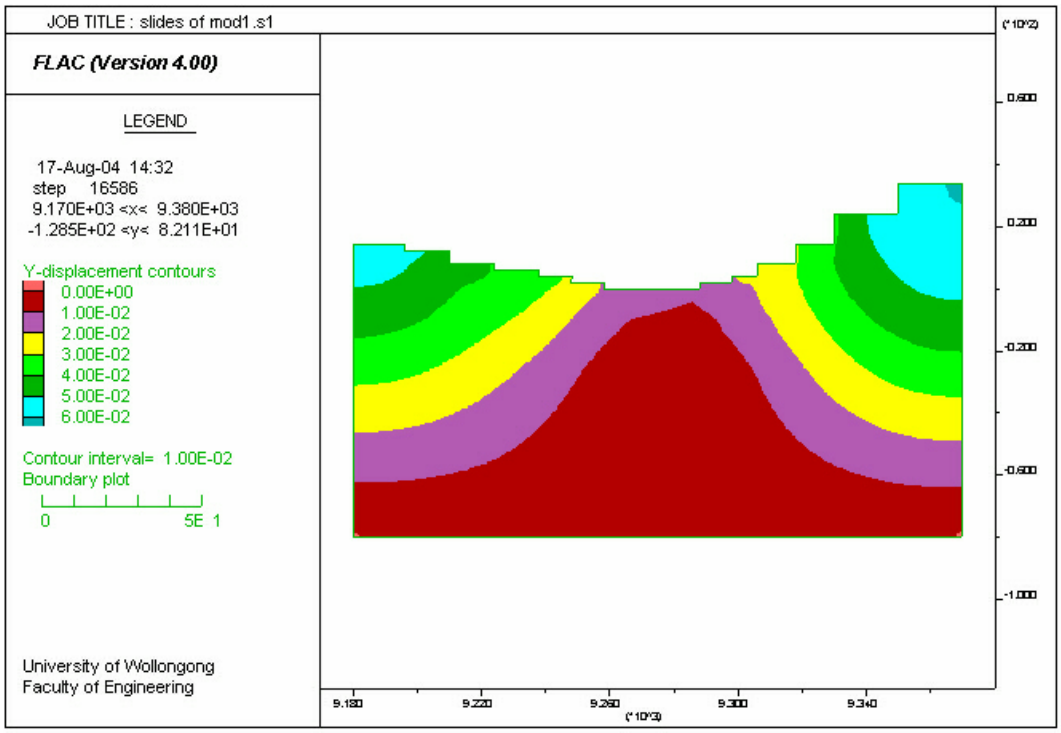

Figure. 5.3 Contours of vertical displacement for Model 1

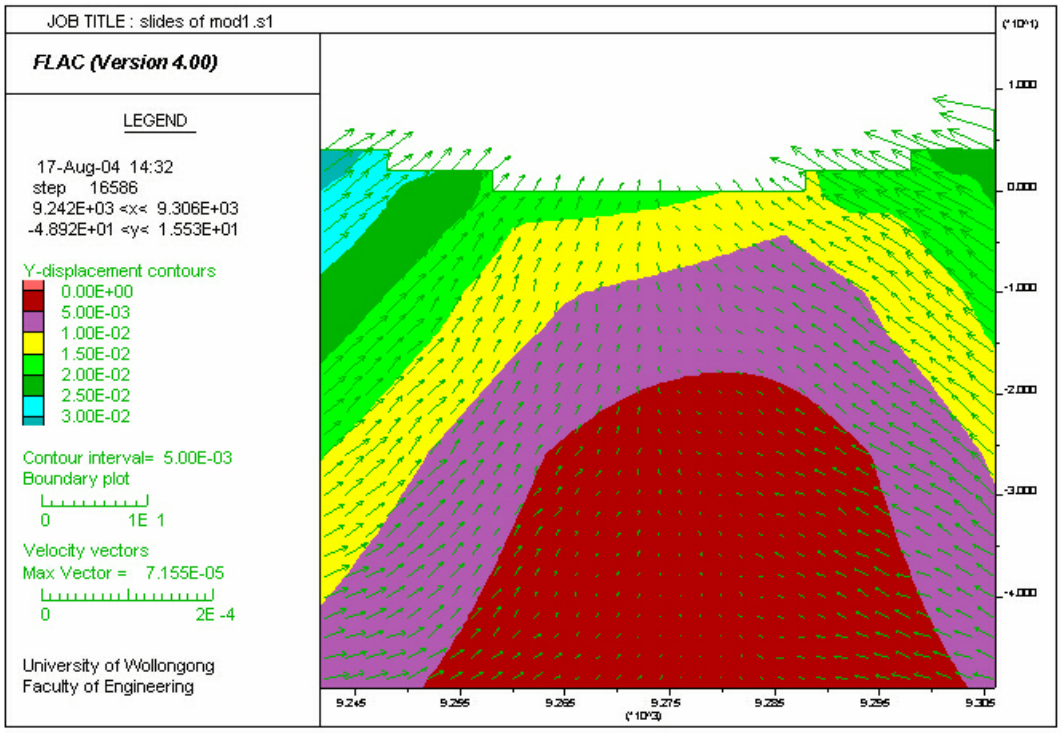

Figure. 5.4 Contours of vertical displacement with vectors for Model 1

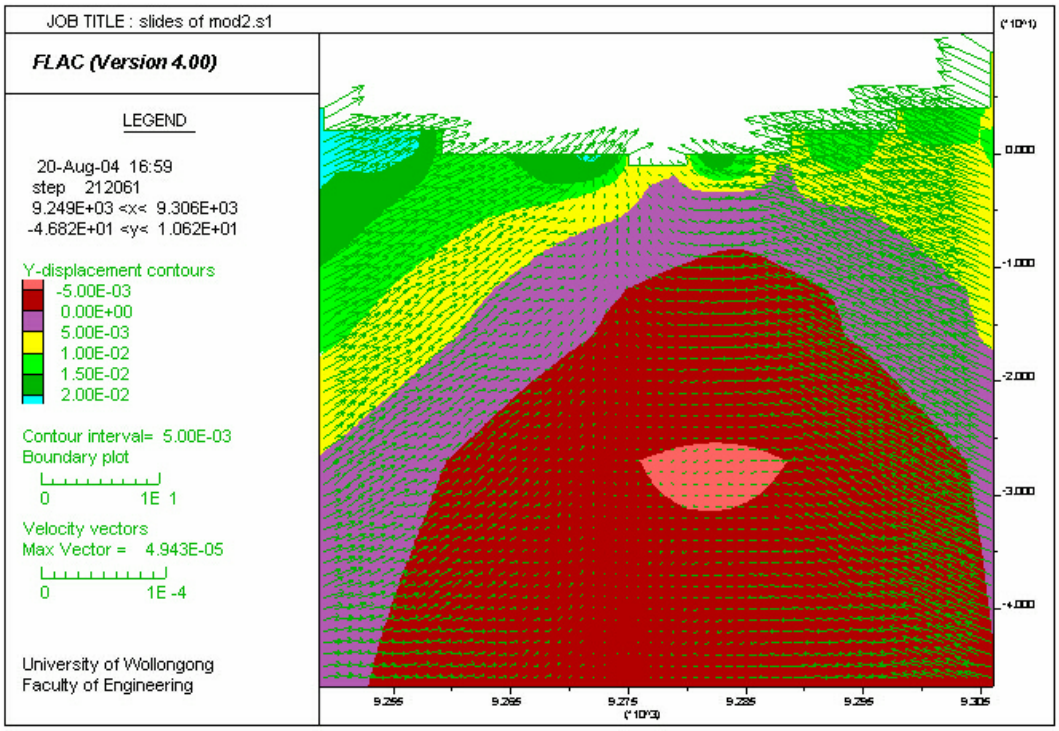

Figure. 5.5 Contours of vertical displacement with vectors for Model 2

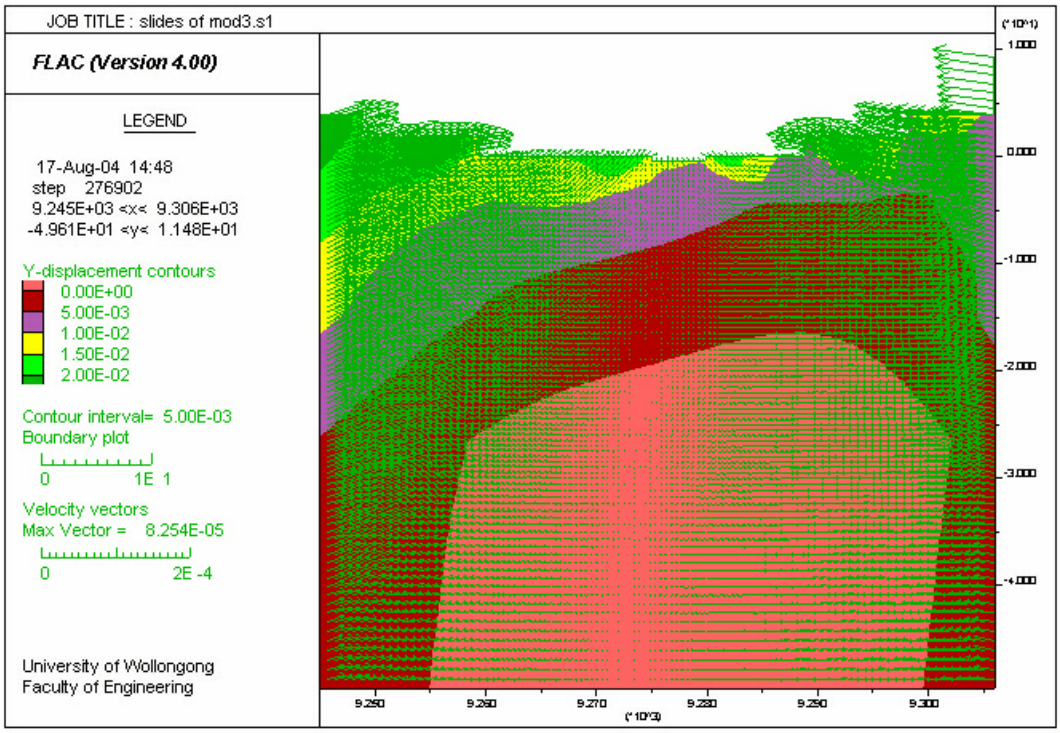

Figure. 5.6 Contours of vertical displacement with vectors for Model 3

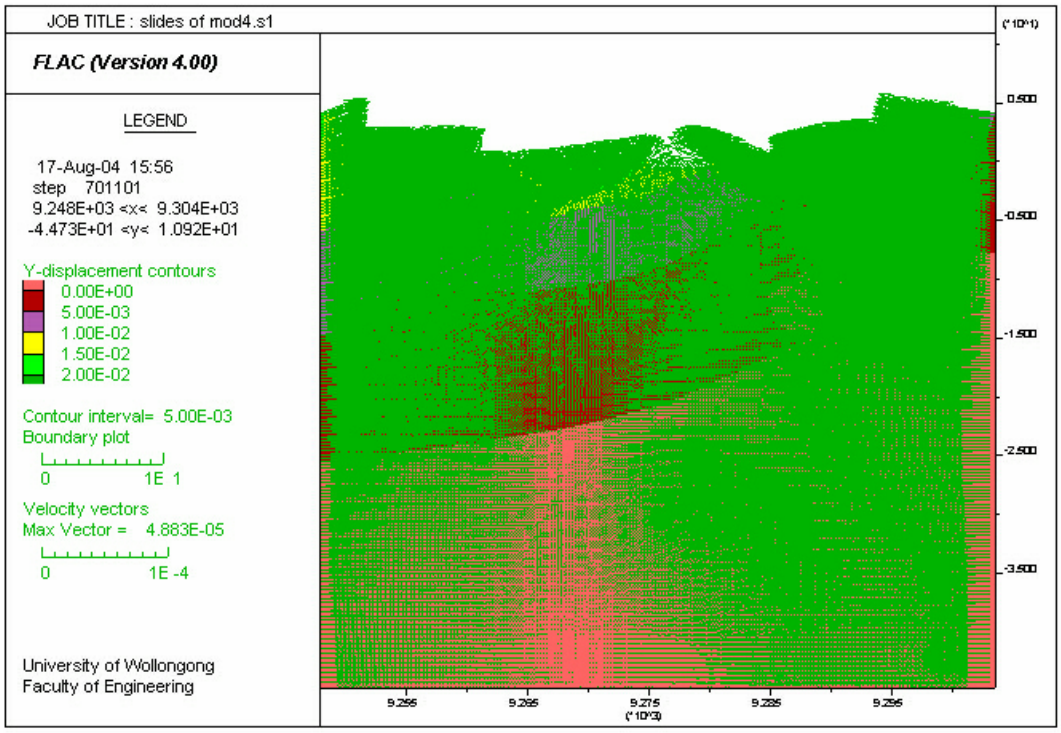

Figure. 5.7 Contours of vertical displacement with vectors for Model 4

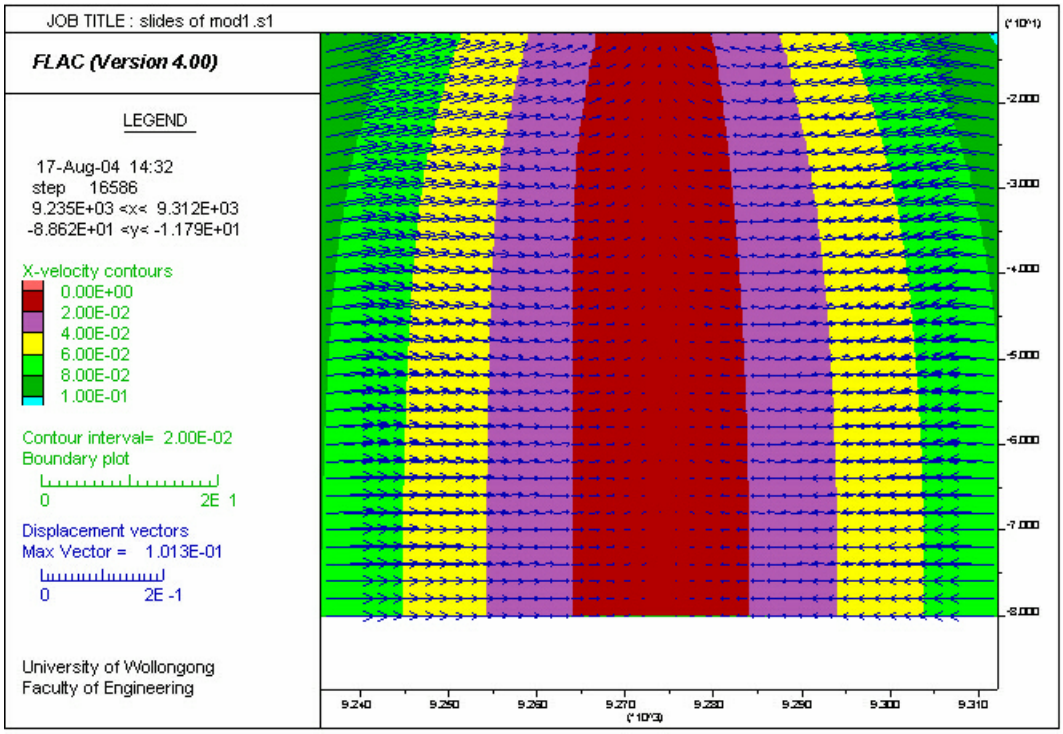

Figure. 5.8 Contours of resultant displacement with vectors for Model 1

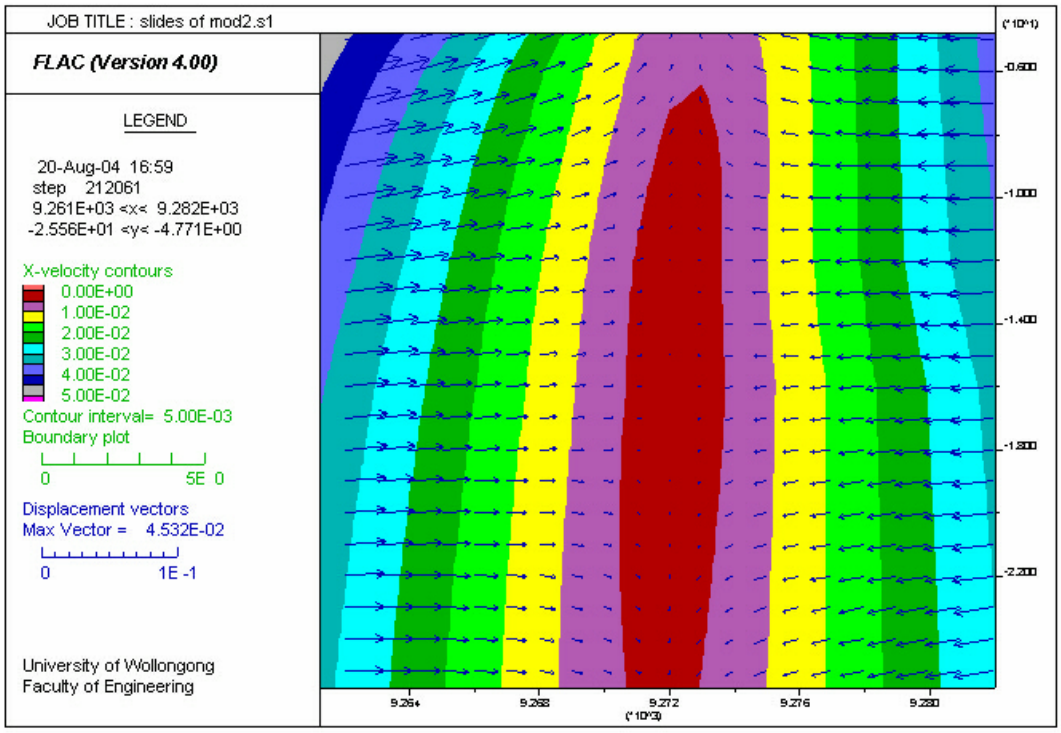

Figure. 5.9 Contours of resultant displacement with vectors for Model 2

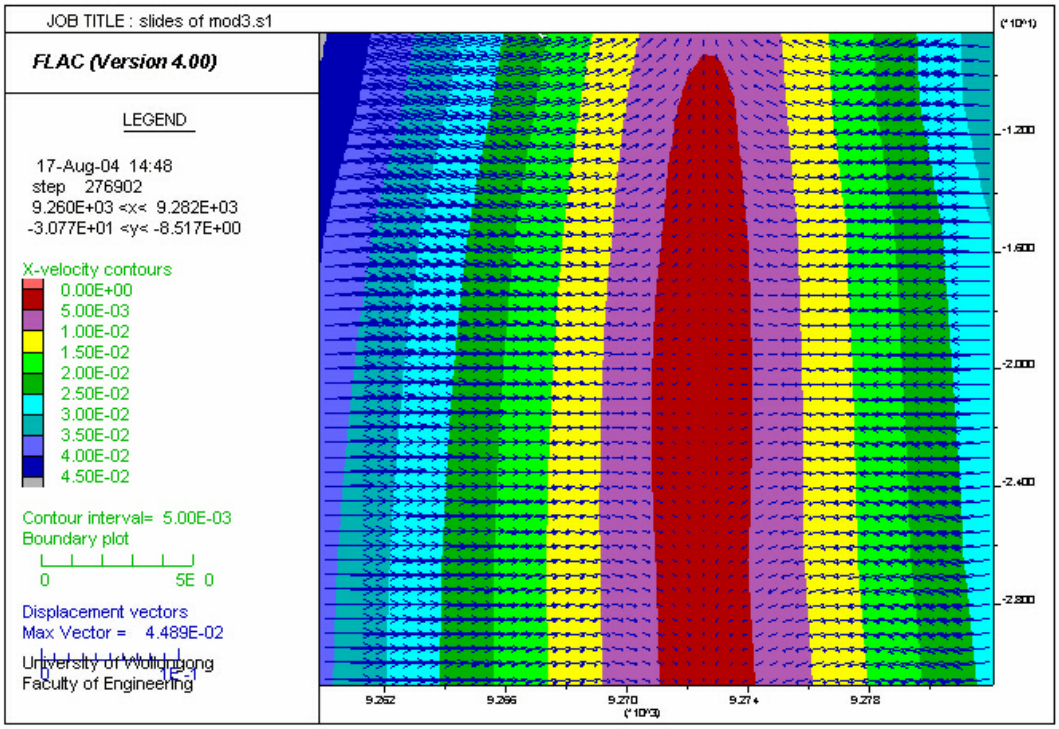

Figure. 5.10 Contours of resultant displacement with vectors for Model 3

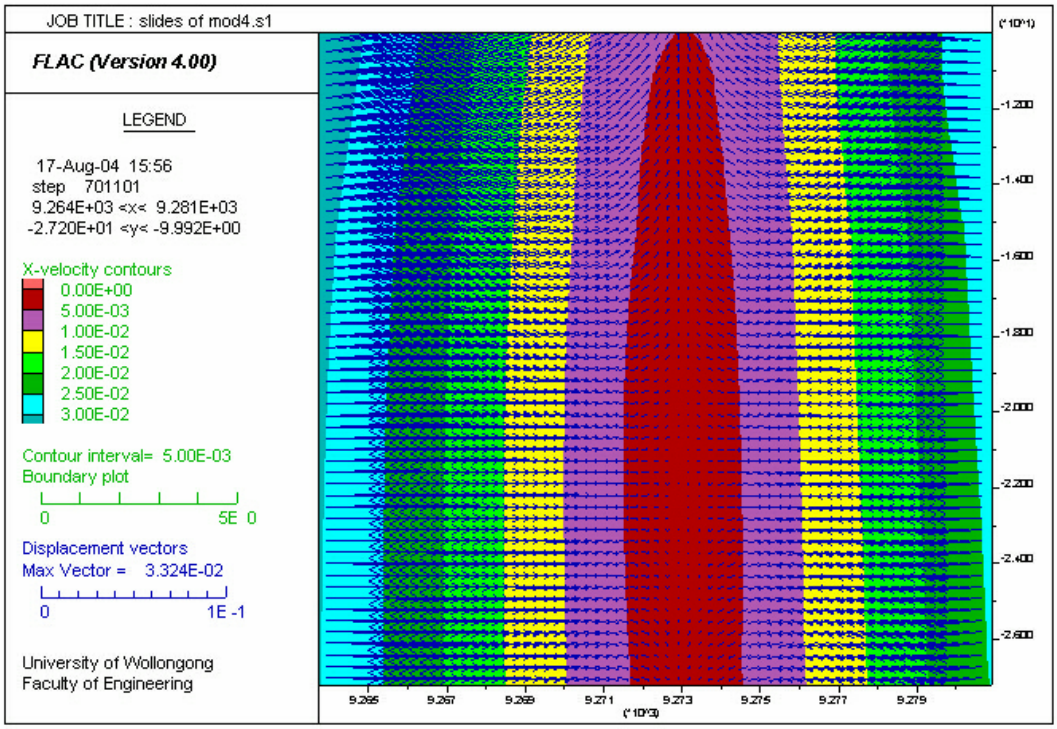

Figure. 5.11 Contours of resultant displacement with vectors for Model 4

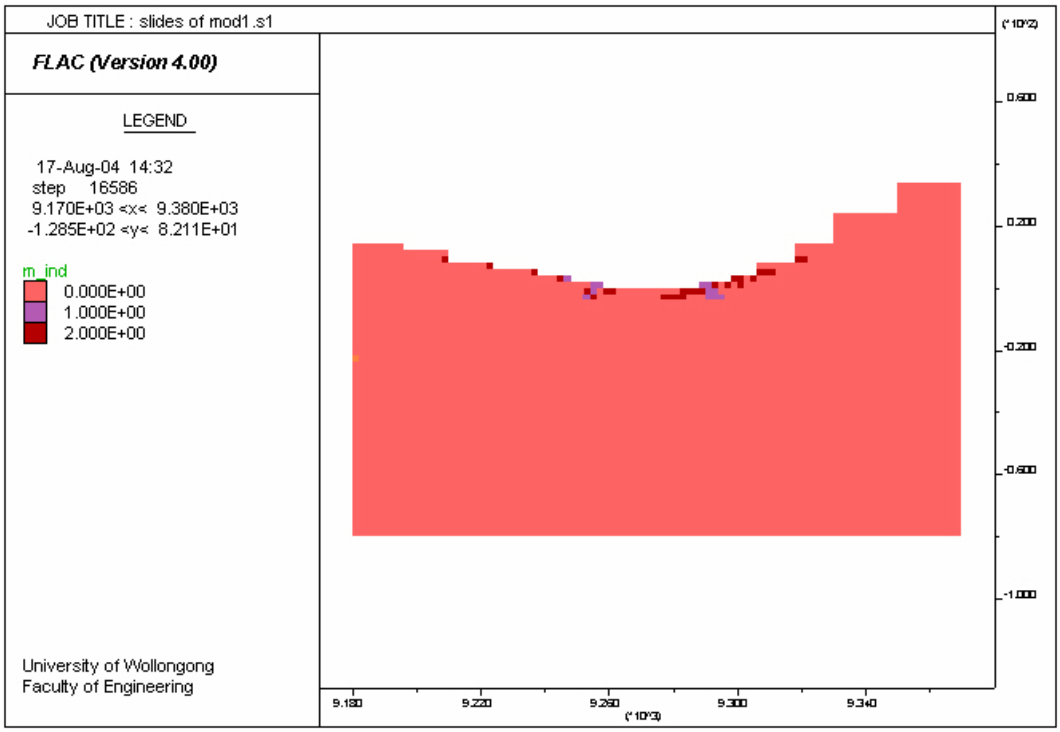

Figure. 5.12 Plastic state for Model 1

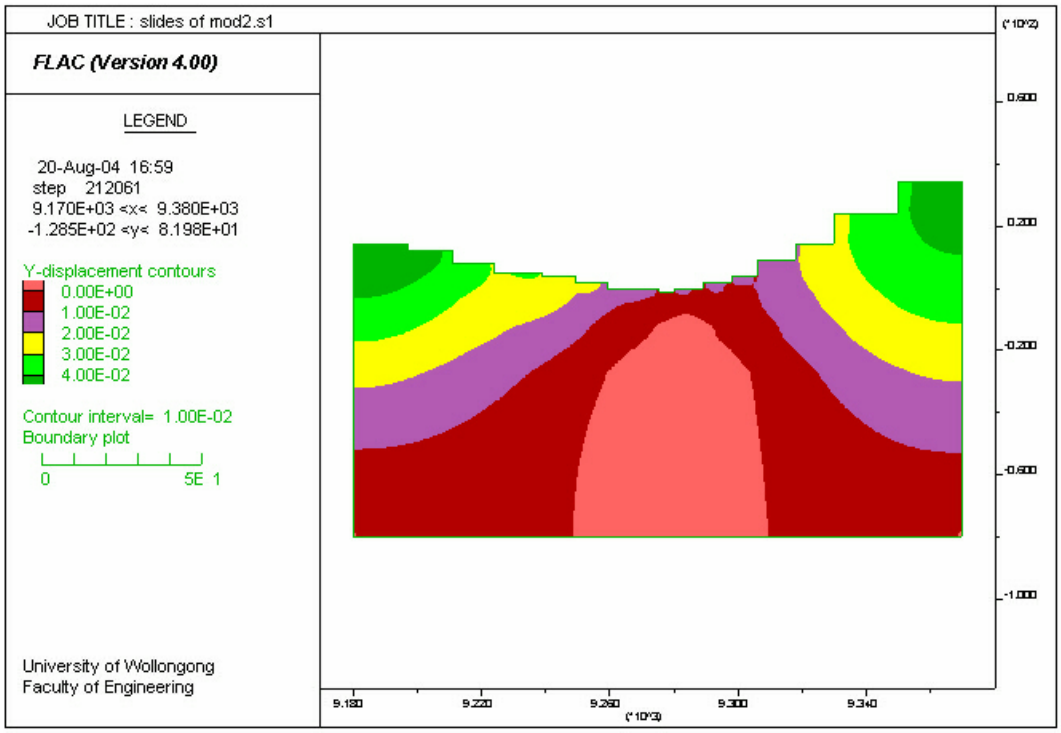

Figure. 5.13 Contours of vertical displacement for Model 2

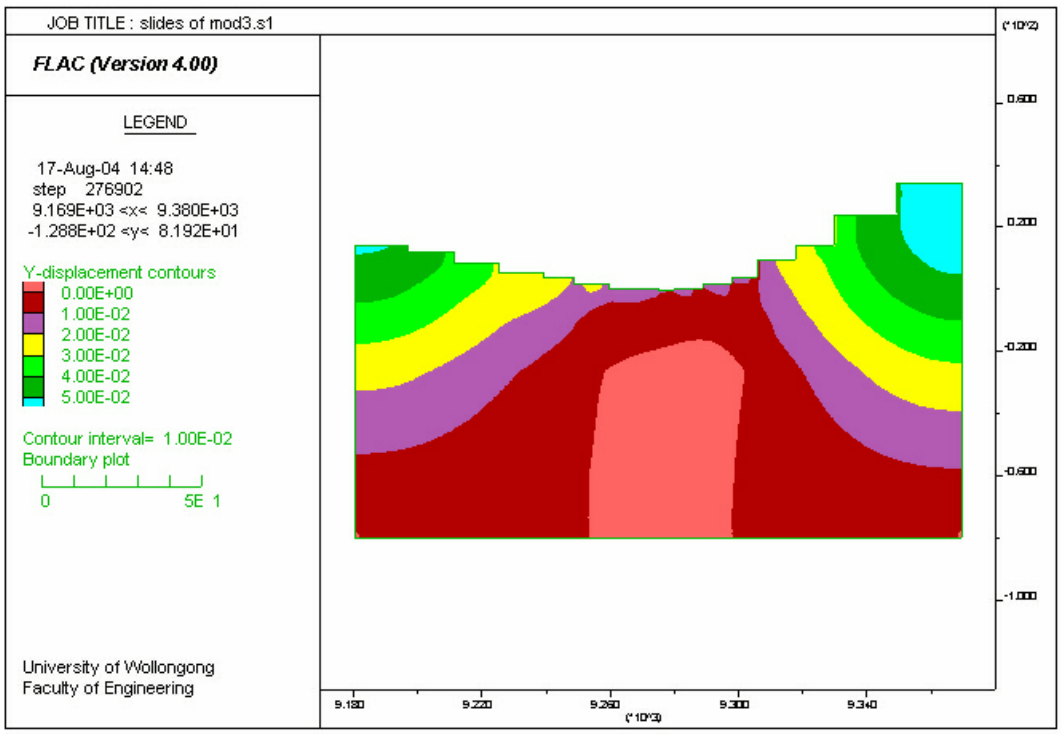

Figure. 5.14 Contours of vertical displacement for Model 3

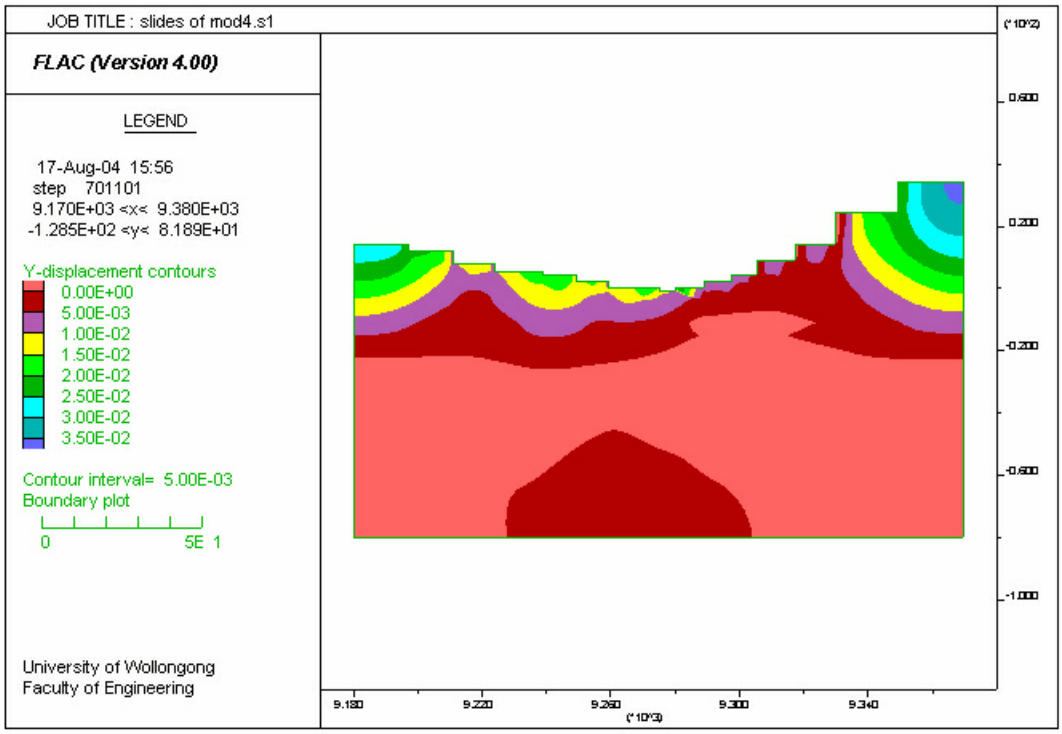

Figure. 5.15 Contours of vertical displacement for Model 4

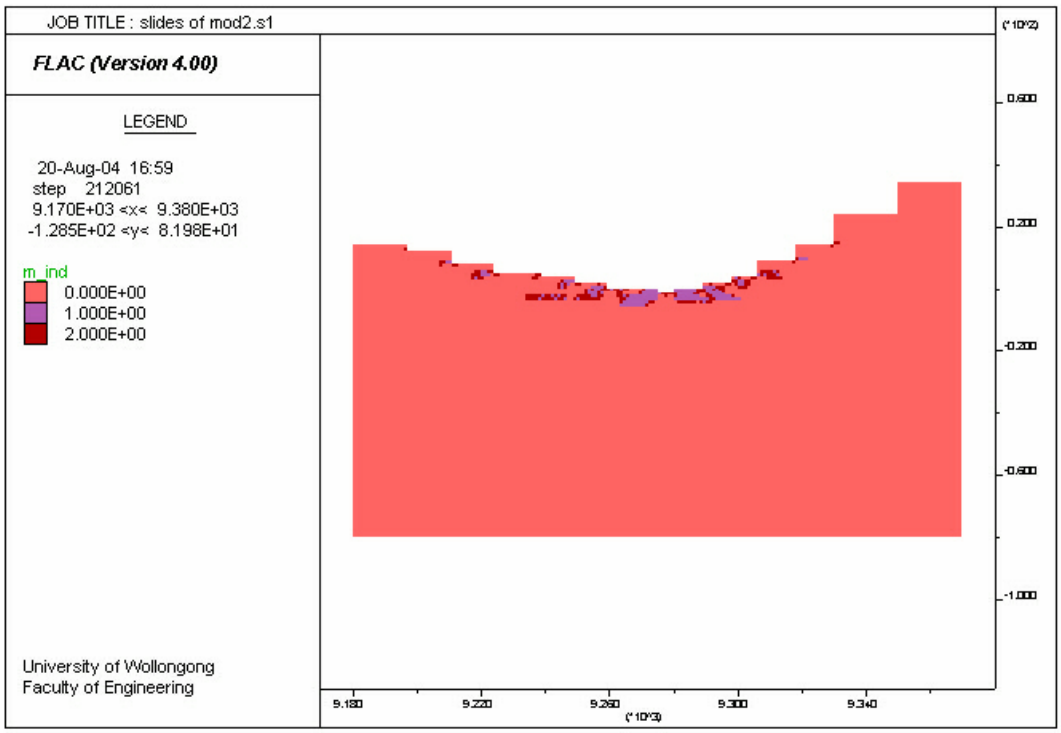

Figure. 5.16 Plastic state for Model 2

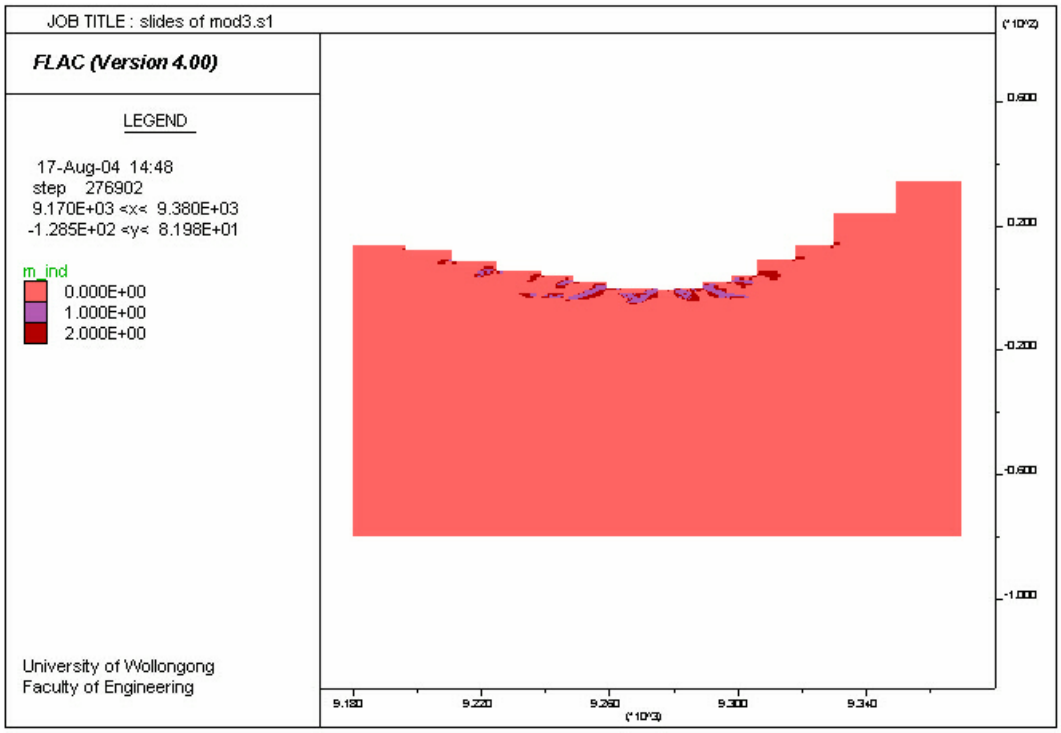

Figure. 5.17 Plastic state for Model 3

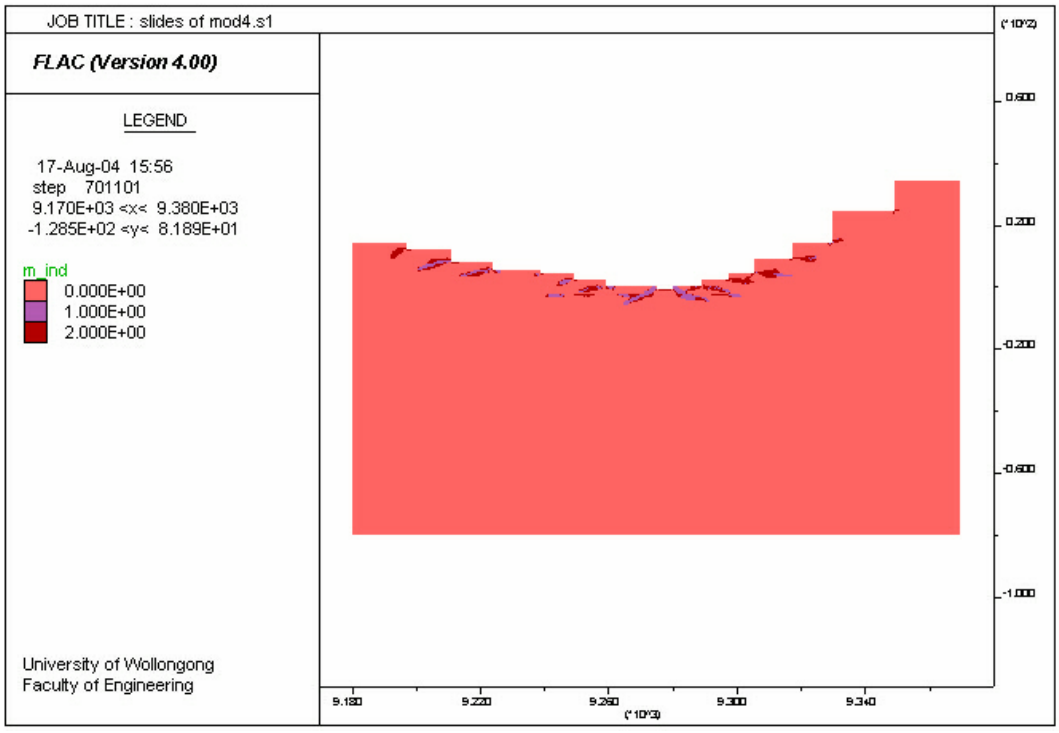

Figure. 5.18 Plastic state for Model 4

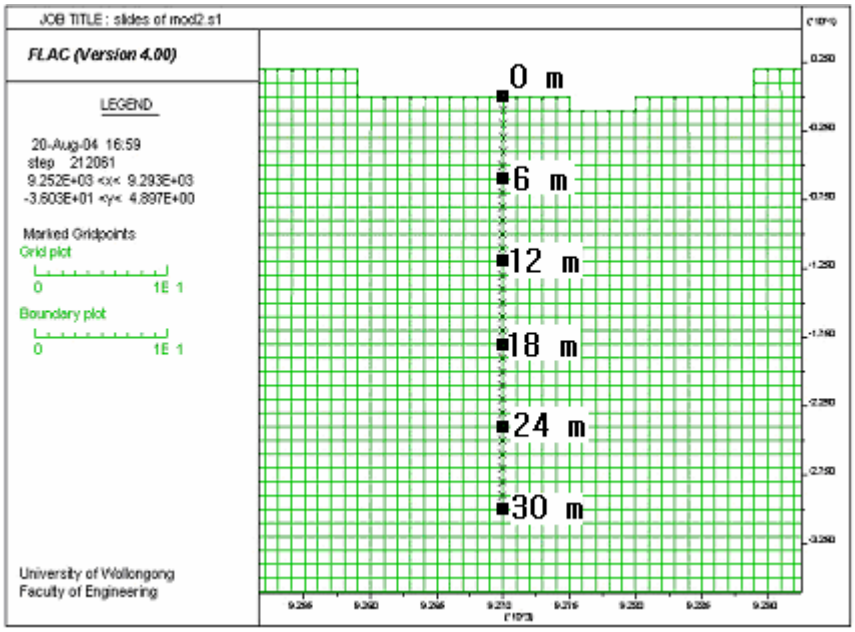

Figure. 5.19 Pre-selected monitoring stations for strata movements

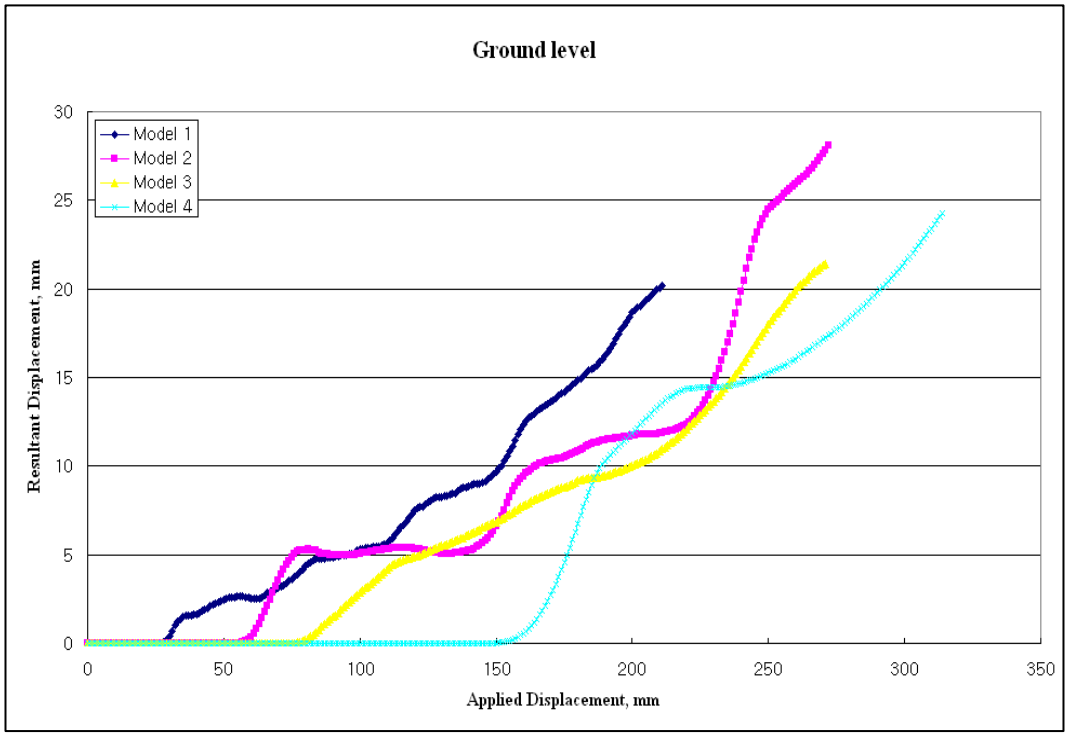

Figure. 5.20 Strata movements at ground level

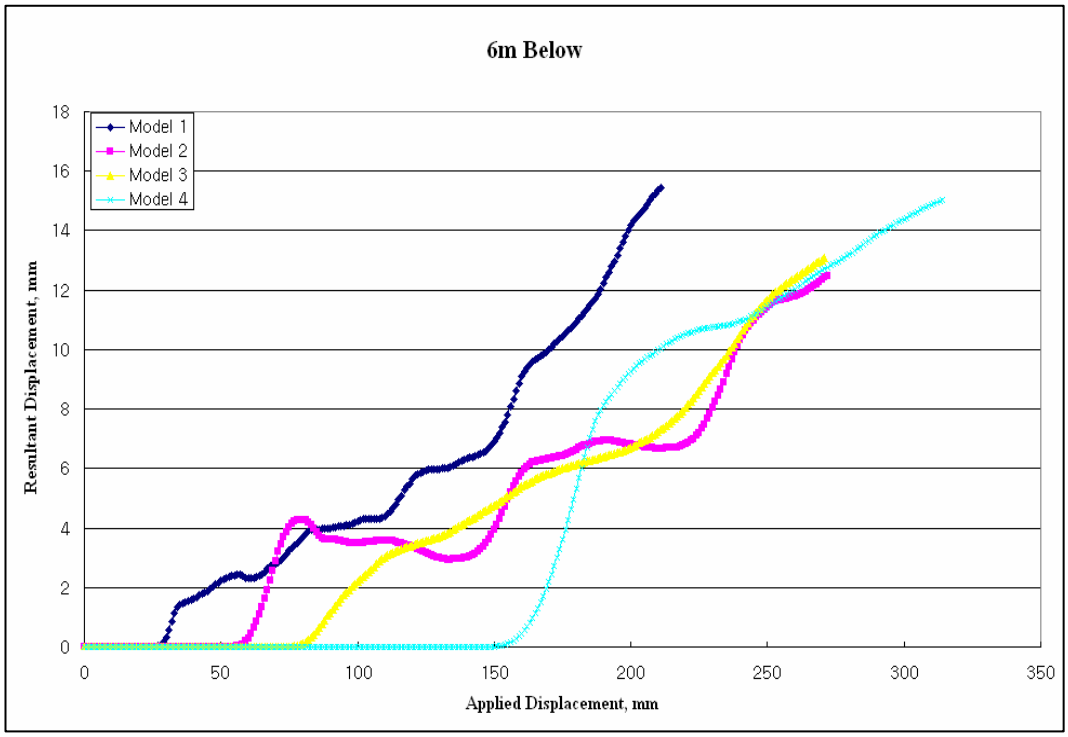

Figure. 5.21 Strata movements at 6 m below ground level

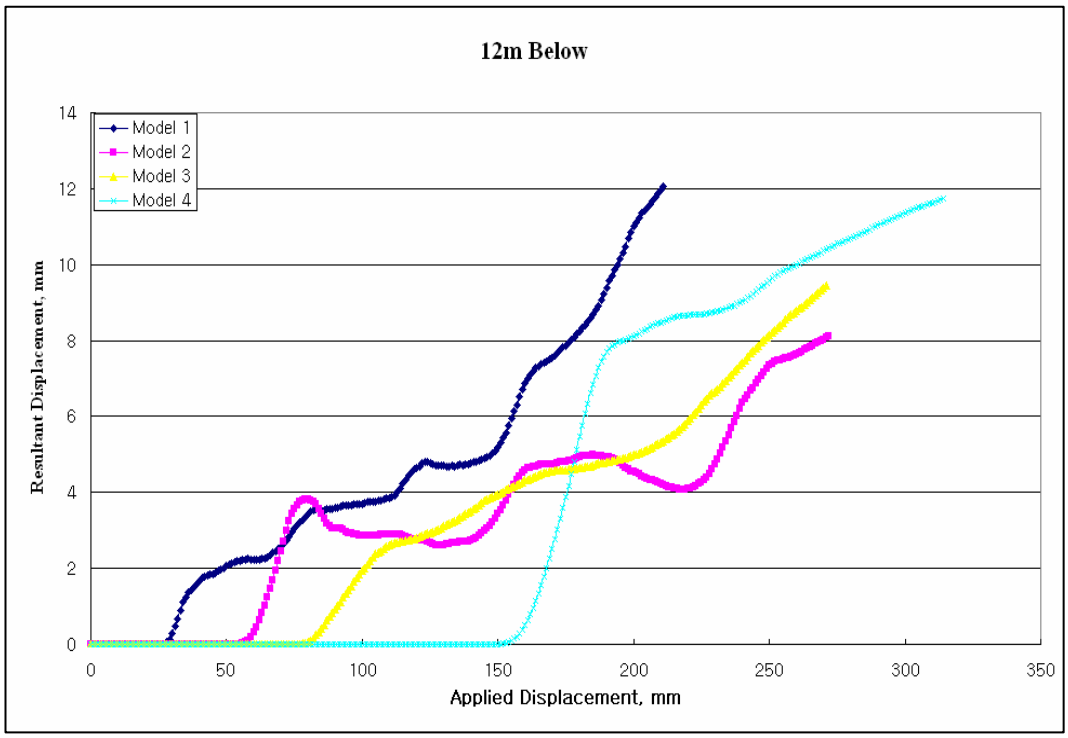

Figure. 5.22 Strata movements at 12 m below ground level

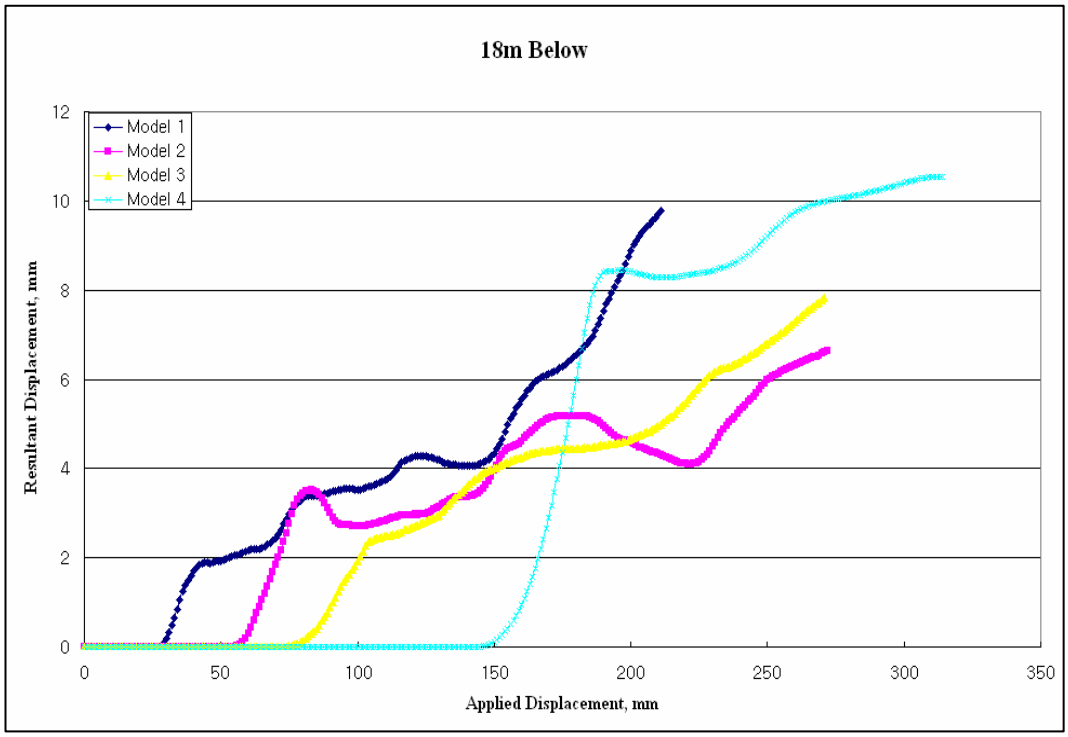

Figure. 5.23 Strata movements at 18 m below ground level

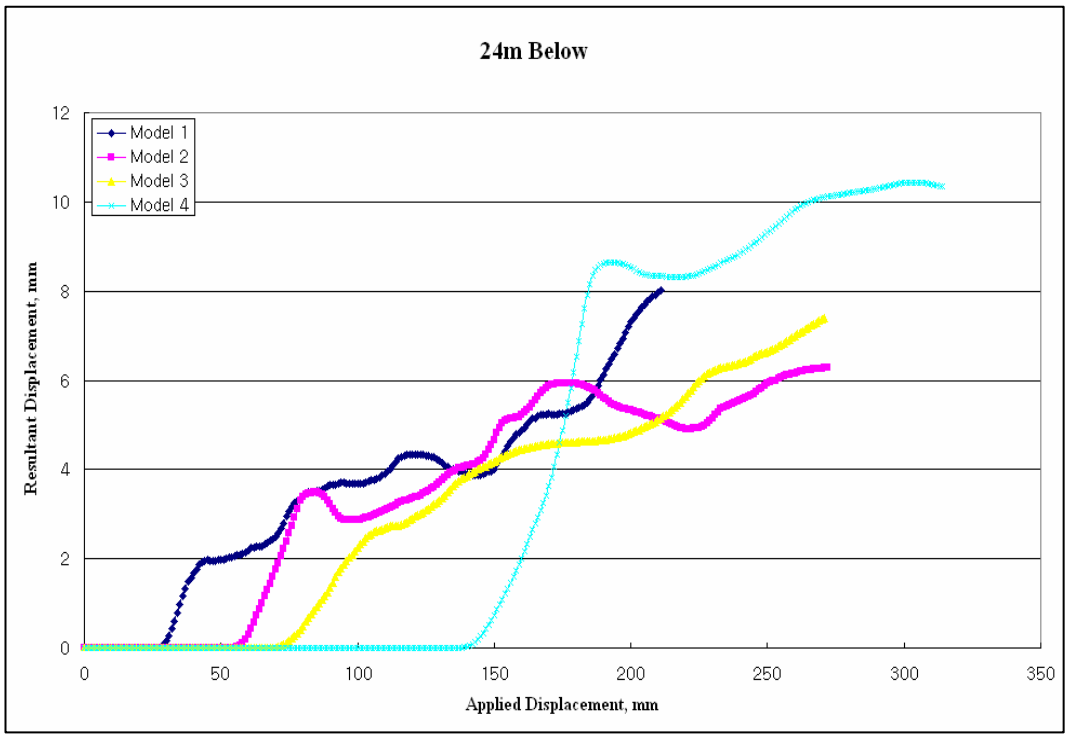

Figure. 5.24 Strata movements at 24 m below ground level

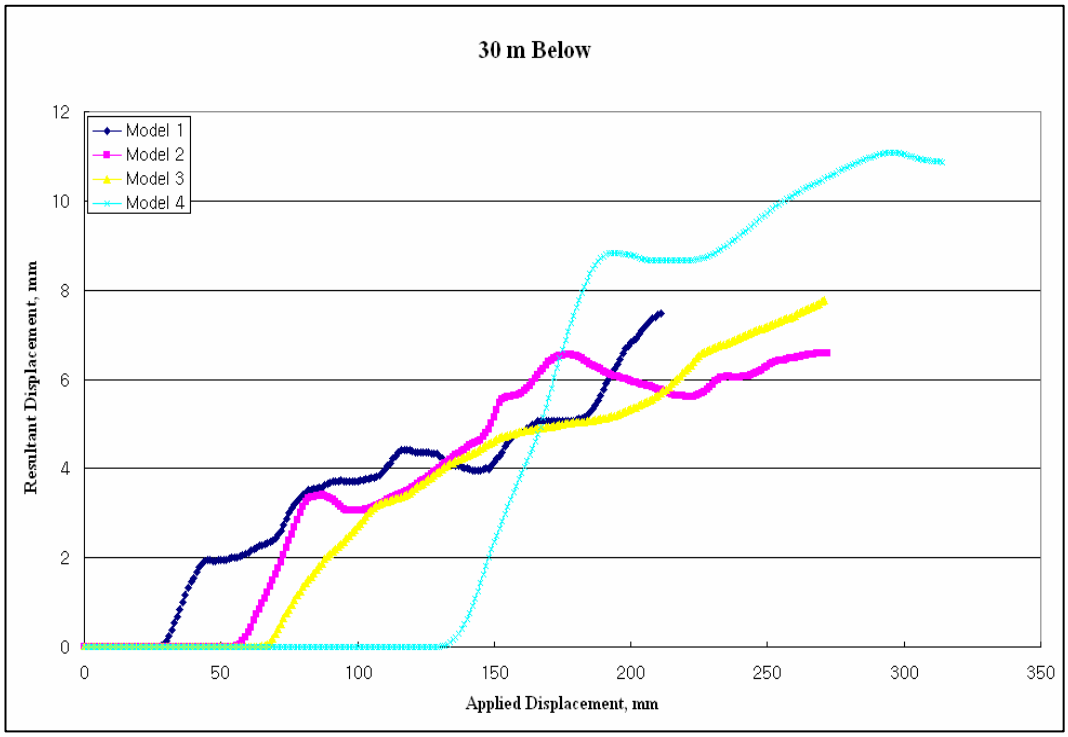

Figure. 5.25 Strata movements at 30 m below ground level

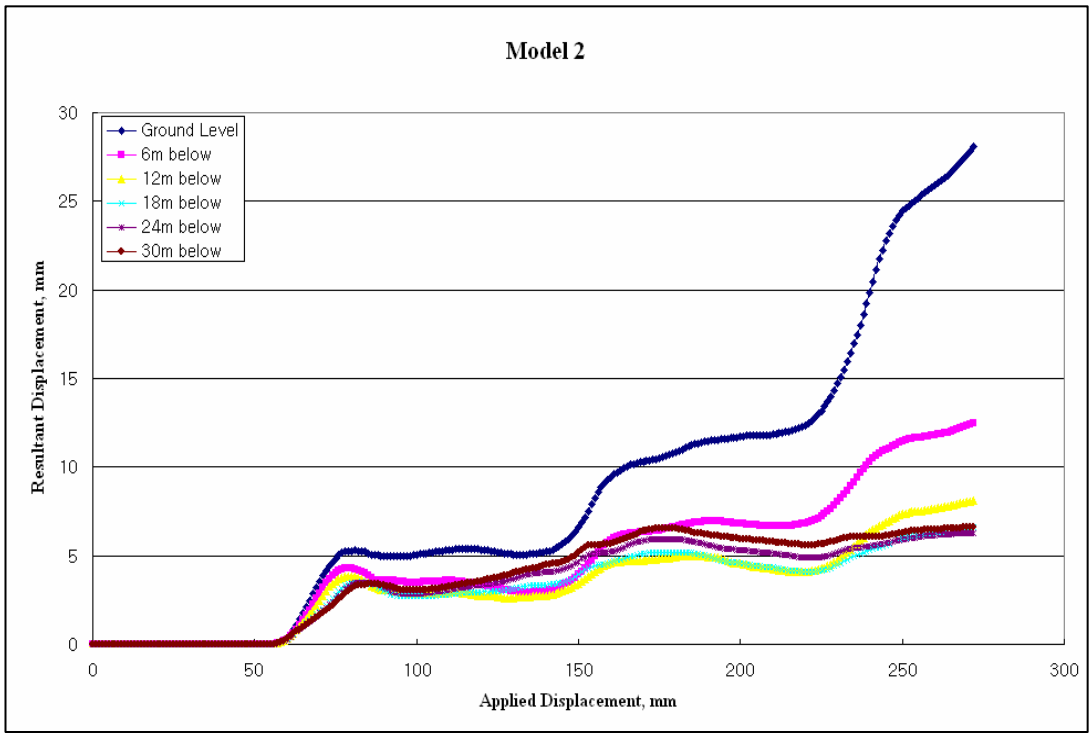

Figure. 5.26 Strata movements for Model 2 at different depths

CHAPTER 6
PARAMETRIC STUDY

6.1 INTRODUCTION

A parametric study was performed based on Model 2 described in Chapter 5. The main objective was to examine how the strata behave under different conditions. In other words, to understand at what extent the input parameters would have affected the overall results of the numerical modelling simulations. The parametric study was divided into two parts:

- Part 1

  The equilibrium state was calculated under different initial conditions. Only one parameter was changed at a time. This condition was saved; and restored later to make alterations. Six additional FLAC files were generated as shown in Table 6.1.

- Part 2

  Alterations were introduced at this stage. Nine different scenarios were evaluated and Table 6.2 shows summary of all files created.

6.2 THE EFFECT OF K RATIO

Two cases of ratio for horizontal to vertical stress were simulated. In case one, the value of k was 1, which meant that the horizontal stress was the same as the vertical stress at any given point on the geometry. For case two, k was 3, indicating that the horizontal stress was three times greater than the vertical stress.

6.2.1 The Case of k = 1

In Fig. 6.1, a valley bulging was observed. The green grid is the original grid before deformation and the purple grid represents the magnified deformed grid.

Valley bulging can also be observed by looking at the displacement vectors which point towards the centre of the valley. Fig. 6.1 also shows that the maximum displacement is about 97 mm for that particular region while the overall maximum displacement is about 281 mm. Note that displacement means the resultant components of horizontal and vertical displacement. Displacement at the surface in the vicinity of the monitoring station is about 28 mm. The profile of displacement versus applied lateral displacement at different monitoring stations for Simulation 2 (Model 2) is shown in Fig. 6.2. Fig. 6.2 shows that up until about 60 mm of Applied Lateral Displacement (ALD), the strata movement was very limited and between 60 mm and 80 mm of ALD, the ratio of strata movement increased significantly. It then increased slowly up until about 220 mm of ALD. When ALD passed 220 mm, the ratio of strata movement increased rapidly until it reached its maximum displacement. This trend was more noticeable at the surface or immediate sub-surface. The turning point defined previously is at about 18 meters below ground level, which is situated almost directly below the centre/base of the valley (refer to Fig. 6.3). At the centre of the turning point, it can be seen that the displacement vector is near zero indicating that the state of stress at turning point would be in compression. This is clearly evident in Fig. 6.4 that most of the regions are in compression except near the surface, particularly in the cliff regions.

6.2.2 The Case of k = 3

In Fig. 6.5, valley bulging is observed. However it is difficult to distinguish between Simulations 2 and 3 results by comparing Fig. 6.1 with Fig. 6.5 alone. Both display almost identical plots at the region of WRS 1. Fig. 6.6 through Fig. 6.11 show that the maximum displacement for both Simulations 2 and 3 is about the same, but the displacement profiles are different. Fig. 6.12 shows the turning point for Simulation 3, and it is at about 16 meters below the surface level. Fig. 6.13 shows plastic state for Simulation 3 after applying about 267 mm of lateral displacement. Although it was difficult to tell from Fig. 6.13 where yield conditions are first detected and how failure propagated, the movie file

"mod2.s3.dcx" which was submitted with this thesis shows that the yield condition was first detected at the base of the valley and propagated toward the artificial boundaries. Based on the yield condition and its trend it is possible to draw a conclusion that fracture will develop at the base of the valley under Simulation 3 conditions and propagate toward the artificial boundaries. At a depth of 6 meters below the bottom of valley, the fractured strata were likely to be in shear.

6.3 THE EFFECT OF REDUCTION FACTOR

In Simulation 1 the strength and stiffness parameters were 50 % of laboratory values. In additional simulations were performed based on different reduction factors. For the first case, the strength and stiffness of the strata was reduced by 75%. In the second case, it was reduced by 15%.

- 75% Reduction:

  Fig. 6.14 shows that valley bulging in Simulation 4 is more visible than in Simulation 1 (refer to Fig. 6.15). The turning point for Simulation 4 was around 20 meters below the surface level (refer to Fig. 6.16).

- 25% Reduction:

  When the strength and stiffness was reduced by 25%, the strata response to lateral displacement was insignificant compared to Simulation 1. Both Simulations 1 and 5 were able to accept about 274 mm of lateral displacement before the artificial boundaries interfered with the model results. Fig. 6.17 shows that the magnitude of the valley bulging was about the same as in Simulation 1 and that the general trend of strata behaviour was also the same. The turning point for Simulation 5 was at a depth of around 13 meters below the surface (Refer to Fig. 6.18).

6.4 THE EFFECT OF BEDDING PLANES

In Simulation 6, a bedding plane was included at 10 meters below the bottom of the valley. Only one bedding plane was assigned to the model to assess its effect on the surrounding areas. It must be noted that the inclusion of a bedding plane required extra time to reach the equilibrium state compared to a model that has no bedding planes. Fig. 6.19 shows the location of the assigned bedding plane in the model. The assigned bedding plane was assumed to be horizontal, and present across the model section, although in reality the bedding plane might not be lying horizontally nor straight. This was necessary to simplify the simulation process. The model plasticity indicators were monitored, following the application of 276 mm of lateral displacement. Fig. 6.20 shows the development of the failure pattern, which was indicated by the plasticity indicators. A failure mechanism is indicated if there is a contiguous line of active plastic zones 'with a state of 1 – purple colour' that joins the two surfaces (refer to Fig. 6.20). Note that initial plastic flow often occurred at the beginning of a simulation, but subsequent stress redistribution unloads the yielding elements so that their stresses no longer satisfy the yield criterion – these elements were represented by a state number of 2 (refer to Fig. 6.20). Only the actively yielding elements (represented by state of 1) are important to the detection of a failure mechanism. Considering the movie file, mod2.s6.dcx on the CD, it can be seen that the yield was first detected at the bottom of the valley and that plastic flow took place toward the artificial boundaries. Fig. 6.21 shows sliding of the bedding plane due to applied lateral displacement.

6.5 THE EFFECT OF PORE PRESSURE

In Simulation 7, an underground water table was included at a depth of 10 meters below the bottom of the valley. Vertical and horizontal stresses were initialised incorporating the pore pressure. Water flow was not simulated and the equilibrium ratio was set as 1×10^{-5}. After 246,430 steps, the equilibrium ratio was $2.183 \times$

10^{-5} and the maximum unbalanced force was 1.238 N. By monitoring the history plot of the maximum unbalanced force, it was determined that no further stepping was required beyond 246,430 steps. Fig. 6.22 shows the contours of pore pressure when the model was at its equilibrium state. Pore pressure was assumed to be zero above the water table and gradually increased below the water table. The contours of the pore pressure shown in Fig. 6.22 indicate that an error might have occurred while initialising the pore pressure. The same simulation was carried out using much smaller geometry to determine the cause of this problem. However, for the smaller geometry displayed there was no obvious error in the FLAC coding (refer to Fig. 6.23). No further simulation was carried out under Simulation 7 since the initial condition of model was not validated.

6.6 THE EFFECT OF MODEL LOADING SHAPE

The loading pattern was modified to study its effect on the model. The lateral displacement was applied in Simulation 8 as shown in Fig. 6.24. Valley bulging under this simulation was different from other simulations. Fig. 6.25 shows that strata moved mostly upward, and only small amount of lateral movement can be seen at the centre of the valley. Plastic flow for this simulation was quite different to other simulations as well. Fig. 6.26 shows that most of plastic flow took place at the centre of the model and near the bottom of the artificial boundary. Only a small area of plastic flow took place at the bottom of the valley. At the upper right hand side of the model, there were plastic indicators of 3, which means that the elements are in plastic tensile. But these elements were insignificant due to the limited plastic flow that took place.

6.7 THE EFFECT OF LOADING VELOCITY

Model 2 used a loading rate of 1×10^{-4} m/s. In addition, two other loading rates were simulated to study the effect of loading on the model. With Simulations 9 and 10, the loading rates were 1×10^{-3} m/s and 1×10^{-5} m/s respectively.

- Loading Velocity of 1×10^{-3} m/s:

The loading rate of 1×10^{-3} m/s was too fast. It caused the model to be unstable and detected plastic flow at the artificial boundary that did not correspond to a physical entity (refer to Fig. 6.27). Hence this solution was considered as not realistic, because of the mechanism of failure being influenced by a non-physical entity.

- Loading Velocity of 1×10^{-5} m/s:

The general trend in Simulation 10 was similar to Simulation 1 (at a loading rate of 1×10^{-4} m/s). Two distinguishable differences were only 181 mm (refer to Fig. 6.28) of lateral displacement, which could be applied before the artificial boundary influenced the mechanism of failure. There was no turning point to be seen in Simulation 10 and Fig. 6.29 shows that all displacement vectors are pointing laterally and upward.

6.8 SUMMARY

The following key points were noted:

- The ratio of horizontal to vertical stress did not have significant effect on the strata movements in the region of the valley bottom (and immediately underneath the base of the valley),

- The reduction of strata strength and stiffness properties has made noticeable change to overall behaviour of the strata movements. When 75% reduction was applied, it caused greater plastic flow than both the 25% and 50% of reduction,

- Shear separation of bedding planes was noticed when a weak bedding plane at 10 meters below the surface was added in the model,

- Incorporating pore pressure in the model proved to be complex. Knowing that pore pressure can be simulated in smaller scale geometry, it suggests that FLAC is geometrically sensitive and results are geometrically dependable,

- Simulation 8 shows that the model will behave differently when the loading pattern is changed. Under existing geometry, the loading pattern used in Simulation 8 would not be viable since the plastic flow took place at the centre of the model rather than at the bottom of the valley or near cliffs, and

- The model stability is sensitive to different rates of loading. Using a higher rate of loading caused instability of the model and caused plastic flow to occur at the artificial boundary particularly at the beginning of simulation.

Table 6.1 Summary of different initial conditions for parametric study in FLAC

Common file is Model 2 (file names are mod2.txt, mod2.ini), grid 190,114 K0x=2.0; 50 % reduction on strength and stiffness; no pore pressure; no bedding plane; model loading shape is →[ ]←; ***Simulation 1***			
Required File	Conditions	Saved File Names	Comment
mod2.2.txt ubi.fis mod2_mark.txt mod2_half_r_fish_properties.txt ininv.fis	Same as mod2.txt, except k0x=1	mod2.2.mark mod2.2.surface mod2.2.ini	Simulation 2
mod2.3.txt ubi.fis mod2_mark.txt mod2_half_r_fish_properties.txt ininv.fis	Same as mod2.txt, except k0x=3	mod2.3.mark mod2.3.surface mod2.3.ini	Simulation 3
mod2.4.txt ubi.fis mod2_mark.txt mod2_threequarter_r_fish_properties.txt ininv.fis	Same as mod2.txt, except reduction of 75 %	mod2.4.mark mod2.4.surface mod2.4.ini	Simulation 4
mod2.5.txt ubi.fis mod2_mark.txt mod2_quarter_r_fish_properties.txt ininv.fis	Same as mod2.txt, except reduction of 25 %	mod2.5.mark mod2.5.surface mod2.5.ini	Simulation 5
mod2.6.txt ubi.fis mod2_mark.txt mod2_half_r_fish_properties.txt ininv.fis	Same as mod2.txt, except it includes bedding plane	mod2.6.mark mod2.6.surface mod2.6.ini	Simulation 6
mod2.7.txt ubi.fis mod2_mark.txt mod2_half_r_fish_properties.txt ininv_1.fis	Same as mod2.txt, except it includes pore pressure	mod2.7.mark mod2.7.surface mod2.7.ini	Simulation 7

Table 6.2 Summary of different scenarios performed in FLAC

Common file is Model 2 (file names are mod2.txt, mod2.ini), grid 190,114 K0x=2.0; 50 % reduction on strength and stiffness; no pore pressure; no bedding plane; model loading shape is →[ ]←; ***Simulation 1***			
Required File	Conditions	Saved File Names	Comment
Mod2.s2.txt, mod2_hist.txt	K0x=1	Mod2.s2.dcx Mod2.s2	Simulation 2
Mod2.s3.txt, mod2_hist.txt	K0x=3	Mod2.s3.dcx Mod2.s3	Simulation 3
Mod2.s4.txt, mod2_hist.txt	Reduction factor = quarter	Mod2.s4.dcx Mod2.s4	Simulation 4
Mod2.s5.txt, mod2_hist.txt	Reduction factor = three-quarter	Mod2.s5.dcx Mod2.s5	Simulation 5
Mod2.s6.txt, mod2.6_hist.txt	Bedding plane	Mod2.s6.dcx Mod2.s6	Simulation 6
Mod2.s7.txt, mod2_hist.txt	Pore pressure	Mod2.s7.dcx Mod2.s7	Simulation 7
Mod2.s8.txt, mod2_hist.txt	Loading shape: →⟨ ⟩←	Mod2.s8.dcx Mod2.s8	Simulation 8
Mod2.s9.txt, mod2_hist.txt	Loading velocity: 1e-3 m/s	Mod2.s9.dcx Mod2.s9	Simulation 9
Mod2.s10.txt, mod2_hist.txt	Loading velocity: 1e-5 m/s	Mod2.s10.dcx Mod2.s10	Simulation 10

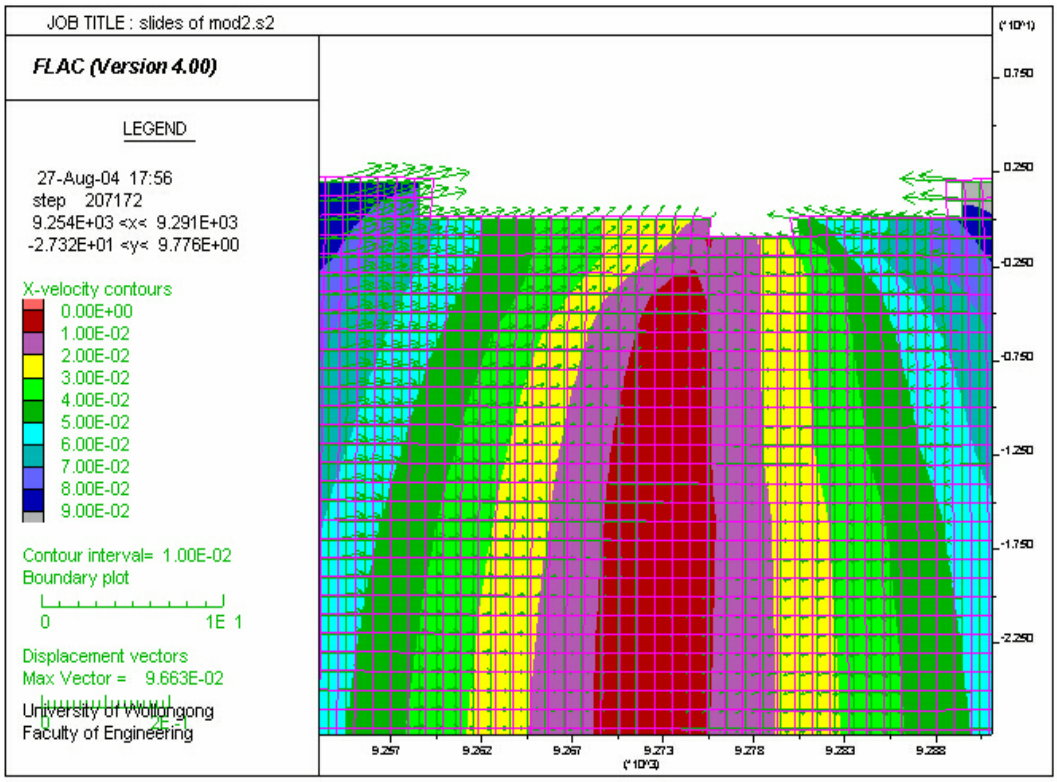

Figure 6.1 Magnified displacement contours with vectors for Simulation 2

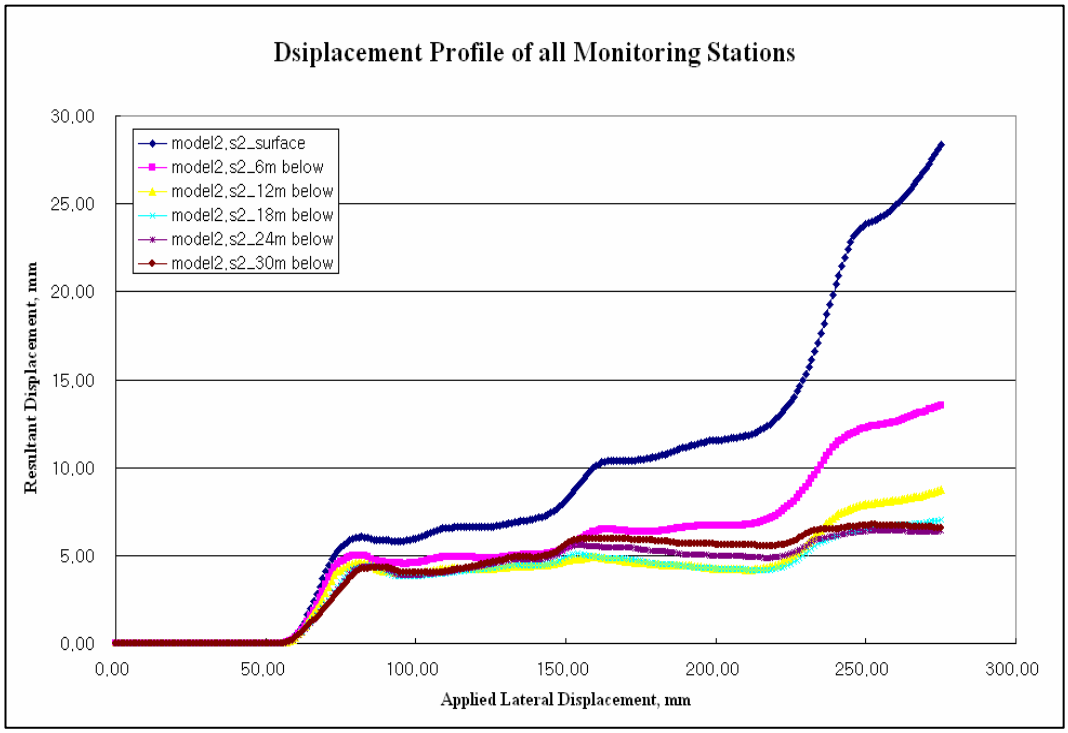

Figure 6.2 Displacement profiles for all monitoring stations for Simulation 2

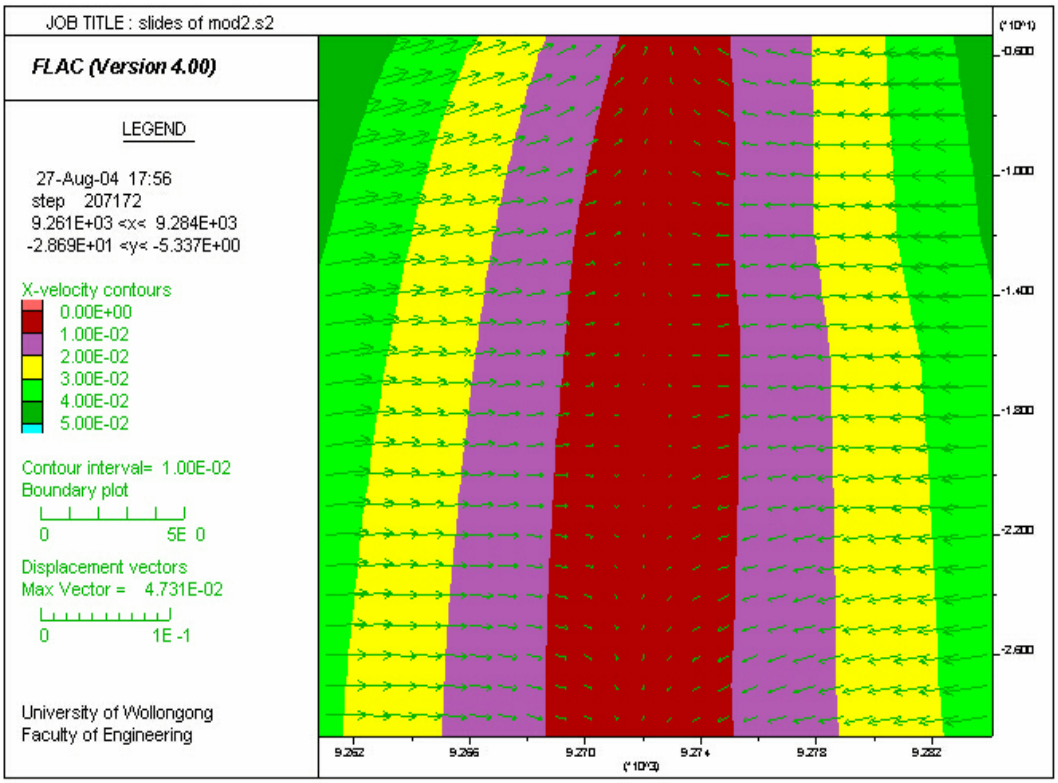

Figure 6.3 Displacement contours with vectors for Simulation 2

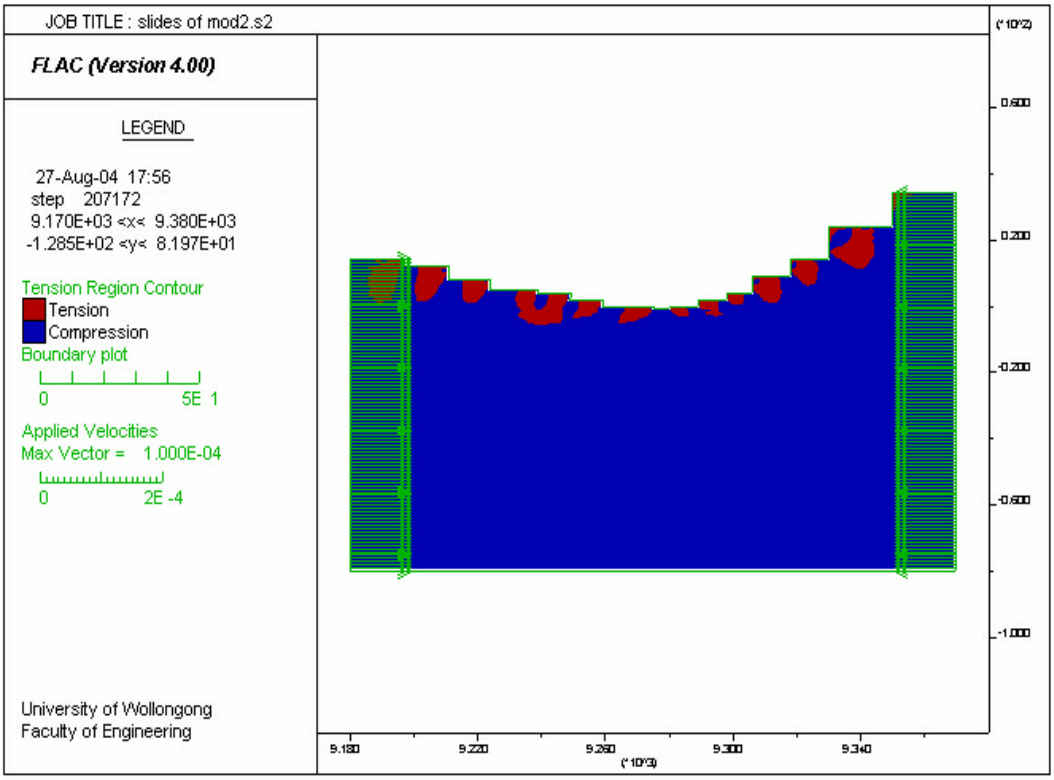

Figure 6.4 Region contours of tension and compression for Simulation 2

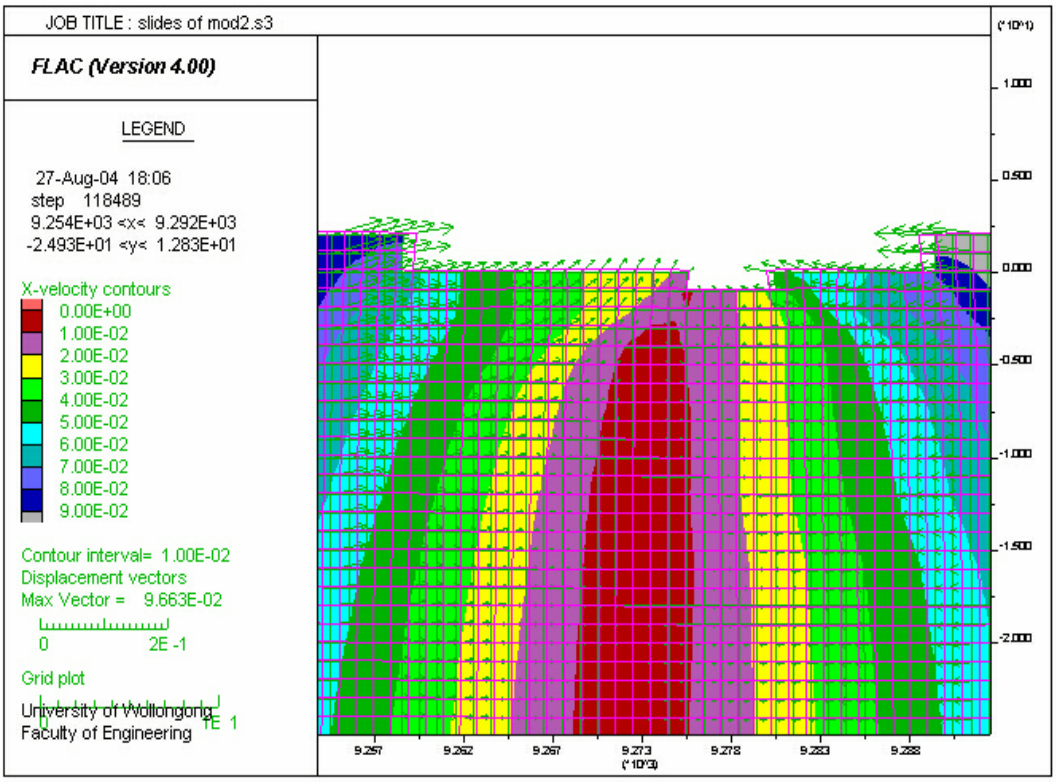

Figure 6.5 Magnified displacement contours with vectors for Simulation 3

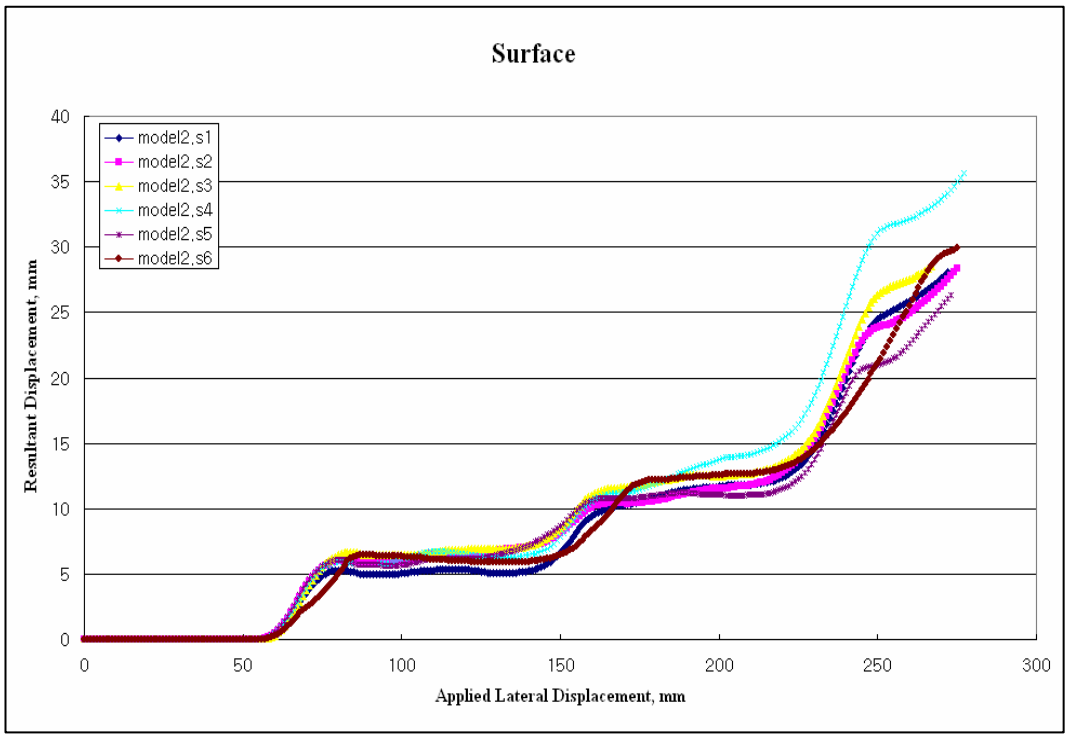

Figure 6.6 Displacement profiles for Simulations 1 to 6 at surface level

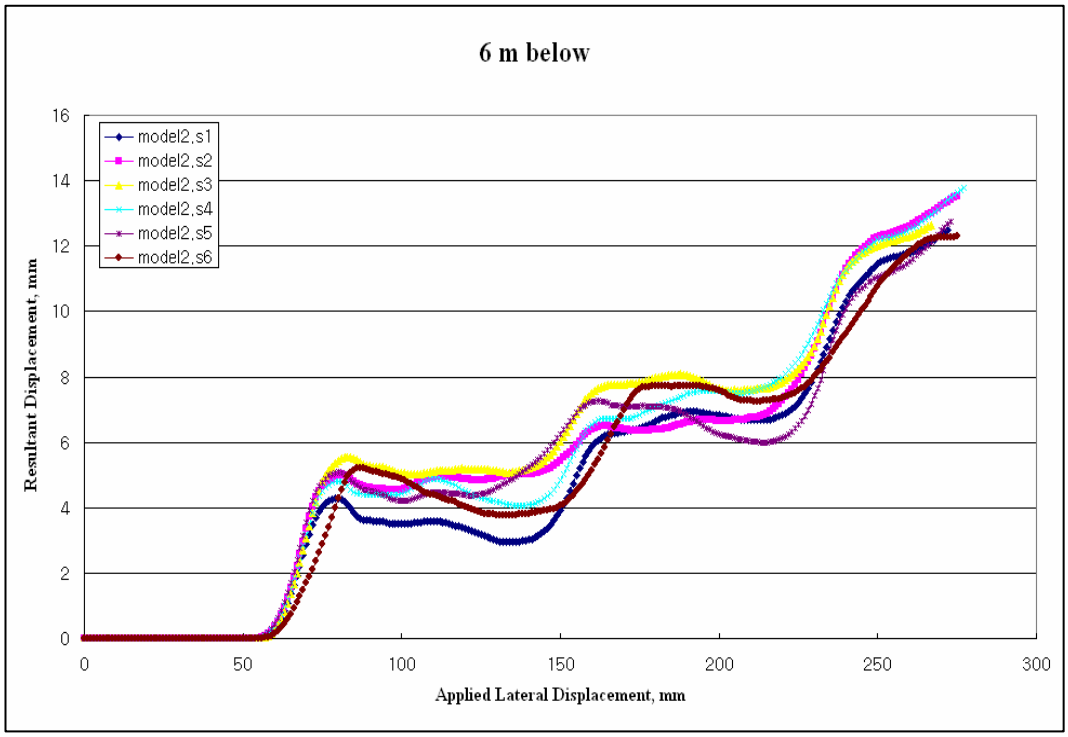

Figure 6.7 Displacement profiles for Simulations 1 to 6 at 6 m below surface level

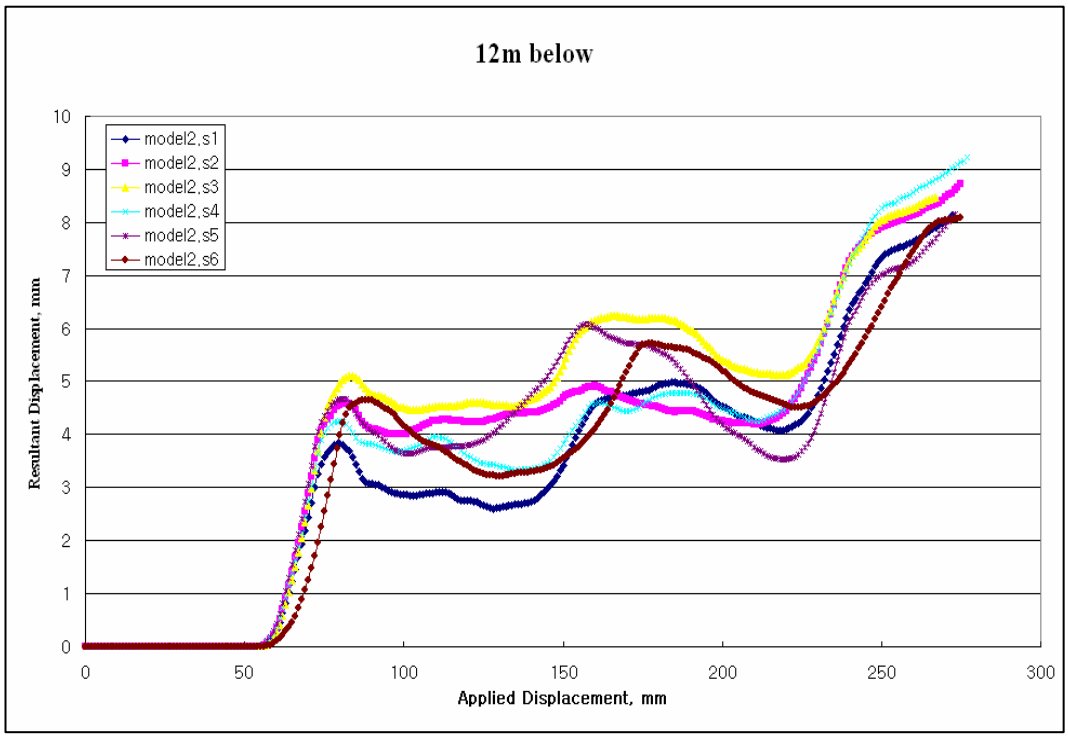

Figure 6.8 Displacement profiles for Simulations 1 to 6 at 12 m below surface level

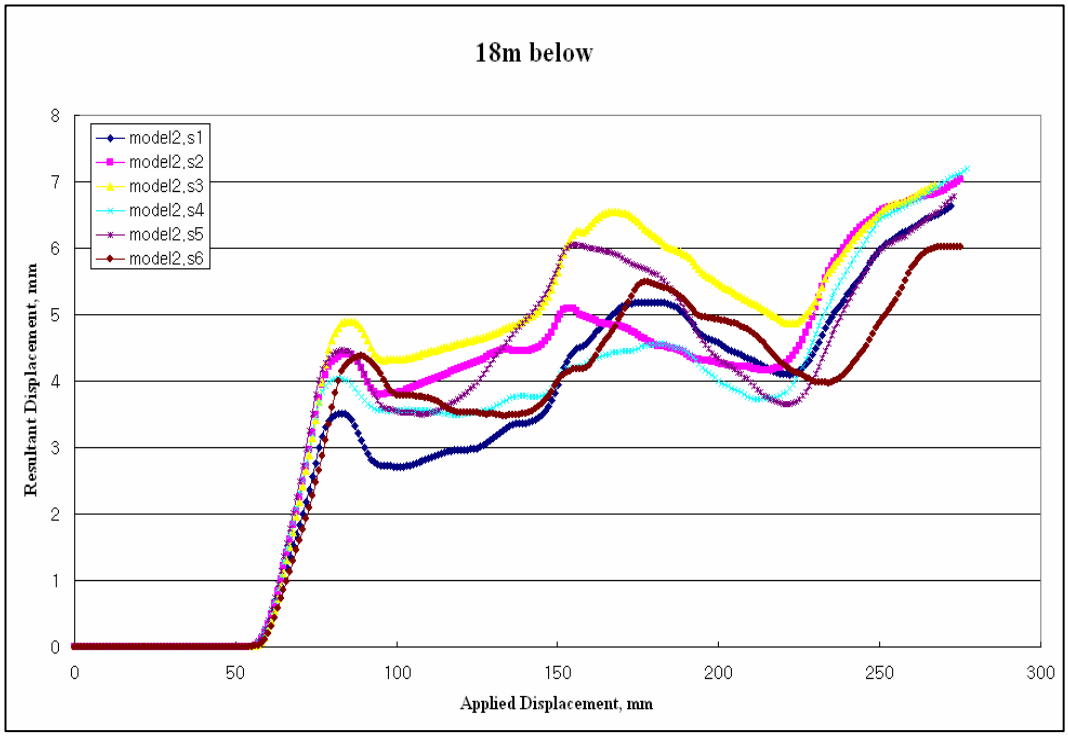

Figure 6.9 Displacement profiles for Simulations 1 to 6 at 18 m below surface level

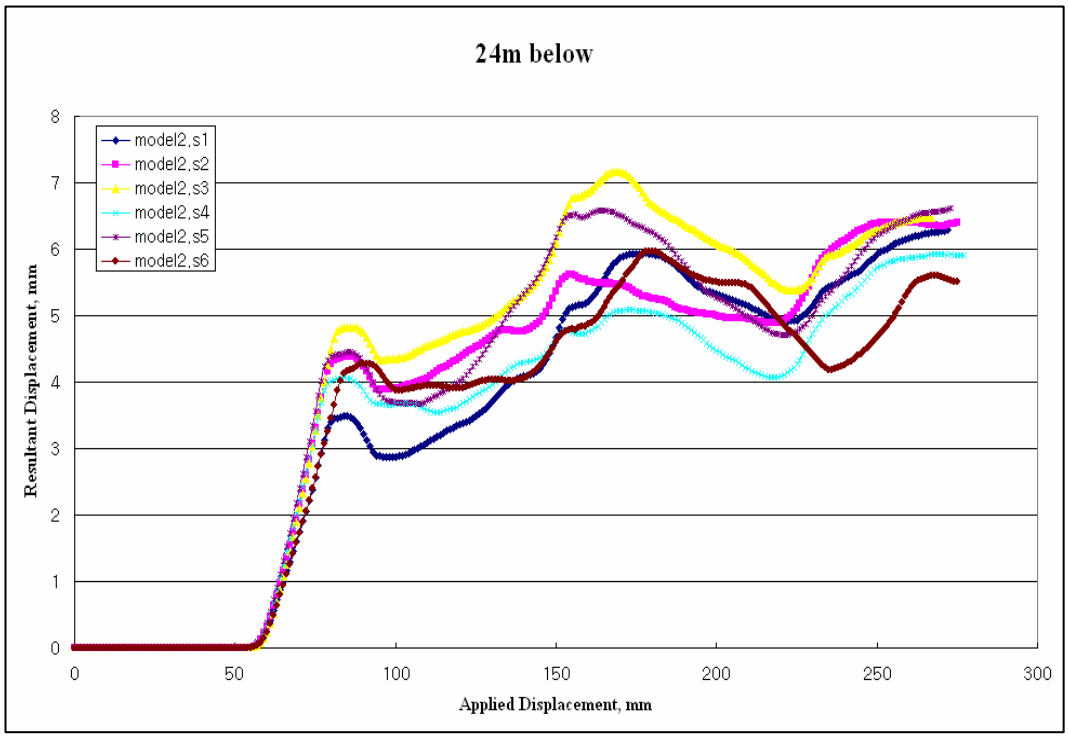

Figure 6.10 Displacement profiles for Simulations 1 to 6 at 24 m below surface level

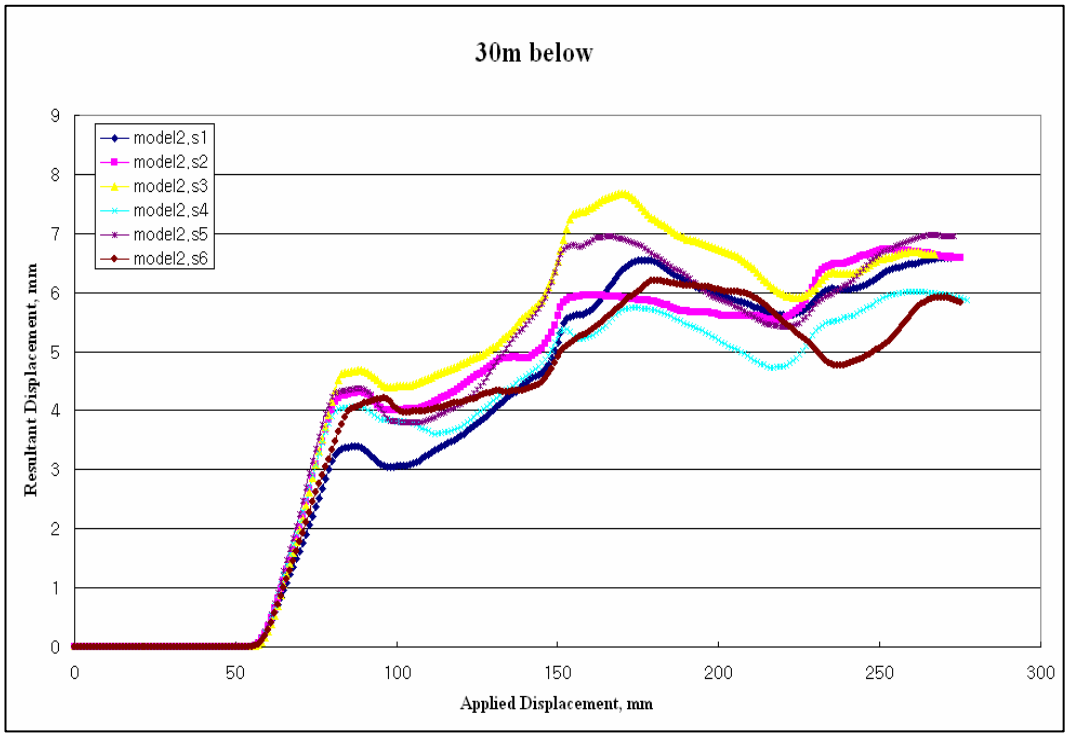

Figure 6.11 Displacement profiles for Simulations 1 to 6 at 30 m below surface level

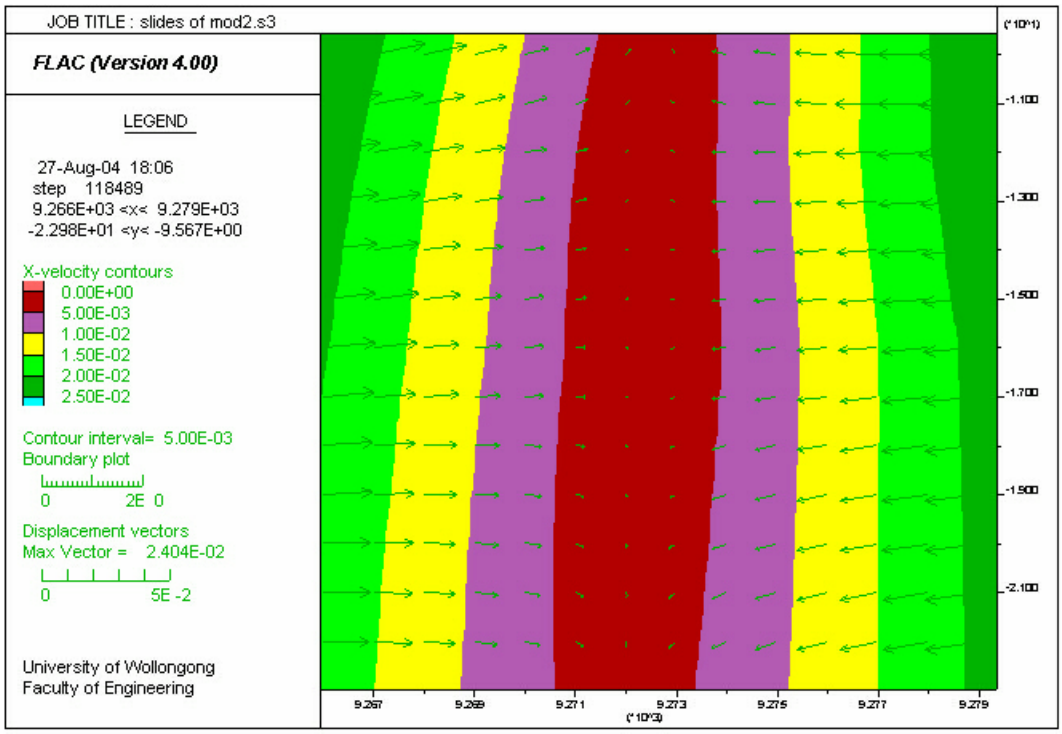

Figure 6.12 Displacement contours with vectors for Simulation 3

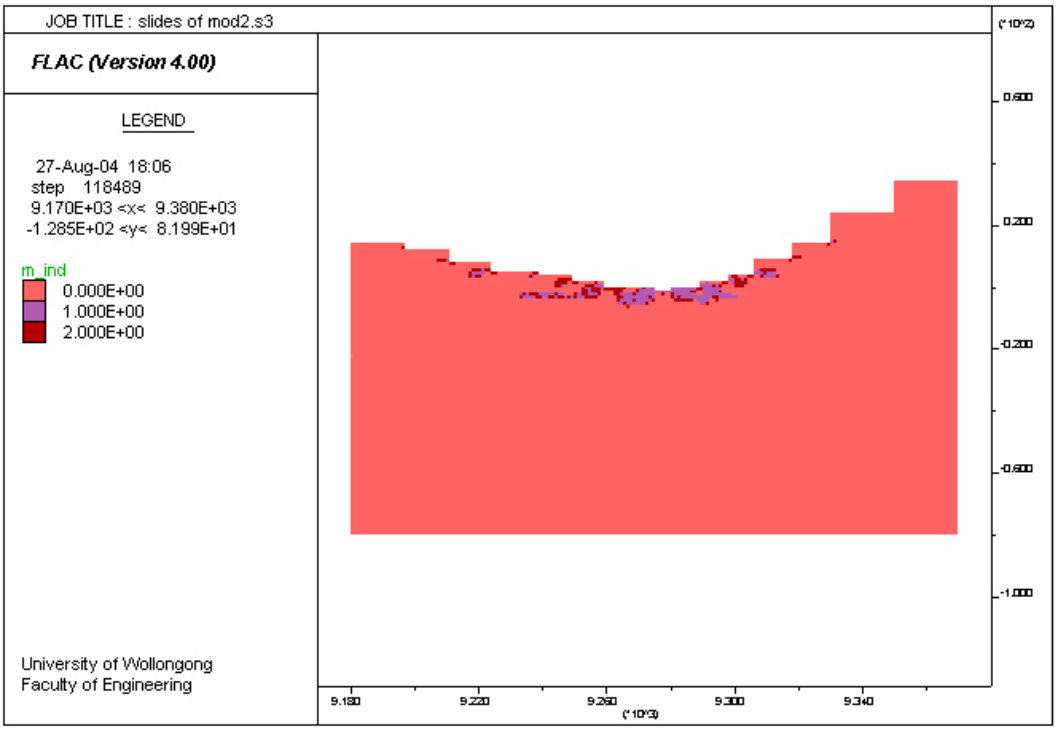

Figure 6.13 Plastic state for Simulation 3 after applying 267 mm of lateral displacement

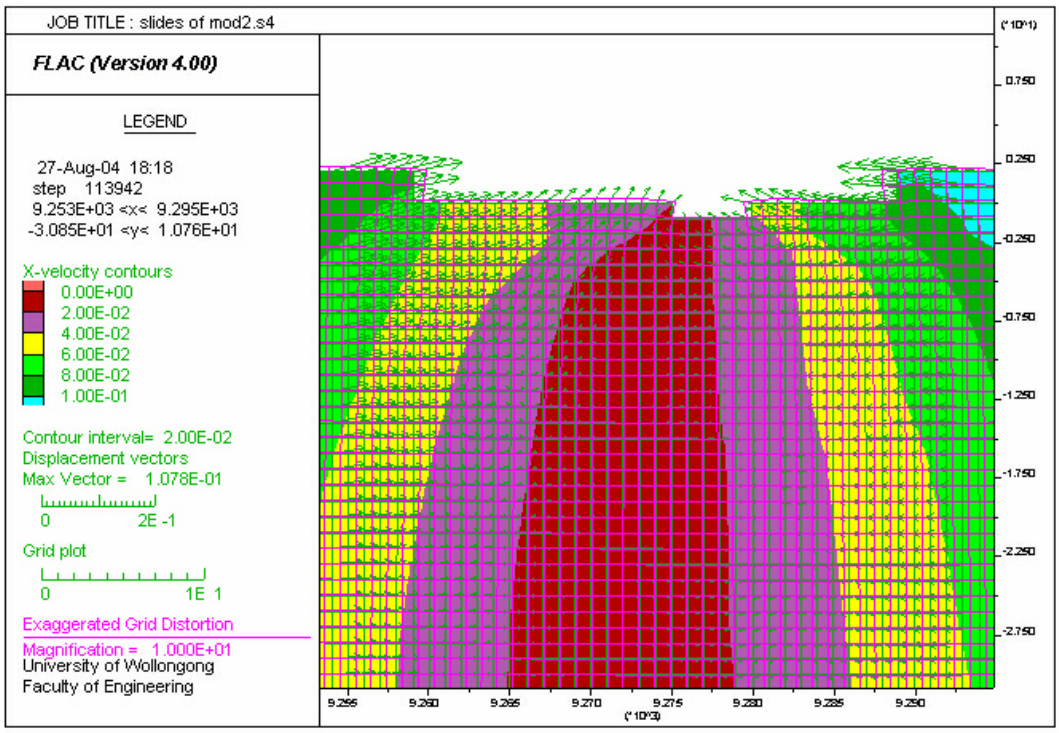

Figure 6.14 Magnified displacement contours with vectors for Simulation 4

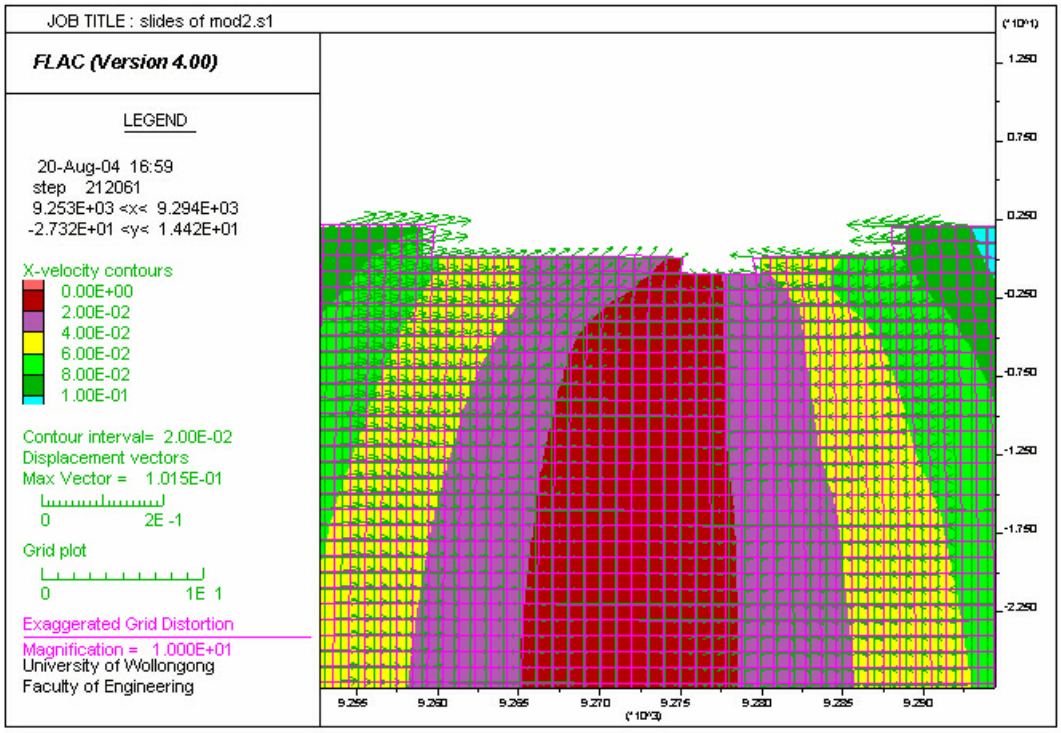

Figure 6.15 Magnified displacement contours with vectors for Simulation 1

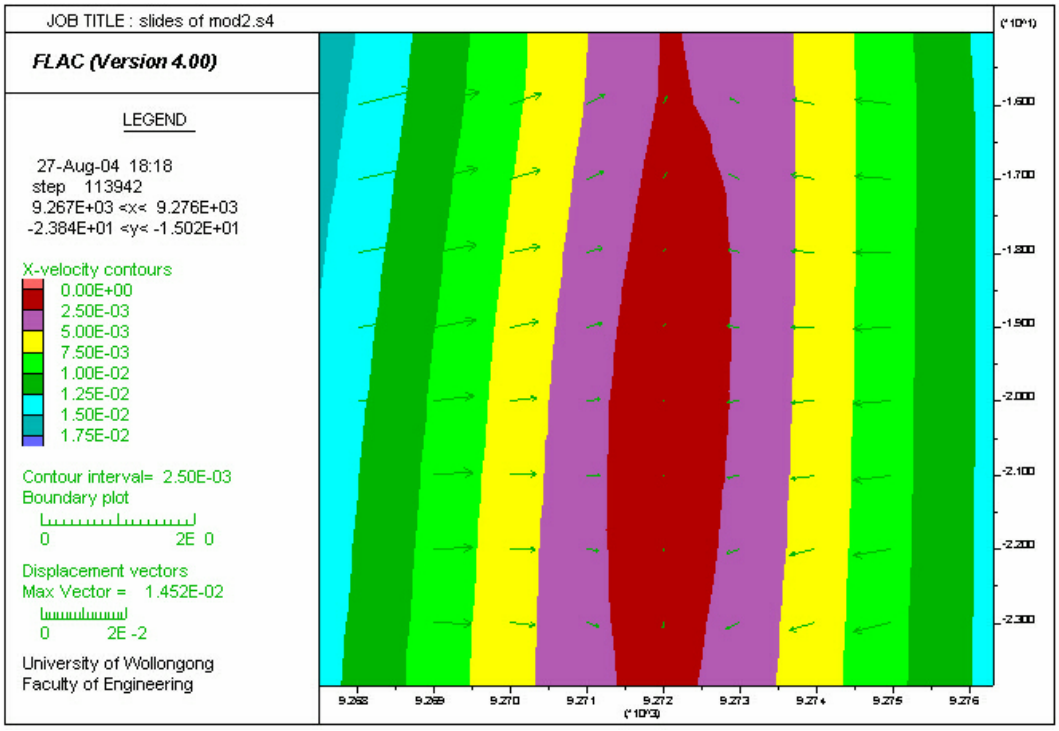

Figure 6.16 Displacement contours with vectors for Simulation 4

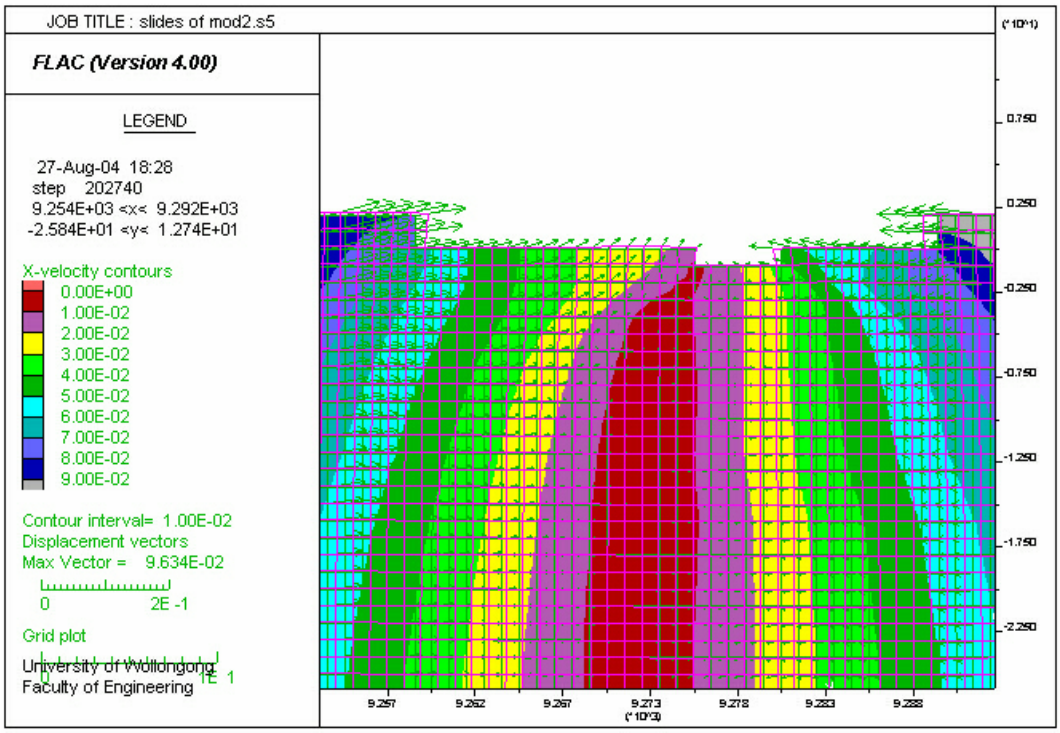

Figure 6.17 Magnified displacement contours with vectors for Simulation 5

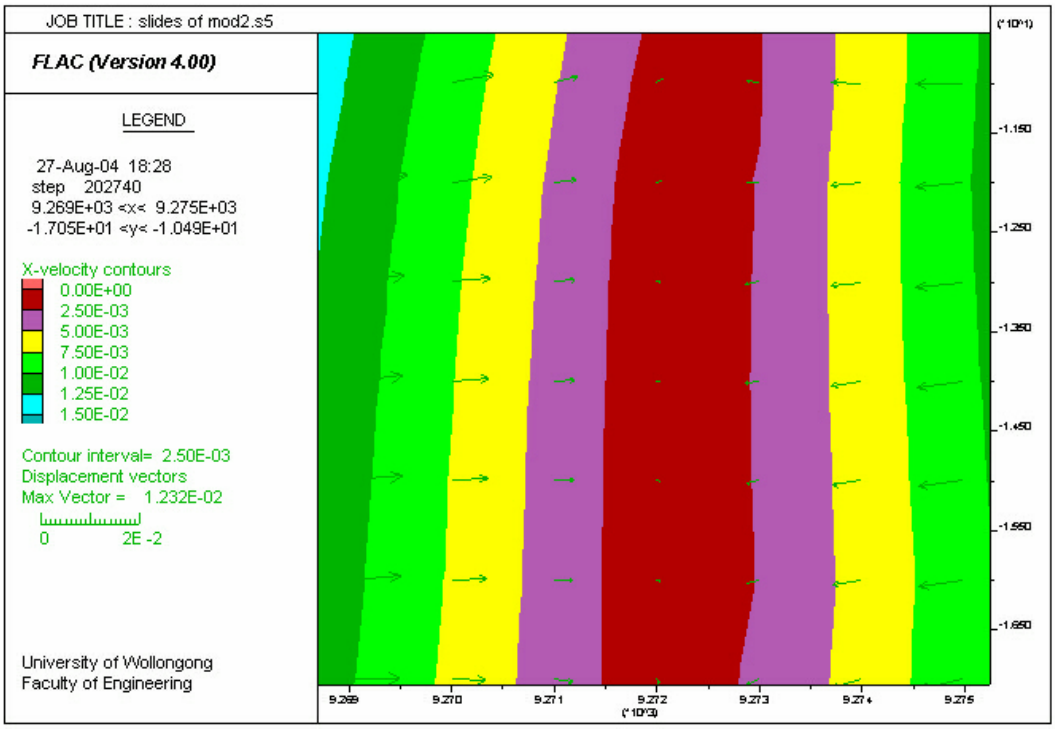

Figure 6.18 Displacement contours with vectors for Simulation 5

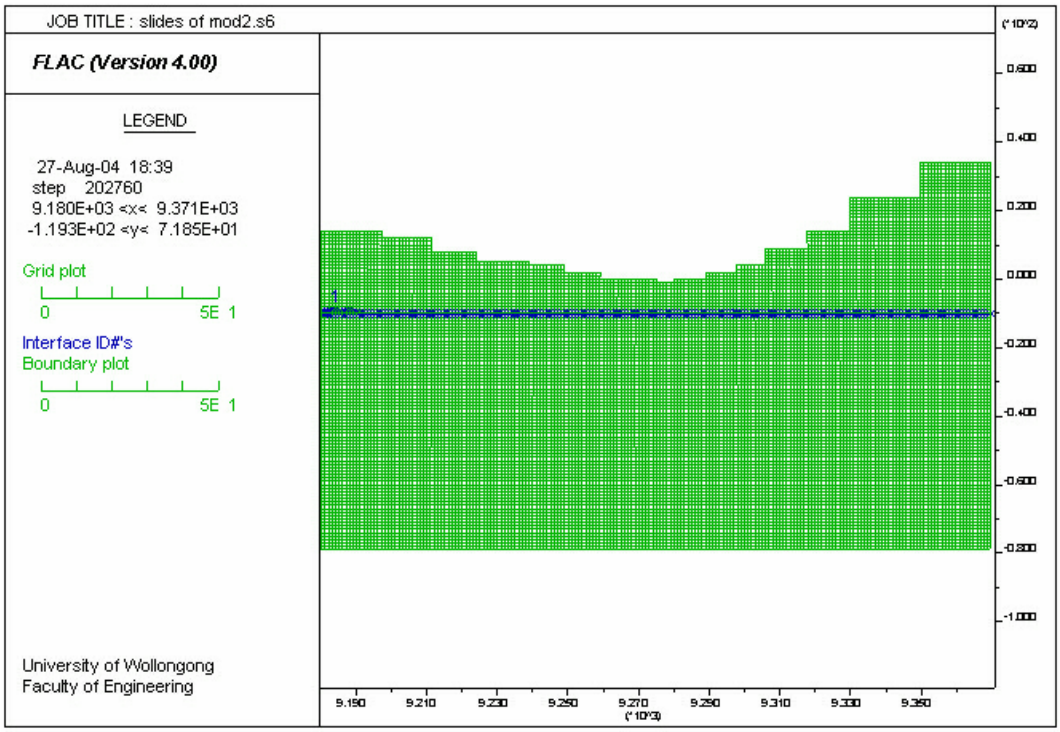

Figure 6.19 Location of bedding plane in Simulation 6

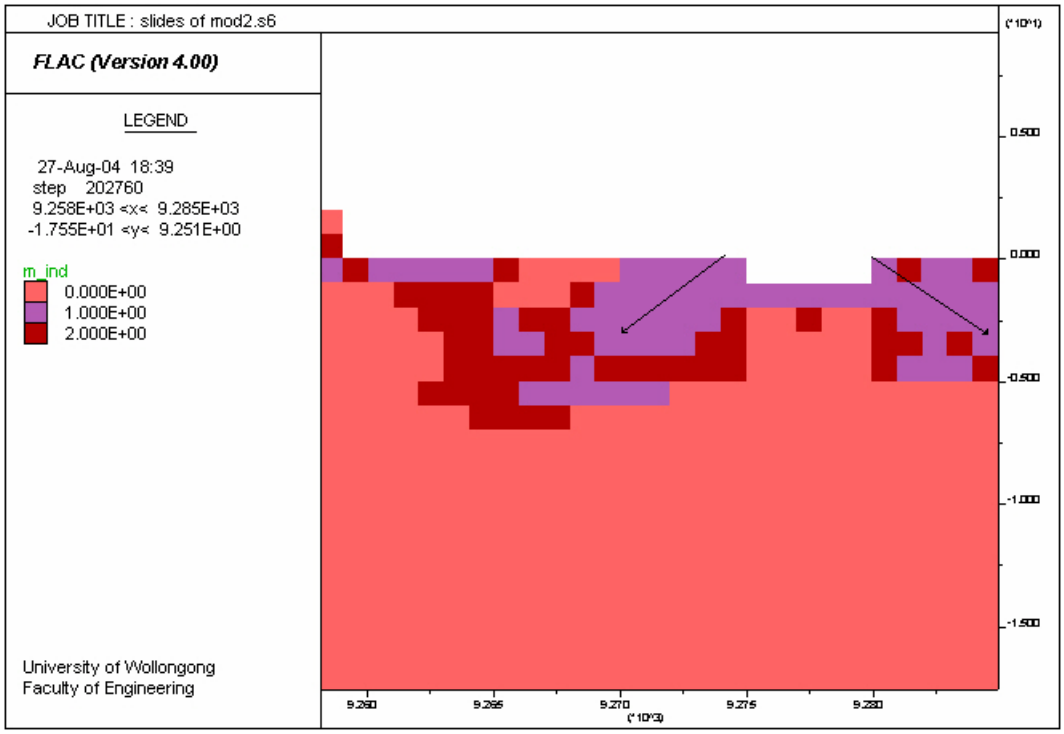

Figure 6.20 Plastic state for Simulation 6 after applying 276 mm of lateral displacement

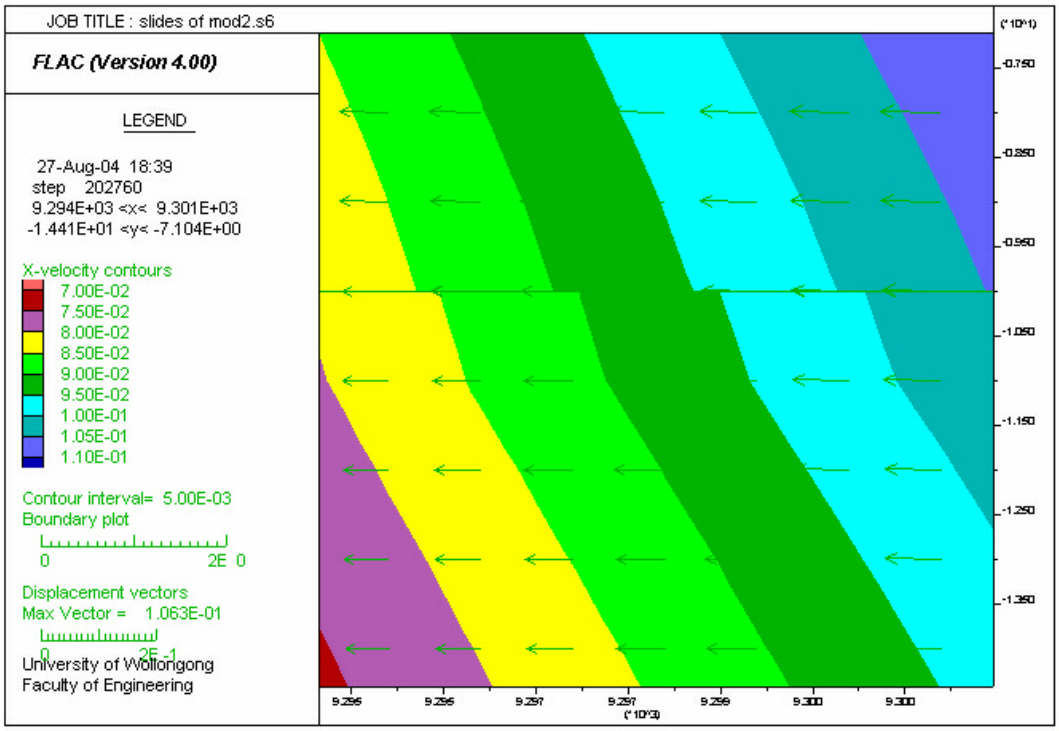

Figure 6.21 Sliding of bedding plane in Simulation 6

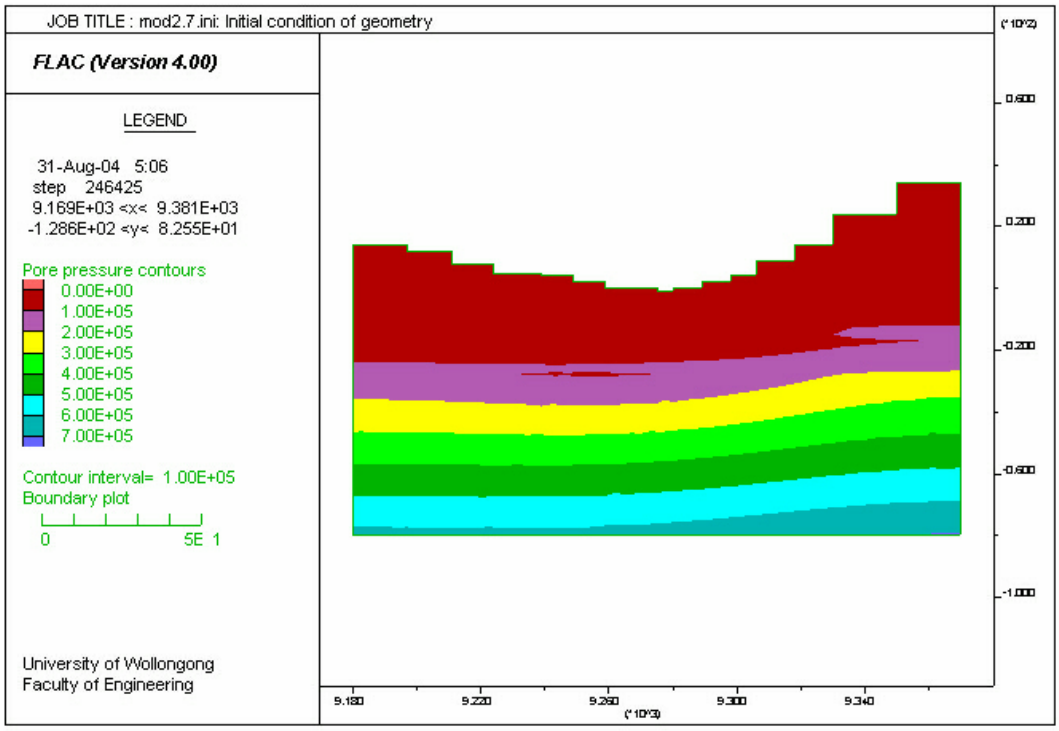

Figure 6.22 Contours of pore pressure in Simulation 7

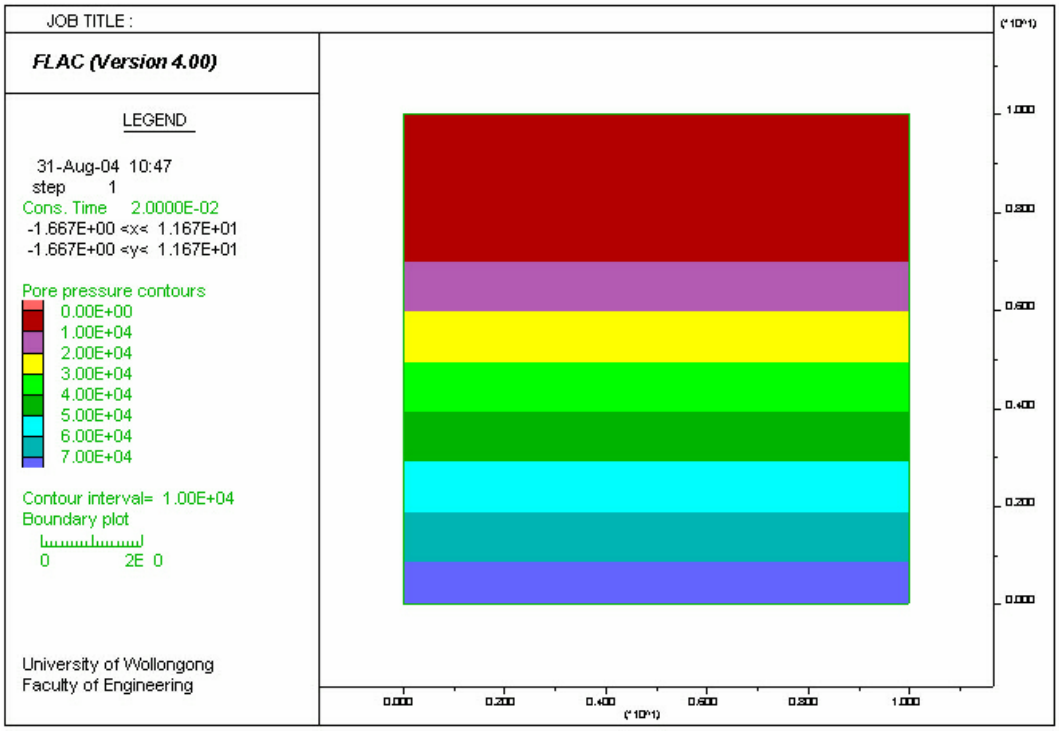

Figure 6.23 Contours of pore pressure for smaller geometry in comparison with Simulation 7

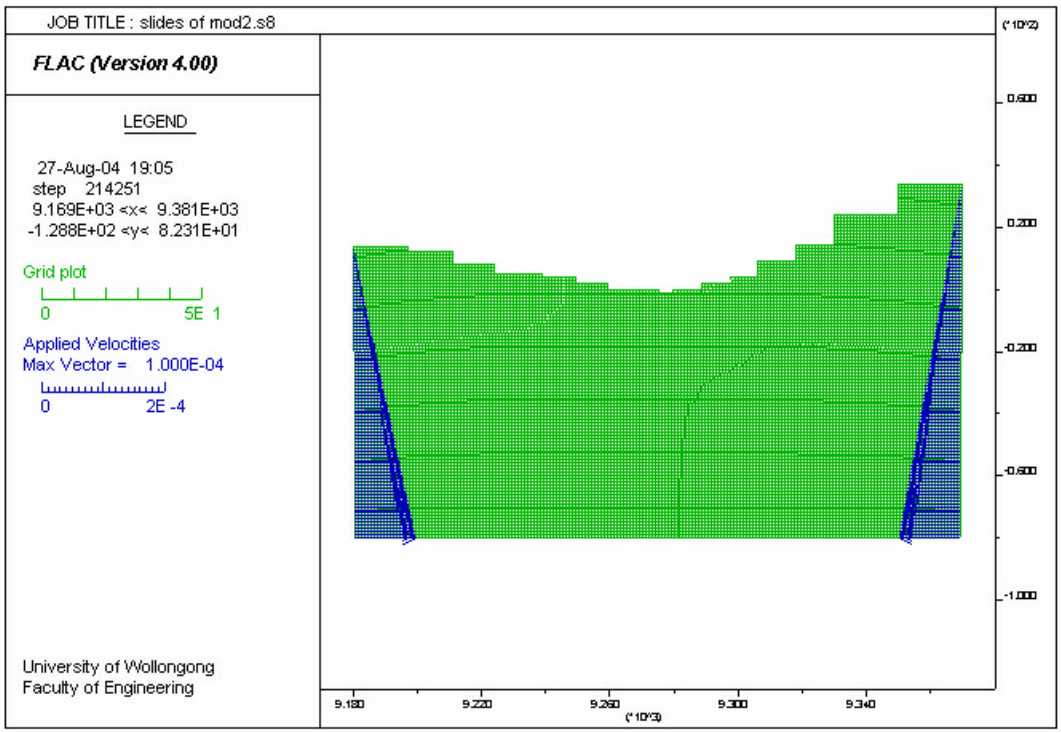

Figure 6.24 Loading pattern for Simulation 8

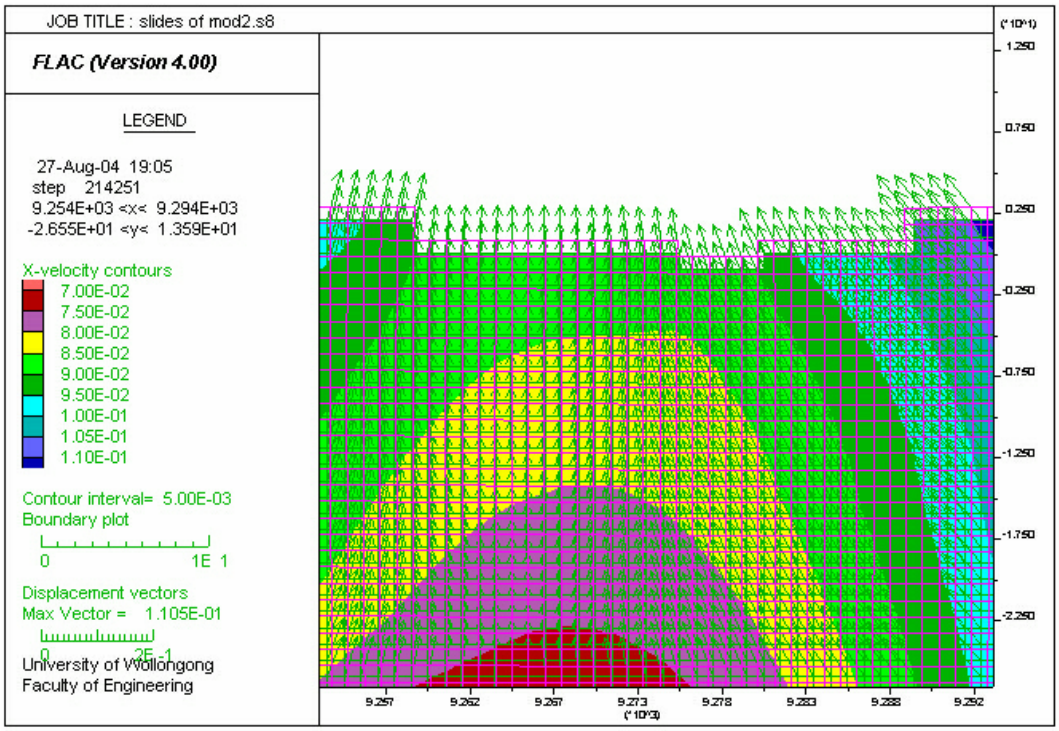

Figure 6.25 Magnified displacement contours with vectors for Simulation 8

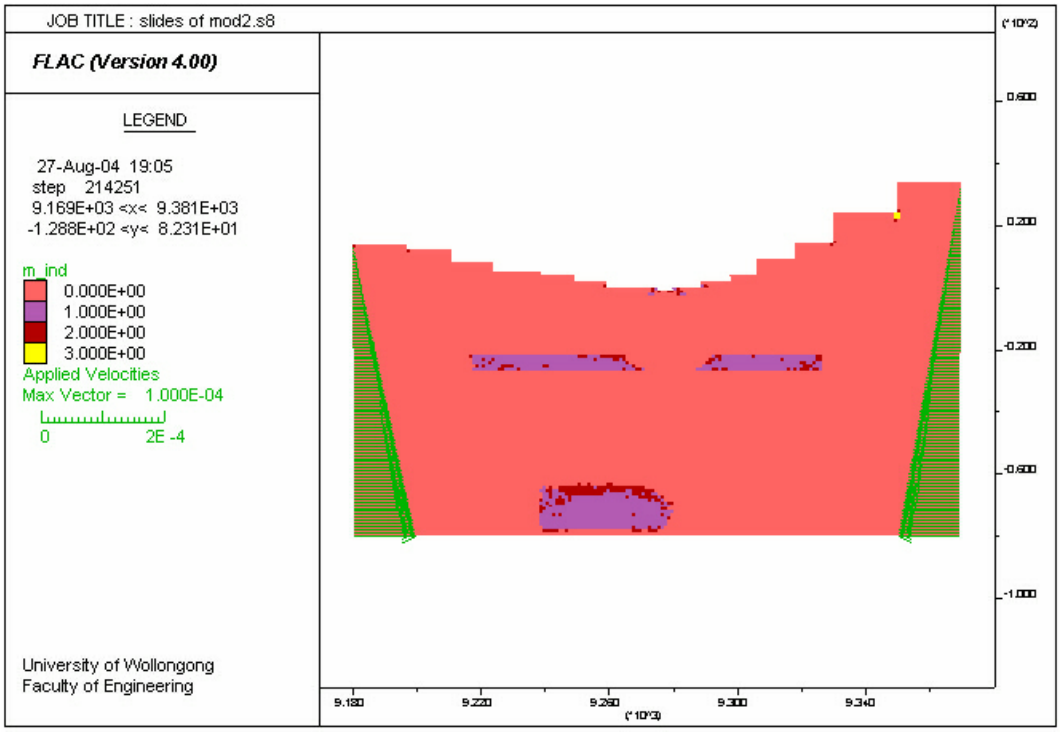

Figure 6.26 Plastic state for Simulation 8 after applying 492 mm of lateral displacement

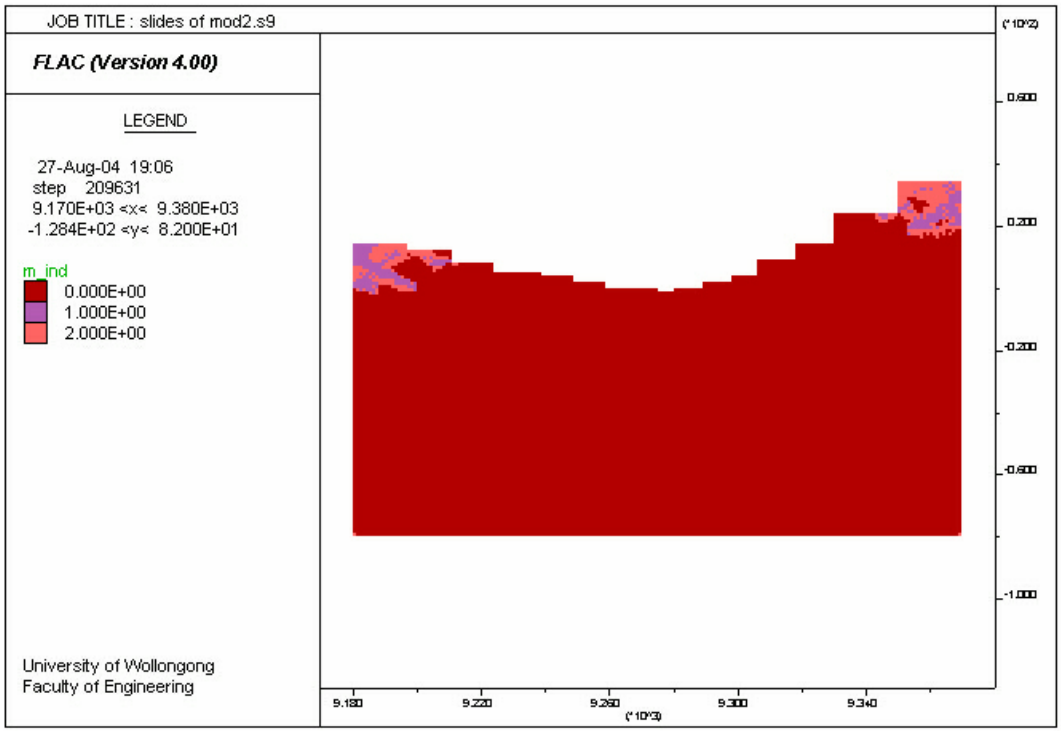

Figure 6.27 Plastic state for Simulation 9 after applying 30 mm of lateral displacement

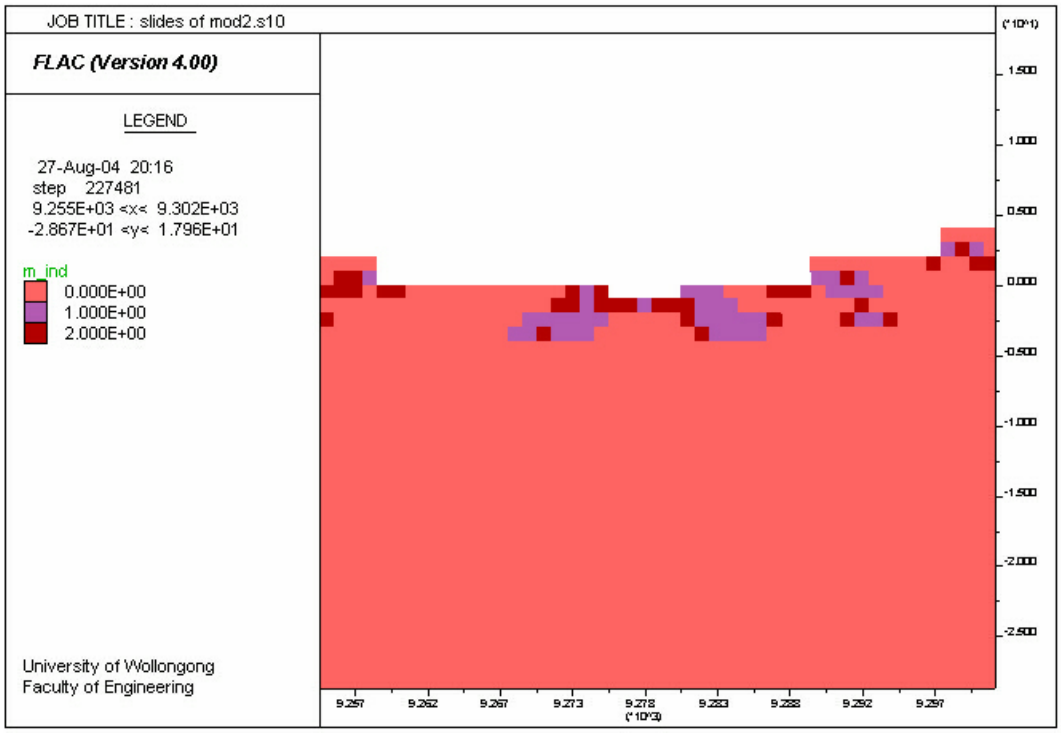

Figure 6.28 Plastic state for Simulation 10 after applying 181 mm of lateral displacement

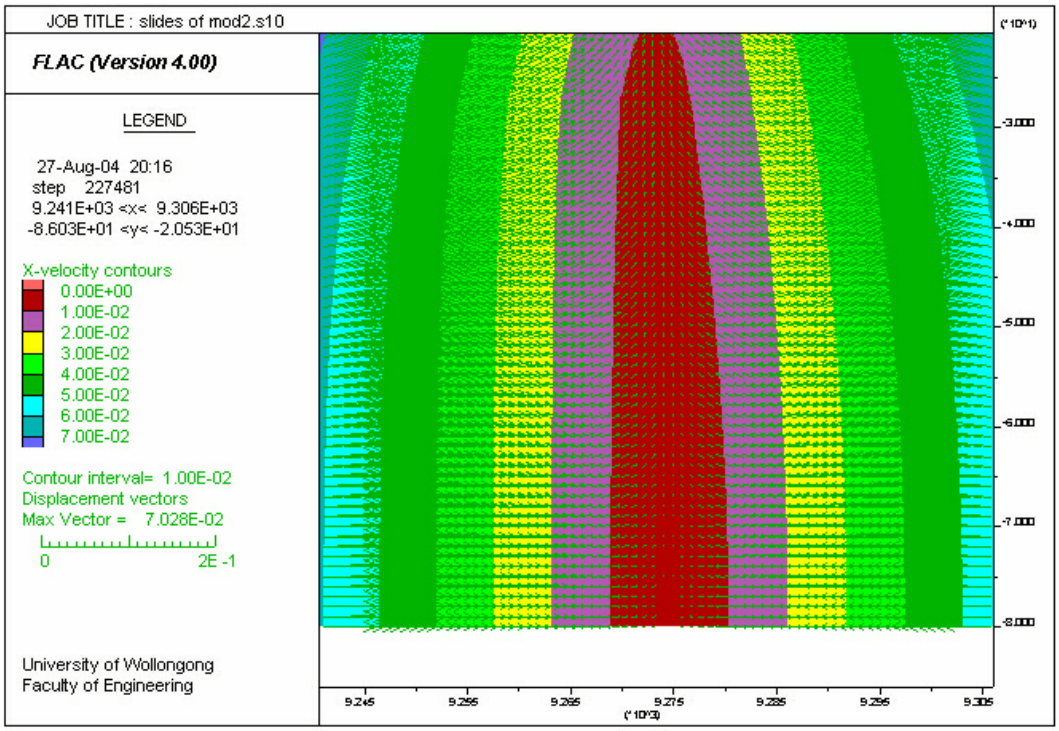

Figure 6.29 Displacement contours with vectors for Simulation 10

CHAPTER 7
CONCLUSIONS AND RECOMMENDATIONS

7.1 CONCLUSIONS

The following conclusions were inferred from the application of FLAC to numerical simulation of the ground deformation in river gorges and valleys:

a) It was possible to successfully simulate ground deformation in river gorges and valley. The quality of the simulation was dependent on the quality and accuracy of the input parameters. The user is at liberty to select and use the parameters of his/her choice in order to obtain the best simulation.

b) A number of indicators were used to assess the state of the numerical model. Indicators such as unbalanced force, grid velocities, plastic indicators and monitoring history of particular interest variables were used to find out what the system was capable of doing and the state of model.

c) FLAC is a geometrically dependent program, and any small changes in model geometry could produce different results. The density of zoning influences the program running time and accuracy of the model results, and accordingly mesh convergence tests should be applied to any particular case under investigation.

d) Model 2 is the optimum model size, and represents the ideal size for further studies under different environments. Using Model 2 as a base, a number of simulations were performed with one parameter being changed at a time.

e) During the simulation process, it was observed that the ratio of horizontal to vertical stress did not have significant impact on the overall results. However, different values of strata properties were found to have considerable impact on the model response. It is also observed that the bedding plane caused shear separation of bedding. Inclusion of more bedding planes and joints in the model with more details such as joint angles with known properties will definitely have an impact on valley bulging of the floor and closure of the valley. Above all, the loading pattern and rate of loading played an important role in the overall results.

7.2 RECOMMENDATIONS

It is recommended that future studies should apply the findings from this thesis to different sites. Where possible, inclusion of bedding planes or joints with known properties would enhance overall results. FLAC might experience some difficulties of simulating multiple joints or bedding planes. For this reason, the author recommends to employ another numerical tool such as UDEC. Further studies are also required for strata interaction when an underground water table is present in the model.

REFERENCES

1. Bieniawski, Z.T., 1974, Estimating the Strength of Rock Materials, J.S. Afr. Inst. Min. Metall., 74, pp.312-320.

2. Brace, W.F., 1963, Brittle Fracture of Rocks, Int. Conf. State of Stress in the Earth's Crust, Santa Monica, California, pp.110-174.

3. Brady, B.H.G. & Brown, E.T. 1993, Rock Mechanics for Underground Mining, 2nd edn, Chapman & Hall, London, 571p.

4. Brown, E.T. and Hoek, E. 1978, Trends in relationships between measured in-situ stresses and depth. International Joint Rock Mechanics Mining Science and Geomechanics, Volume 15, pp.211-215.

5. Central Mapping Authority of NSW [Map] Topographic Maps, 1:25000, Zone 56/I Appin 9029-I-S, 6212700 N 309250 E.

6. Fell, R., Hungr, O., Leroueil, S. and Riemer, W., 2000, Geomechanical Engineering of the Stability of Natural Slopes, and Cuts and Fills in Soils. GeoEng 2000, Proceedings of the International Conference on Geotechnical and Geological Engineering, Melbourne, Australia. Int. Soc. For Rock Mechanics, pp.21-120.

7. Fell, R., MacGregor, P. and Stapledon, D., 1992, Weathering Processes and Profiles in Valleys. Geotechnical Engineering of Embankment Dams. Balkema, 675p.

9 Geoscience Australia, Australia Government., Department of Industry, Tourism and Resources [Online] www.ga.gov.au/Free Data Downloads [Accessed July 2003].

10 Griggs, D. and Handin, J., 1960, Observations on fracture and a hypothesis of earthquakes. Geol. Soc. Am. Memoir 79, pp.347-364.

11 Heard, H.C., 1963, "The Effect of Large Changes in Strain Rate in the Experimental Deformation of Rocks", Journal of Geology, Vol. 71, p162.

12 Hoek, E. and Brown, E.T., 1980, Underground Excavations in Rock, London, Inst. Min. Metall, 525p.

13 Hooker, V.E., Bickel, D.L. and Aggson, J.R. 1972, In-situ Determination of Stresses in Mountainous Topography, US Bur. Mines Rep. Invest. 7654.

14 Hutchinson, J.N., 1987, Mechanisms Producing Large Displacements in Landslides on Pre-existing Shears, Memoir of the Geological Society of China, No. 9, pp.175-200.

15 Itasca Consulting Group, 2001a. FLAC Manual: FISH in FLAC. Minneapolis, MN: Itasca Consulting Group.

16 Itasca Consulting Group, 2001b. FLAC Manual: Fluid-Mechanical Interaction. Minneapolis, MN: Itasca Consulting Group.

17 Itasca Consulting Group, 2001c. FLAC Manual: Theory and Background. Minneapolis, MN: Itasca Consulting Group.

18 Itasca Consulting Group, 2001d. FLAC Manual: User's Guide. Minneapolis, MN: Itasca Consulting Group.

19 Johnston, I.W., 1985, Strength of Intact Geomechanical Materials, J. Geotech. Eng. Div., ASCE, Vol. 111, pp.730-749.

20 Jumikis, A.R., 1979, Rock Mechanics, 1st edn, Trans Tech Publications, Germany, 356p.

21 McClintock, F.A. and Walsh, J.B., 1962, Friction on Griffith Cracks in Rocks Under Pressure. 4th U.S. Nat. Cong. Appl. Mech., Berkeley, California, Vol. 2, pp.1015-1021.

22 Metropolitan Colliery, July 2002, Metropolitan Colliery Subsidence Coordinates, Metropolitan Colliery Survey, Wollongong.

23 Mills, K., 2002, Report to Metropolitan Colliery (MET2367): In-situ Measurements and Installation of Monitoring Instruments at WRS 1, report of investigation, Strata Control Technology (SCT) Pty. Ltd., Wollongong, 53p.

24 Mohammad, N., Reddish, D.J. and Stace, L.R., 1997, The Relation Between In-situ and Laboratory Rock Properties Used in Numerical Modeling, Int. J. Rock Mech. Min. Sci. Vol. 34, No. 2, pp.289-297.

25 Obert, L., and Duvall, W.I., 1967, Rock Mechanics and the Design of Structures in Rock, John Wiley and Sons, Inc., New York, 495p.

26 Patton, F.D. and Hendron, A.J., 1972, General Report on Mass Movements, Proc. 2nd Intl. Congress of International Association of Engineering Geology, pp.1-57.

27 Vutukuri, V.S. & K. Katsuyama, K., 1994, Introduction to Rock Mechanics, Industrial Publishing & Consulting, Inc, 275p.

28 Waddington, A.A., and Kay, D.R., June 2002, Management Information Handbook on the Undermining of Cliffs, Gorges and River Systems, ACARP Projects No. C9067, Chapter 6.

APPENDIX A
FAILURE CRITERIA

1. Maximum Tensile Stress Criterion

The material is assumed to fracture in tension if the minimum principal stress σ_3 is equal or less than the uniaxial tensile strength σ_t. This is formulated in Equation A.1:

$$\sigma_3 = -\sigma_t \tag{A.1}$$

2. Coulomb's Shear Strength Criterion

This criterion postulated that shear strength of rock is made up of two parts – a constant cohesion and a normal stress-dependent frictional component. Thus, the shear strength can be developed on a plane such as *ab* in Fig. A1.

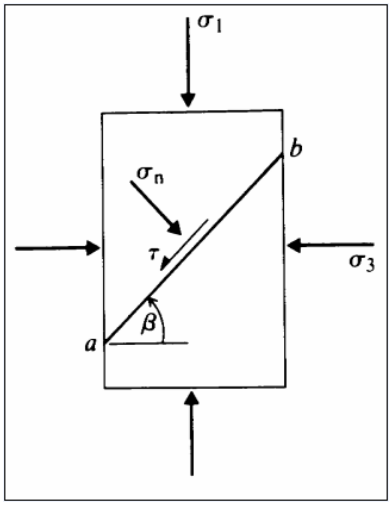

Figure A.1 Shear Failure on Plane *ab*

Fig. A1 can be transformed to different equations as follows:

$$\sigma_n = \frac{1}{2}(\sigma_1 + \sigma_3) + \frac{1}{2}(\sigma_1 - \sigma_3)\cos 2\beta \tag{A2}$$

and

$$\tau = \frac{1}{2}(\sigma_1 - \sigma_3)\sin 2\beta \tag{A3}$$

where,

σ_n = normal stress, Pa
τ = shear stress, Pa

There will be a critical plane on which the available shear strength will be first reached as σ_1 is increased. The Mohr circle construction of Fig. A2 (a) gives the orientation of this critical plane as:

$$\beta = \frac{\pi}{4} + \frac{\phi}{2} \tag{A4}$$

where,

ϕ = angle of internal friction, °

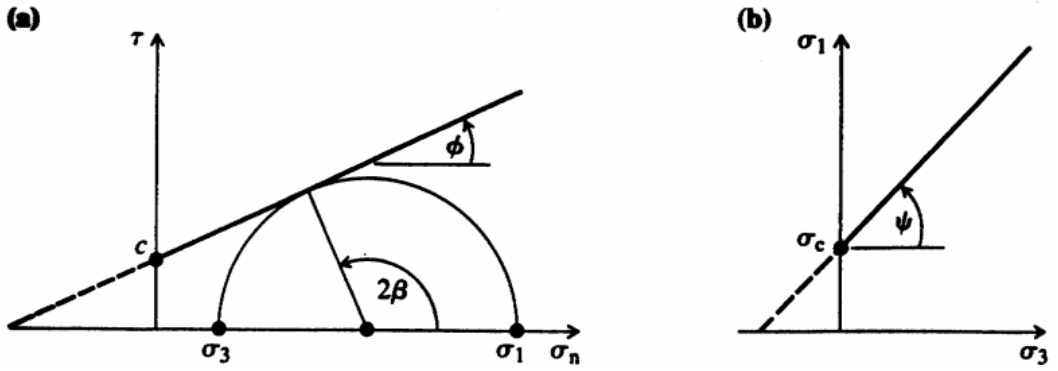

Figure A2 Coulomb strength envelopes in terms of (a) shear and normal stress and (b) principal stresses

For the critical plane, the fracture criterion can be expressed as follows:

$$\sigma_1 = \frac{2c\cos\phi + \sigma_3(1+\sin\phi)}{1-\sin\phi} \tag{A5}$$

This linear relation between σ_3 and the peak value of σ_1 is shown in Fig. A2 (b). Note that the uniaxial compressive strength is related to c and ϕ by the equation:

$$\sigma_c = \frac{2c\cos\phi}{1-\sin\phi} \tag{A6}$$

where,

c = cohesion, Pa

If the Coulomb envelope shown in Fig. A2 (b) is extrapolated to $\sigma_1 = 0$, it will intersect the σ_3 axis at an apparent value of uniaxial tensile strength of the material given by

$$\sigma_t = \frac{2c\cos\phi}{1+\sin\phi} \tag{A7}$$

This criterion predicts that the compressive strength is greater than the tensile strength, but the ratio is not as large (10 to 50) as found in practice. The angle of fracture is the same for tension and compression fracture. In compression the angle of fracture is relatively constant for most rock types, but in tension the fracture surface is usually normal to the direction of the tensile stress. This criterion assumes shear fracture, so that σ_t should not be the actual (brittle) tensile strength but the value at which shear fracture in tension would take place if in fact brittle fracture did not occur in practice before this value reached. The difference in the appearance of the fracture surface created in tension and shear also indicates the mechanism of fracture is not the same in the two cases.

3. Mohr's Criterion

A material may fracture when either the shear stress τ in the plane of fracture has increased to a certain value which in general will depend also on the normal stress σ_n active across the same plane or when the numerically largest tensile principal stress has reached a limiting value σ_t dependent on the properties of the material. Thus at fracture either:

$$\tau = f(\sigma_n) \quad \text{(A8)}$$

$$\sigma_3 = -\sigma_t \quad \text{(A9)}$$

The functional relationship $\tau = f(\sigma_n)$ must be determined experimentally and is represented by a typical curve '$A\ \sigma_t\ c\ B$' (Fig. A3). As this curve is the envelope to the Mohr's circle for the value of σ_3 and σ_1 at fracture, for any state of stress represented by a Mohr's circle lying completely within the envelope, the material will not fracture.

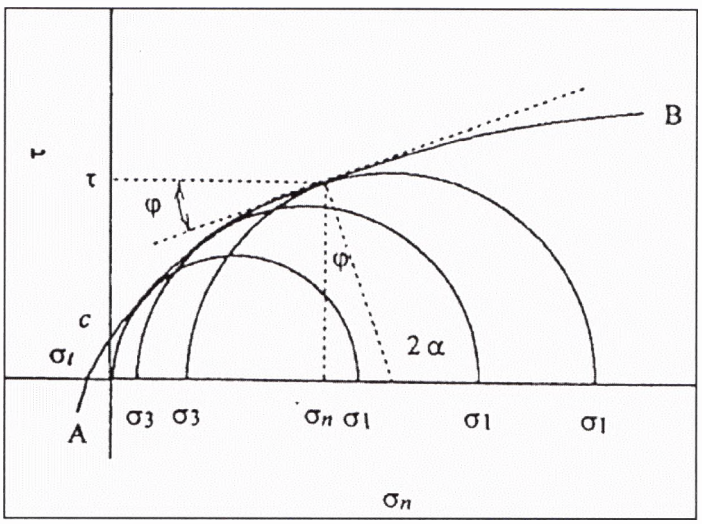

Figure A3 Representation of Mohr's criterion of fracture
(Vutukuri & Katsuyama, 1994)

If any part of the circle lies outside the envelope, the critical stresses will thus be exceeded. For the circle tangent to the envelope, the material will fracture on the plane making the angle α with respect to the minor principal stress. Mohr's criterion further implies that the intermediate principal stress, σ_2 has no influence on fracture. Only the major σ_1 and minor σ_3 principal stresses play an active part in this criterion.

4. Griffith Criterion

It is known that crystalline substances contain microfractures. It is assumed in Griffith criterion of failure, the existence of thin, flat, narrow, elliptical uniform

microcracks in the material. These cracks bring about stress concentration at the tips or ends of Griffith microcracks. When the tensile stress at or near the tip attains a certain critical value, it causes the crack to propagate and ultimately contributing to macroscopic failure of the material. Also, this criterion postulates that fracture is initiated in a brittle material by failure in tension around the tips of the microcracks, and that the crack retains its form until the moment of failure. According to this criterion, the stress necessary to cause brittle fracture varies inversely with the length of the existing cracks. The Griffith criterion of fracture predicts that the magnitude of the uniaxial compressive strength should be exactly eight times the uniaxial tensile strength ($\sigma_c = 8\sigma_t$), a condition that is not consistent with observation, as the uniaxial compressive strength of most rocks varies from 10 to 50 times the uniaxial tensile strength.

McClintock and Walsh (1962) extended the Griffith criterion for the case of high biaxial conditions, where the compression forces are sufficient to close the crack and thereby allow the action of friction forces on the crack surfaces. This modified Griffith criterion includes two criterial quantities, namely, the criterial tensile stress at the tip, expressed by the values of uniaxial tensile strength of the material (as in the original Griffith criterion) and the coefficient of friction between crack surfaces. Fracture occurs when:

$$\sigma_1[1+\mu^2)^{0.5}-\mu]-\sigma_3[(1+\mu^2)^{0.5}+\mu]=4\sigma_t(1+\frac{\sigma_{cr}}{\sigma_t})^{0.5}-2\mu\sigma_{cr} \qquad \text{(A10)}$$

where,

μ = the coefficient of friction for the crack surfaces

σ_{cr} = the stress normal to the crack required to close it.

It should be noted that the coefficient of friction of the crack surface is not the same as the coefficient of internal friction that appears in Mohr's criterion of fracture, although these quantities may be related.

Brace (1963) pointed out that σ_{cr} is small and can be neglected. Hence the above Equation (A10) becomes:

$$\sigma_1[1+\mu^2)^{0.5}-\mu]-\sigma_3[(1+\mu^2)^{0.5}+\mu]=4\sigma_t \qquad \text{(A11)}$$

The relationship between σ_1 and σ_3 is linear as in the Coulomb's criterion. If $\sigma_1 = \sigma_c$ and $\sigma_3 = 0$ are the conditions for simple compression, the ratio of uniaxial compressive to uniaxial tensile strength is:

$$\frac{\sigma_c}{\sigma_t}=\frac{4}{[(1+\mu^2)^{0.5}-\mu]} \qquad \text{(A12)}$$

For $\mu = 1$, the ratio of the uniaxial compressive to uniaxial tensile strength is approximately 10, which is an improvement over the Coulomb's predicted ratio of 5.8; but lower than generally observed values.

5. Bieniawski's Criterion

The criterion proposed by Bieniawski (1974) is as follows:

$$\frac{\sigma_1}{\sigma_c}=1+A(\frac{\sigma_3}{\sigma_c})^k \qquad \text{(A13)}$$

or

$$\frac{\tau_m}{\sigma_c}=0.1+B(\frac{\sigma_m}{\sigma_c})^c \qquad \text{(A14)}$$

where,

A = 3 for siltstone and mudstone
= 4 for sandstone
= 4.5 for quartzite
= 5 for norite

B = 0.7 for siltstone and mudstone
= 0.75 for sandstone
= 0.78 for quartzite
= 0.8 for norite

$k \cong 0.75$ for all rock types

c = 0.9 for all rock types

$$\tau_m=\frac{1}{2}(\sigma_1-\sigma_3) \qquad \sigma_m=\frac{1}{2}(\sigma_1+\sigma_3)$$

6. Hoek and Brown Criterion

The criterion proposed by Hoek and Brown (1980) is as follows:

$$\frac{\sigma_1}{\sigma_c} = \frac{\sigma_3}{\sigma_c} + (1 + m\frac{\sigma_3}{\sigma_c})^{0.5} \quad \text{(A15)}$$

where,

m = 9.6 for sandstone

Substitution of σ_1 = 0 in this criterion, and solution of the resulting quadratic equation for σ_3, gives the uniaxial tensile strength of a rock, σ_t as follows:

$$\sigma_3 = \sigma_t = \frac{1}{2}\sigma_c[m - (m^2 + 4)^{0.5}] \quad \text{(A16)}$$

7. Johnston's Criterion

The criterion proposed by Johnston (1985) is as follows:

$$\frac{\sigma_1}{\sigma_c} = [(\frac{M}{B})(\frac{\sigma_3}{\sigma_c}) + 1]^B \quad \text{(A17)}$$

Where M and B are constants. These constants depend upon σ_c as follows:

$$M = 2.065 + \text{k } (\log\sigma_c)^2 \quad \text{(A18)}$$

$$B = 1 - 0.0172 \ (\log\sigma_c)^2 \quad \text{(A19)}$$

where,

k = 0.170 for dolomite, limestone and marble
= 0.231 for mudstone, shale, slate and clay
= 0.270 for sandstone and quartzite
= 0.659 for amphobolite, gabbro, gneiss, granite, norite and grano-diorite
= 0.276 for all rock types combined (overall)

σ_c = uniaxial compressive strength, kPa

When σ_1 = 0, σ_3 becomes tensile strength, σ_t and then

$$\frac{M}{B} = -\frac{\sigma_c}{\sigma_t} \tag{A.20}$$

This is the only criterion that suggests that the values of the parameters are not only dependent on rock types but also on uniaxial compressive strength of the rock.

8. Summary of Failure Criteria

Comparison of the various failure criteria is summarised in Table A.1. Strength of a rock was evaluated using these criteria and the results were compared with one of a rock sample from laboratory. These results were plotted, σ_1 versus σ_3, as shown in Fig. A4. As can be seen from Fig. A4, the Hoek-Brown criterion matches well with the laboratory sample.

Table A1 Summary of failure criteria

Lab Data		Griffith		Mohr-Coulomb		Johnston		Hoek-Brown		Bieniawski	
σ_3, KPa	σ_1, KPa	σ_3, KPa	σ_1, KPa	σ_3, KPa	σ_1, KPa	σ_3, KPa	σ_1, KPa	σ_3, KPa	σ_1, KPa	σ_3, Kpa	σ_1, KPa
0	55000	0	55002	0	56540	0	55000	0	55000	0	55000
500	57910	500	56710	500	59315	500	58976	500	57850	500	61477
1000	60000	1000	58417	1000	62091	1000	62790	1000	60607	1000	65893
1500	65000	1500	61831	1500	67641	1500	70013	1500	65883	1500	73320
2000	70000	2000	65245	2000	73191	2000	76794	2000	70890	2000	79831
2500	75000	2500	68659	2500	78741	2500	83216	2500	75673	2500	85810
3000	80000	3000	72073	3000	84291	3000	89340	3000	80266	3000	91423
Required Equation/s		Required Equation/s		Required Equation/s		Required Equation/s		Required Equation/s		Required Equation/s	
None		A11 & A12		A.5		A17, A18 & A19		A15		A13	

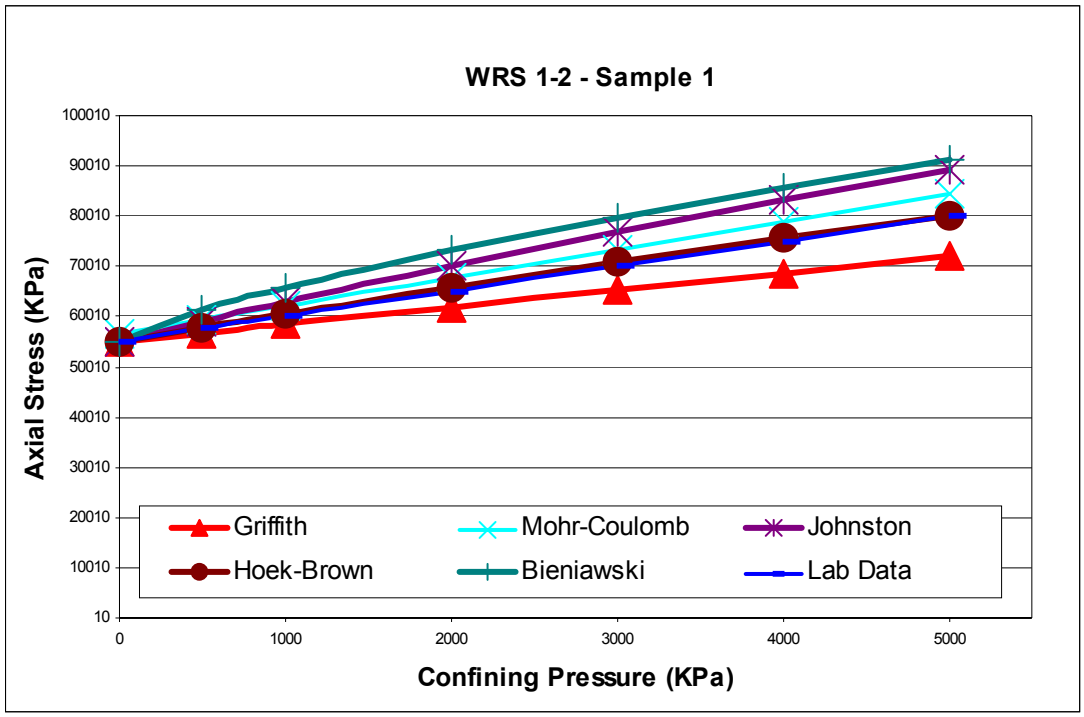

Figure A4 Comparison of failure criteria

APPENDIX B

GENERAL MODELLING PROCEDURE

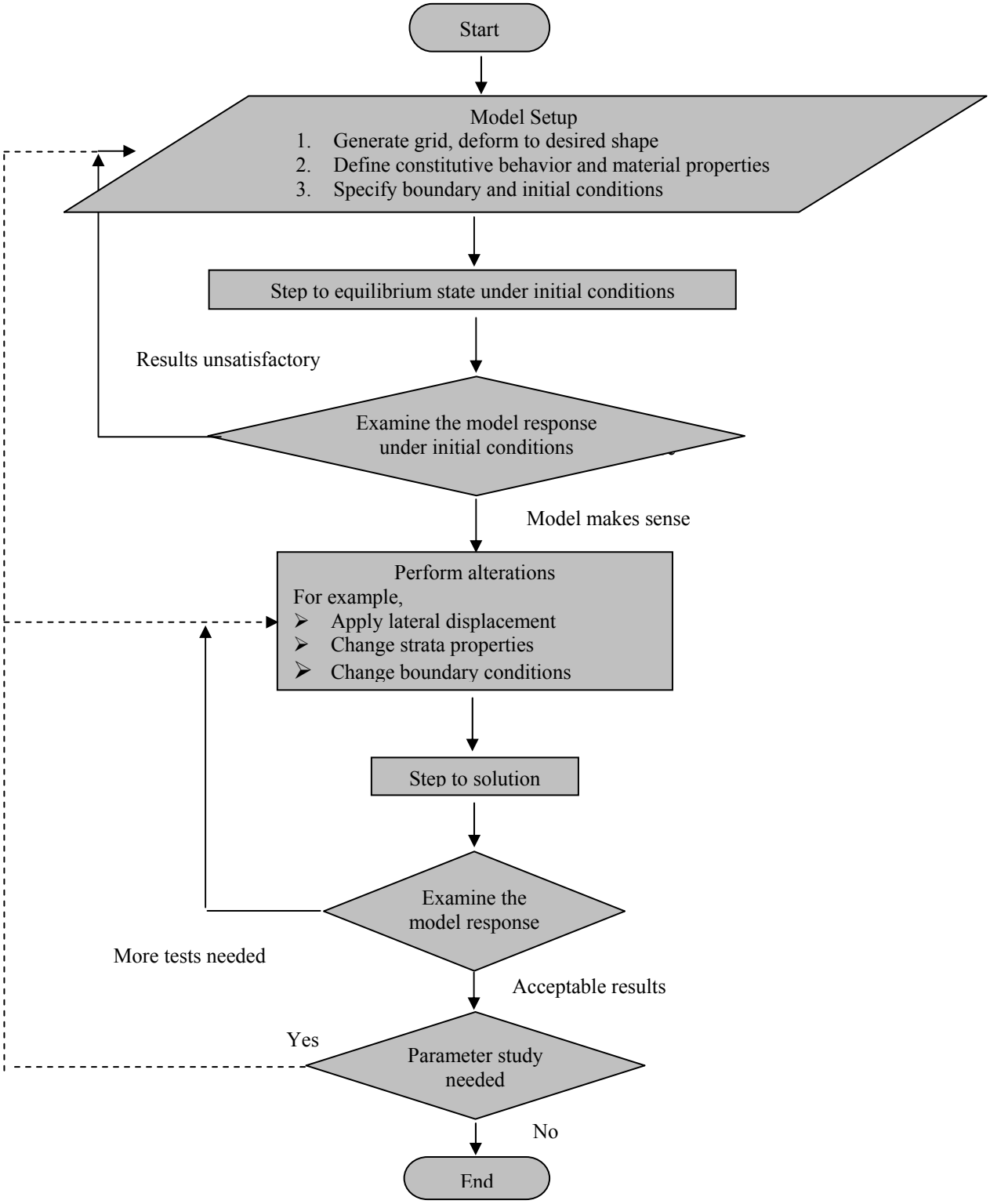

APPENDIX C
NUMERICAL MODEL CODE FOR FLAC

```
;***************
;*************** Section 1
;*************** Generation of grid
;***************

grid 190,114

gen 9180,-80    9180,-30    9260,-30    9260,-80    i=1,81      j=1,51
gen 9180,-30    9180,0      9260,0      9260,-30    i=1,81      j=51,81
gen 9180,0      9180,34     9260,34     9260,0      i=1,81      j=81,115
gen 9260,-80    9260,-30    9290,-30    9290,-80    i=81,111    j=1,51
gen 9260,-30    9260,0      9290,0      9290,-30    i=81,111    j=51,81
gen 9260,0      9260,34     9290,34     9290,0      i=81,111    j=81,115
gen 9290,-80    9290,-30    9370,-30    9370,-80    i=111,191   j=1,51
gen 9290,-30    9290,0      9370,0      9370,-30    i=111,191   j=51,81
gen 9290,0      9290,34     9370,34     9370,0      i=111,191   j=81,115

;***************
;*************** Section 2
;*************** Constitutive model
;***************

call ubi.fis
model m_ubi
mod null j=70
ini y add 1 j=1,70

int 1 Aside from 1,70 to 191,70 Bside from 1,71 to 191,71

;***************
;*************** Section 3
;*************** External boundary
;***************

title
mod2.mark: Assigning natural surface topography
set echo off
```

```
ca mod2_mark.txt
set echo on
save mod2.surface

;***************
;*************** Section 4
;*************** Assigning strata properties
;***************

set echo off
ca mod2_half_r_fish_properties.txt
set echo on

int 1 ks=6.3e10 kn=6.3e10 fric=44

;***************
;*************** Section 5
;*************** Excavation to form the ground surface
;***************

mod nul reg 110,110

;***************
;*************** Section 6
;*************** Assigning gravity
;***************

set grav 9.8
set large

;***************
;*************** Section 7
;*************** Initialising horizontal and vertical stress
;***************

set echo off
ca ininv.fis
set k0x=2
set k0z=1
ininv
set echo on
```

```
;***************
;*************** Section 8
;*************** Boundary conditions
;***************

fix x y j=1
fix x i=1
fix x i=191

;***************
;*************** Section 9
;*************** Monitoring equilibrium state of model
;***************

hist unbal
ca mod2_hist.txt

;***************
;*************** Section 10
;*************** Step to equilibrium state
;***************

solve sratio 1e-5 step 50000
save mod2.ini

solve sratio 1e-5 step 50000
save mod2.ini

solve sratio 1e-5 step 50000
save mod2.ini

solve sratio 1e-5 step 50000
save mod2.ini

ret
```

APPENDIX D

MODIFIED FISH VERSION OF UBI MODEL

```
;------------------------------------------------------------ ------------------------------------
----
; FISH version of Ubiquitous joint model
; Assume a weak plane embedded in a Mohr-Coulomb solid
;-------------------------------------------------------------------------------------------------
---
set echo off
def m_ubi
  constitutive_model
  f_prop  m_g m_k m_coh m_fric m_dil m_ten m_ind
  f_prop  m_jang m_jcoh m_jfric m_jdil m_jten
  f_prop  m_csnp m_nphi m_npsi m_e1 m_e2 m_x1 m_sh2

  float $sphi $spsi $s11i $s22i $s12i $s33i $sdif $s0 $rad $s1 $s2 $s3
  float $si $sii $psdif $fs $alams $ft $alamt $bisc $pdiv $tco $alamjs
  float $cs2 $si2 $dc2 $dss $s22p $s12p $ds12p $s11p $s33p
  float $apex $anphi $tau $taum $tand $fach $e21 $uang $tdil
  float $muj $theta $cs $sn $cla $clb $csn $clc $clab $dts
  int   $icase $m_err

  Case_of  mode
; ----------------------
; Initialisation section
; ----------------------
    Case 1
      $m_err = 0
      if m_fric > 89.0 then
        $m_err = 1
      end_if
      if abs(m_dil)  > 89.0 then
        $m_err = 2
      end_if
      if m_coh  < 0.0 then
        $m_err = 3
      end_if
      if m_jfric > 89.9 then
         $m_err = 4
      end_if
      if m_jcoh  < 0.0 then
        $m_err = 5
      end_if
      if $m_err # 0 then
        nerr = 126
        error = 1
```

```
    end_if

    $sphi    = sin (m_fric * degrad)
    $spsi    = sin (m_dil * degrad)
    m_nphi  = (1.0 + $sphi) / (1.0 - $sphi)
    m_npsi  = (1.0 + $spsi) / (1.0 - $spsi)
    m_csnp  = 2.0 * m_coh * sqrt(m_nphi)
    m_e1    = m_k + 4.0 * m_g / 3.0
    m_e2    = m_k - 2.0 * m_g / 3.0
    m_x1    = m_e1 - m_e2*m_npsi + m_e1*m_npsi*m_nphi - m_e2*m_nphi
    m_sh2   = 2.0 * m_g
    if abs(m_x1) < 1e-6 * (abs(m_e1) + abs(m_e2)) then
      $m_err = 6
      nerr  = 126
      error = 1
    end_if
; --- set tension to prism apex if larger than apex ---
    $apex = m_ten
    if m_fric # 0.0 then
      $apex = m_coh / tan(m_fric * degrad)
    end_if
    m_ten = min($apex,m_ten)
; --- set joint tension to joint apex if larger than apex ---
    $apex = m_jten
    if m_jfric # 0.0 then
      $apex = m_jcoh / tan(m_jfric * degrad)
    end_if
    m_jten = min($apex,m_jten)

  Case 2
; ---------------
; Running section
; ---------------
    zvisc = 1.0
    if m_ind # 0.0 then
      m_ind = 2.0
    end_if
    $anphi = m_nphi
;--- get new trial stresses from old, assuming elastic increments ---
    $s11i = zs11 + (zde22 + zde33) * m_e2 + zde11 * m_e1
    $s22i = zs22 + (zde11 + zde33) * m_e2 + zde22 * m_e1
    $s12i = zs12 + zde12 * m_sh2
    $s33i = zs33 + (zde11 + zde22) * m_e2 + zde33 * m_e1
    $sdif = $s11i - $s22i
    $s0   =  0.5 * ($s11i + $s22i)
    $rad  =  0.5 * sqrt ($sdif*$sdif + 4.0 * $s12i*$s12i)
;--- principal stresses ---
```

```
    $si    =  $s0 - $rad
    $sii   =  $s0 + $rad
    $psdif =  $si - $sii
;--- determine case ---
    section
     if $s33i > $sii then
;--- s33 is major p.s. ---
       $icase = 3
       $s1    = $si
       $s2    = $sii
       $s3    = $s33i
       exit section
     end_if
     if $s33i < $si then
;--- s33 is minor p.s. ---
       $icase = 2
       $s1    = $s33i
       $s2    = $si
       $s3    = $sii
       exit section
     end_if
;--- s33 is intermediate ---
     $icase = 1
     $s1    = $si
     $s2    = $s33i
     $s3    = $sii
    end_section
;--------------------------
    section
; --- shear yield criterion ---
     $fs    = $s1 - $s3 * $anphi + m_csnp
     $alams = 0.0
; --- tensile yield criterion ---
     $ft    = m_ten - $s3
     $alamt = 0.0
; --- tests for failure ---
     if $ft < 0.0 then
       $bisc = sqrt(1.0 + $anphi * $anphi) + $anphi
       $pdiv = -$ft + ($s1 - $anphi * m_ten + m_csnp) * $bisc
       if $pdiv < 0.0 then
; ---     shear failure ---
         $alams = $fs / m_x1
         $s1 = $s1 - $alams * (m_e1 - m_e2 * m_npsi)
         $s2 = $s2 - $alams * m_e2 * (1.0 - m_npsi)
         $s3 = $s3 - $alams * (m_e2 - m_e1 * m_npsi)
         m_ind = 1.0
           m_coh=0.0          ;addition<<<<<<<<<<<<<<<<<<<<<<<<<<<<<<<
```

```
        else
; ---     tension failure ---
          $alamt = $ft / m_e1
          $tco= $alamt * m_e2
          $s1 = $s1 + $tco
          $s2 = $s2 + $tco
          $s3 = m_ten
          m_ind = 3.0
            m_coh=0.0          ;addition<<<<<<<<<<<<<<<<<<<<<<<<<<<<<<<<
        end_if
      else
        if $fs < 0.0 then
; ---     shear failure ---
          $alams = $fs / m_x1
          $s1 = $s1 - $alams * (m_e1 - m_e2 * m_npsi)
          $s2 = $s2 - $alams * m_e2 * (1.0 - m_npsi)
          $s3 = $s3 - $alams * (m_e2 - m_e1 * m_npsi)
          m_ind = 1.0
          m_coh=0.0            ;addition<<<<<<<<<<<<<<<<<<<<<<<<<<<<<<<<
        else
; ---     no failure ---
          zs11 = $s11i
          zs22 = $s22i
          zs33 = $s33i
          zs12 = $s12i
          exit section
        end_if
      end_if
; --- direction cosines ---
      if $psdif = 0.0 then
        $cs2   = 1.0
        $si2   = 0.0
      else
        $cs2   = $sdif      / $psdif
        $si2   = 2.0 * $s12i / $psdif
      end_if
;--- resolve back to global axes ---
      case_of  $icase
        case 1
          $dc2  = ($s1 - $s3) * $cs2
          $dss  =  $s1 + $s3
          zs11  = 0.5 * ($dss + $dc2)
          zs22  = 0.5 * ($dss - $dc2)
          zs12  = 0.5 * ($s1  - $s3) * $si2
          zs33  = $s2
        case 2
          $dc2  = ($s2 - $s3) * $cs2
```

```
        $dss  =  $s2 + $s3
        zs11  = 0.5 * ($dss + $dc2)
        zs22  = 0.5 * ($dss - $dc2)
        zs12  = 0.5 * ($s2  - $s3) * $si2
        zs33  = $s1
      case 3
        $dc2  = ($s1 - $s2) *$cs2
        $dss  =  $s1 + $s2
        zs11  = 0.5 * ($dss + $dc2)
        zs22  = 0.5 * ($dss - $dc2)
        zs12  = 0.5 * ($s1  - $s2) * $si2
        zs33  = $s3
    end_case
    zvisc = 0.0
  end_section
;
; --- check for yield along the weak plane ---
;   The joint angle is given in prop as m_jang.

  if m_ind = 6.0 then
    m_ind = 7.0
  else
    if m_ind = 8.0 then
      m_ind = 7.0
    end_if
  end_if

  $muj   = tan (m_jfric * degrad)
  $tdil  = tan (m_jdil  * degrad)
  $theta = m_jang * degrad
  $cs    = cos ($theta)
  $sn    = sin ($theta)
  $cla   = $cs  * $cs
  $clb   = $sn  * $sn
  $csn   = $cs  * $sn
  $clc   = 2.0  * $csn
  $clab  = $cla - $clb
; --- Find stresses referred to the shear plane ---
  $s22p = zs11 * $clb + zs22 * $cla - zs12 * $clc
  $s12p = 0.5 * (zs22 - zs11) * $clc + zs12 * $clab
  $tau  = abs($s12p)
  $taum = -$s22p * $muj + m_jcoh
  $ft   = m_jten - $s22p
  $fs   = $tau - $taum
  section
; --- test for failure on shear plane ---
  if $ft < 0.0 then
```

```
        $tand = sqrt(1.0 + $muj * $muj) - $muj
        $fach = m_jcoh - m_jten * ($muj + $tand)
        if $tau - $s22p * $tand - $fach > 0.0 then
; ---    shear failure on plane ---
          m_ind = 6.0
          $ds12p = $taum * float(sgn($s12p)) - $s12p
          zs11 = zs11 - $ds12p * $clc
          zs22 = zs22 + $ds12p * $clc
          zs12 = zs12 + $ds12p * $clab
          if m_jdil # 0.0 then
            $alamjs = - $fs / (m_sh2 + m_e1 * $muj * $tdil)
            $s11p   = m_e2 * $alamjs * $tdil
            $s22p   = m_e1 * $alamjs * $tdil
            $s33p   = $s11p
            zs11    = zs11 + $s11p * $cla + $s22p * $clb
            zs22    = zs22 + $s11p * $clb + $s22p * $cla
            zs33    = zs33 + $s33p
            zs12    = zs12 + ($s11p - $s22p) * $csn
          end_if
        else
; ---    tension failure on plane ---
          m_ind = 8.0
          $e21 = m_e2 / m_e1
          zs11 = zs11 + $ft * ($e21 * $cla + $clb)
          zs22 = zs22 + $ft * ($e21 * $clb + $cla)
          zs12 = - $ft * $clc * m_g / m_e1
          zs33 = zs33 + $ft * $e21
        end_if
      else
        if $fs > 0.0 then
; ---    shear failure on plane ---
          m_ind = 6.0
          $ds12p = $taum * float(sgn($s12p)) - $s12p
          zs11 = zs11 - $ds12p * $clc
          zs22 = zs22 + $ds12p * $clc
          zs12 = zs12 + $ds12p * $clab
          if m_jdil # 0.0 then
            $alamjs = - $fs / (m_sh2 + m_e1 * $muj * $tdil)
            $s11p   = m_e2 * $alamjs * $tdil
            $s22p   = m_e1 * $alamjs * $tdil
            $s33p   = $s11p
            zs11    = zs11 + $s11p * $cla + $s22p * $clb
            zs22    = zs22 + $s11p * $clb + $s22p * $cla
            zs33    = zs33 + $s33p
            zs12    = zs12 + ($s11p - $s22p) * $csn
          end_if
        else
```

```
; ---    no failure on plane ---
          exit section
        end_if
      end_if
      zvisc = 0.0
      end_section

      if large # 0 then
; --- Update joint angle ---
        $dts   = zde12 * $clab + $csn * (zde22-zde11)
        $uang = $uang + $dts + zdrot
        if zsub > 0.0 then
          m_jang = m_jang + $uang / (zsub * degrad)
          $uang = 0.0
        end_if
      end_if

    Case 3
; ----------------------
; Return maximum modulus
; ----------------------
      cm_max = m_k + 4.0 * m_g / 3.0
      sm_max = m_g

    Case 4
; ---------------------
; Add thermal stresses
; ---------------------
      ztsa = ztea * m_k
      ztsb = zteb * m_k
      ztsc = ztec * m_k
      ztsd = zted * m_k
  End_case
end

opt m_ubi
set echo=on
```